Multi-Objective Optimization of Facade Geometry for Wind and Thermal Resilience

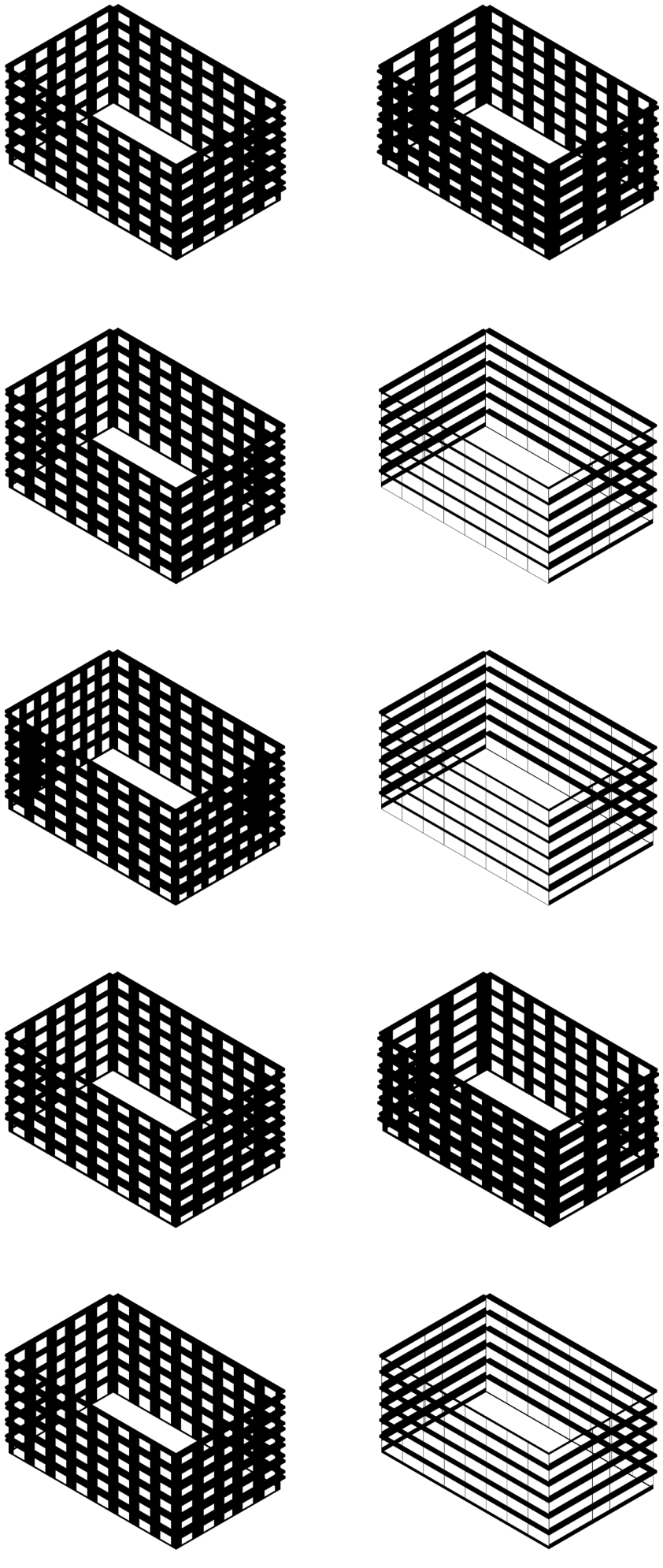

Muhammad Rafif Cahyadi Agung

Master's Thesis
Building Technology

Technische Universiteit Delft

TU Delft

Report

Multi-Objective Optimization of Façade Geometry for Wind and Thermal Resilience

By

Muhammad Rafif Cahyadi Agung
6166962

In fulfilment of the requirements for the degree of:

Master of Science
in Architecture, Urbanism, and Building Sciences

at the Delft University of Technology,
Faculty of Architecture and the Built Environment

to be defended publicly on Wednesday, June 24th 2026 at 11:30 AM.

Mentors:	Dr. Simona Bianchi, Structural Design and Mechanics,	TU Delft
	Dr. Gabriele Mirra, Design Informatics	TU Delft
Delegate:	Dr.ir. M.G.H. Schoonderbeek	

This thesis was funded by:
Indonesia Endowment Fund for Education (LPDP Scholarship)



An electronic version of this thesis is available at http://repository.tudelft.nl/.

Contents

Acknowledgements **5**

Abstract **6**

List of Figures **7**

List of Tables **8**

1 Introduction **9**
1.1 Background 9
1.1.1 Climate change, heatwaves and windstorms 9
1.1.2 From Energy Efficiency to Climate Resilience 9
1.1.3 Façade Resilience and the complexity of multi-hazard behaviour 10
1.2 Problem Statement 10
1.3 Relevance 10
1.3.1 Scientific Relevance 10
1.3.2 Societal / professional relevance 11
1.4 Objective and motivation 11
1.4.1 General Objective 11
1.4.2 Sub-objectives 11
1.4.3 Motivation 11
1.5 Research and/or design questions 12
1.6 Scope 12

2 Approach **13**
2.1 Methodology 13
2.1.1 Literature Review 14
2.1.2 Dataset Generation 14
2.1.3 Resilience Quantification 14
2.1.4 Exploratory Data Analysis 14
2.1.5 Surrogate Model Training 14
2.1.6 Multi-Objective Optimization 15
2.2 Theoretical Framework 15
2.2.1 Façade Resilience 15
2.2.2 Multi-hazard Framework 16
2.2.3 Quantitative Resilience Assessment 18
2.2.4 Thermal Resilience Quantification 20
2.2.5 Wind Resilience Quantification 22
2.2.6 Multi-Objective Optimization 33

3 Case Study **35**
3.1 Building Selection 35
3.2 Façade Parameter Space 36
3.3 Design Variable Ranges 38

3.4 Latin Hypercube Sampling 39

4 Thermal Resilience Quantification 41
4.1 Thermal Simulation 41
4.1.1 Heatwave Identification 41
4.1.2 Thermal Simulation Setup 42
4.1.3 Example Use on Case Study 42
4.2 Thermal Resilience Score Calculator 45
4.2.1 Grasshopper Python Component 45
4.3 Heatwaves Surrogate Model Training 47
4.3.1 Correlation Analysis 47
4.3.2 Random Forest Regression 50
4.3.3 Sobol Sensitivity Analysis 52
4.3.4 Key Findings and Implications 54

5 Wind Resilience Quantification 55
5.1 Wind Simulation 55
5.1.1 CFD Simulation Setup 55
5.1.2 Example Use on Case Study 56
5.2 Wind Resilience Score Calculator 57
5.2.1 Grasshopper Python Component 57
5.2.2 Fragility Curve Viewer 61
5.3 Wind Surrogate Model Training 62
5.3.1 Correlation Analysis 63
5.3.2 Random Forest Regression 67
5.3.3 Sobol Sensitivity Analysis 69
5.3.4 Key Findings and Implications 70

6 Multi-Objective Optimization 72
6.1 Defining Parameters 72
6.2 Defining Objectives 72
6.3 Results 73

7 Conclusion and Discussion 77
7.1 Conclusion 77
7.2 Discussion 78
7.3 Answer to research questions 82
7.4 Further development 84

References 86

Appendix A 93

Appendix B 102

Appendix C 122

Acknowledgements

The AE+T faculty has provided me with positive experience and guidance throughout the whole master's study. Various insights from different topics have opened up my way of thinking towards the world.

I would like to express my deepest gratitude to my mentors, Dr. Simona Bianchi and Dr. Gabriele Mirra. Their guidance and expertise motivated me to work in the right direction. Their patience in answering my questions and the constructive feedback they offered at every stage of this thesis shaped not only the outcome of this work but also the way I approach research itself.

My sincere appreciation goes to LPDP (Lembaga Pengelola Dana Pendidikan) for the scholarship that made this master's study possible. Beyond the financial support, being part of the LPDP community has been a constant reminder of the responsibility and privilege of pursuing education abroad, and of the contribution I hope to make in return.

To my friends, both those I met during this chapter and those who have been with me long before it — Vadya, Rizqi, Gazza, Krishna, Sana, Purvi, Janvi, Thanassis, Bart, Andres, and everyone else I couldn't mention — thank you for the conversations, the shared meals, the late-night study sessions, and the moments of laughter that kept everything in perspective. Above all, my deepest thanks go to my mom and dad, whose love and trust have been the foundation of everything I have done, and to my girlfriend, Lintang Kirana, whose patience, encouragement, and quiet support carried me through the hardest stretches of this work. This journey would have felt far heavier without all of you.

Muhammad Rafif Cahyadi Agung
Delft, June 2024

Abstract

Climate change is increasing the frequency and severity of heatwaves and windstorms, shifting the focus of façade design from energy efficiency and sustainability towards climate resilience. Façades sit at the boundary between the indoor environment and an increasingly hostile climate, and they are now expected to deliver thermal comfort under extreme heat and to retain structural integrity under extreme wind in a single, coherent design. **Current façade design workflows, however, lack the computational efficiency and the multi-hazard framework necessary to systematically balance the non-linear trade-offs between thermal and wind resilience.**

Three gaps in current practice motivate this work. First, thermal and wind hazards are typically evaluated separately and combined only after the design has been fixed, which prevents trade-offs from being navigated generatively. Second, the dynamic simulations required for both hazards (EnergyPlus and CFD) are too computationally expensive to be embedded inside a design exploration loop, forcing designers to rely on a few pre-selected variants. Third, the literature offers resilience indicators for each hazard but provides little guidance on how to recast them into a single, simulation-ready, comparable form that can drive an optimisation.

To address these gaps, this thesis develops and tests a data-driven workflow that links eleven façade design parameters to thermal and wind resilience metrics. The parameters comprise four aperture ratios, four shading depths, two window-subdivision ratios, and the outer-pane glass thickness. Hazard-specific simulations are coupled with a resilience quantification framework that translates literature-based indicators into simulation-ready, normalised resilience scores on [0, 1] for both hazards. A Latin Hypercube Sampling dataset is generated across the eleven-variable design space and explored through correlation, feature-importance, and Sobol sensitivity analyses to identify the drivers of each hazard. Because the underlying simulations are too expensive to evaluate inside an optimisation loop, a random forest surrogate model is trained on this dataset to predict the two resilience scores in near-real time, and the surrogate is embedded inside an NSGA-II multi-objective optimisation routine that generates Pareto-optimal façade designs making cross-hazard conflicts and synergies explicit.

The workflow is illustrated on *De Centrale IJburg*, a residential case study located in the IJburg district of Amsterdam, the Netherlands. The building has a footprint of approximately 32 × 20 m and a height of approximately 20 m, and the analysis uses climate data and building-code references relevant to the Dutch context. The results show that thermal and wind resilience engage disjoint subsets of the design space: thermal performance is governed primarily by the orientation-specific apertures and the South shading depth, while wind performance is governed almost entirely by the window subdivision parameters. This separation produces a Pareto front with a clear knee region in which both objectives can be jointly maximised. The top-ranked Pareto solutions share a coherent geometric signature combining moderate apertures across all four orientations, deeper shading on the North and East orientations, and the thicker outer-pane glass option.

By translating high-level EU climate adaptation targets into a practical, Grasshopper-based design tool, this thesis contributes to resilience-based design practice and demonstrates how multi-hazard resilience can be treated as a generative design objective embedded within the optimisation process, rather than as a separate evaluation step applied only after the design is fixed.

List of Figures

Figure 1. Graphical representation of overall workflow (Author) 13
Figure 2. Resilience criteria for facade and components (Navarro et al., 2024) 16
Figure 3. De Centrale IJburg Floor Plan and Section (vurbarchitects, 2020) 35
Figure 4. Type of apartments in De Centrale IJburg (vurbarchitects, 2020) 36
Figure 5. Dataset Generation Workflow (Author) 40
Figure 6. Historical Heatwave Events from 1901-2025 (Author) 41
Figure 7. Most Intense Heatwave Recorded (Author) 41
Figure 8. Graphical Representation of Thermal Simulation Workflow (Author) 42
Figure 9. Thermal Resilience Workflow Application on Case Study (Author) 43
Figure 10. Cooling EUI during Heatwave (Author) 43
Figure 11. Cooling EUI Typical (Author) 44
Figure 12. Example of Thermal Resilience Workflow Output - SET (Author) 44
Figure 13. Example of Thermal Resilience Workflow Output - Functionality Curve (Author) 45
Figure 14. Thermal Resilience Calculator Grasshopper Component (Author) 45
Figure 15. Correlation Analysis of Thermal Resilience of Corridor Rooms (Author) 48
Figure 16. Correlation Analysis of Thermal Resilience of Living Area (Author) 49
Figure 17. Correlation Analysis of Thermal Resilience of the Whole Building (Author) 49
Figure 18. Strongest per Input Feature (Author) 50
Figure 19. Target Variable Distributions for EUI and Thermal Resilience (Author) 50
Figure 20. OOB Convergence for Thermal Resilience (Author) 51
Figure 21. Feature Importance Averaged Across Floors for Thermal Resilience (Author) 51
Figure 22. Parity Plots Averaged Across Floors for Thermal Resilience (Author) 52
Figure 23. Overall Input Sensitivity for Thermal Resilience (Author) 53
Figure 24. Graphical Representation of Wind Simulation Workflow (Author) 55
Figure 25. Wind Resilience Workflow Application on Case Study (Author) 56
Figure 26. Pressure Coefficient on Probing Points (Author) 57
Figure 27. Graphical Representation of Wind Resilience Calculator Workflow (Author) 58
Figure 28. Wind Resilience Calculator Grasshopper Component (Author) 58
Figure 29. Fragility Curve Viewer - Interactive Hazard Intensity Slider 62
Figure 30. Fragility Curve Viewer - Demand vs Capacity per Orientation (Author) 62
Figure 31. Correlation Analysis of Design Inputs vs Wall Cp Outputs (Author) 64
Figure 32. Correlation Analysis of Design Inputs vs Shading Cp Outputs (Author) 65
Figure 33. Correlation Analysis of Design Input vs Wind Resilience Outputs (Author) 66
Figure 34. Target Variable Distributions for Wind Resilience Score (Author) 67
Figure 35. OOB Convergence for Wind Resilience (Author) 68
Figure 36. Feature Importance for Wind Resilience (Author) 68
Figure 37. Parity Plots for Wind Resilience Models (Author) 69
Figure 38. Overall Input Sensitivity for Wind Resilience (Author) 70
Figure 39. NSGA-II Convergence of the MOO Result (Author) 73
Figure 40. All iterations and Final Pareto Front Results (Author) 74
Figure 41. Top 5 Pareto Solutions with Scores (Author) 74
Figure 42. Top 5 and Bottom 5 Solutions Facade Geometry (Author) 75

List of Tables

Table 1. Multi-Hazard Resilient Façade Framework (Author) 18
Table 2. Key Performance Indicators Identified in Literature (Author) 19
Table 3. Wind Hazard Intensity from various sources (Author) 23
Table 4. Glazing Design Bending Strength Parameters (Various Sources) 26
Table 5. Coefficient k1 and k4 for calculation of the maximum stress (NEN 16612, 2019) 27
Table 6. Independent Variables used in the study (Author) 38
Table 7. Design Parameter of Selected Iteration 42
Table 8. Thermal Resilience Score Calculator Grasshopper Component Input (Author) 45
Table 9. Thermal Resilience Score Calculator Grasshopper Component Output (Author) 46
Table 10. Building Geometry Input (Author) 59
Table 11. Site and Wind Parameters (Author) 59
Table 12. Facade Parameters (Author) 59
Table 13. Glass Properties (Author) 60
Table 14. Window Geometry Parameter (Author) 60
Table 15. Shading Element Capacity (Author) 60
Table 16. Fragility Parameter (Author) 61
Table 17. Wind Resilience Component Output (Author) 61
Table 18. Top 5 MOO Result (Author) 75
Table 19. Bottom 5 MOO Result (Author) 76

1 Introduction

1.1 Background

1.1.1 Climate change, heatwaves and windstorms

Over recent decades, weather and climate-related extremes have caused very large and rising losses. Globally, the “big five” disasters: earthquakes, floods, storms, droughts, and heatwaves are responsible for more than 95% recorded direct losses in the past 20 years, and a total annual disaster costs, when social and ecosystem impacts are included, are estimated to approach USD 2.3 trillion (United Nations Office for Disaster Risk Reduction (UNDRR), 2025). In Europe alone, economic losses from such events are estimated at about EUR 822 billion (1980-2024), with a quarter of these losses occurring just between 2021 and 2024. Hydrological hazards (floods) account for around 47% of this total, meteorological hazards (storms, including windstorms, lightning and hail) for about 27%, and climatological hazards such as heatwaves for almost 18% (European Environment Agency (EEA), 2025).

This shows that climate-related extremes such as heatwaves and windstorms are now structural drivers of risk. At building scale, heatwaves translate into more frequent overheating, higher cooling energy demand and discomfort to its occupants (Pyrgou et al., 2017). While windstorms lead to higher wind pressures, suction and wind-driven rain on facades, increasing the probability of cladding damage, glazing failure and costly downtime (Eissa et al., 2025). This situates façade performance under extreme heat and wind as a core climate-risk question not just a comfort or serviceability issue (Calvin et al., 2023).

1.1.2 From Energy Efficiency to Climate Resilience

European policy is recognizing this growing climate risk. The EU Adaptation Strategy (2021) aims to build resilience and ensure that the EU is prepared to manage climate risks, explicitly acknowledging that climate-related extremes will intensify and that associated economic losses are likely increasing (European Comission, 2021). The same indicator used for monitoring the 8th Environment Action Program emphasizes that adaptation and resilience must be mainstreamed, and that overall monetary losses from climate-related events should be reduced through better risk management and adaptation measures (European Environment Agency (EEA), 2025).

Within this policy landscape, the Energy Performance of Buildings Directive (EPBD) has historically focused on energy efficiency. However, the 2024 EPBD recast represents a significant shift; Article 8 now mandates that Member States address adaptation to climate change alongside fire safety and seismic risks during major renovations (Directive (EU) 2024/1275, 2024). Furthermore, this include optional indicators for the "increase in resilience against disaster risks," officially linking building upgrades to climate-risk management.

Renovation is thus framed as the main lever for both mitigation and adaptation. Research conducted under the IEA EBC Annex 80: Resilient Cooling of Buildings highlights that upgrading façades, becomes important, not only to reduce energy demand but also to manage exposures and

vulnerabilities that drive economic losses (Attia et al., 2021). This reinforces the need for façade-scale methods that allow designers to consider resilience to multiple hazards explicitly during renovation and design decisions.

1.1.3 Façade Resilience and the complexity of multi-hazard behaviour

Multi-hazard conditions are intrinsically complex: hazards can occur sequentially or concurrently, interact in non-linear ways and produce conflicting demands on the same building component. This complexity is recognized in recent international work on building and urban resilience, which stresses that combining hazards and performance criteria often leads to trade-offs and non-additive effects rather than simple “sum of single hazards” behavior (Bruneau et al., 2017).

Understanding how multi-hazard scenarios affect façade performance is therefore essential. The relationships between façade parameters and hazard impacts are likely non-linear, with threshold behaviors, interaction effects and conflicting objectives across hazards and performance domains (Kim et al., 2025). This complexity justifies treating façade resilience as a multi-hazard systems problem rather than a set of independent checks, and motivates quantitative methods that can explore these non-linear, sometimes conflicting relationships systematically during design.

1.2 Problem Statement

The accelerating frequency and intensity of climate-related extremes, specifically heatwaves and windstorms, have transformed building façade design from a matter of energy efficiency and occupant comfort into a critical risk challenge. While the 2024 EPBD recast and the EU Adaptation Strategy mandate that the existing building stock be adapted to these risks, designers currently lack the methods and tools to evaluate multi-hazard resilience during the early design stages.

Façade parameters that optimize for multi-hazard resilience often create conflicting demands or non-linear trade-offs. Without an integrated, rapid-feedback workflow, design decision risk being sub-optimal, leading to increased economic loss, occupant discomfort, or structural failure. **Current façade design workflows lack the computational efficiency and multi-hazard framework necessary to systematically balance the non-linear trade-offs between thermal and wind resilience.**

1.3 Relevance

1.3.1 Scientific Relevance

This research contributes to the emerging field of resilience-based design by transitioning from single-hazard checks to a unified multi-hazard system. It builds upon the framework by introducing Machine Learning (ML) surrogate modeling strategy to replace relatively slow, physics-based simulations with rapid surrogate models. Furthermore, this study explores the “design space” of facades more comprehensively using Multi-Objective Optimization in order to generate the optimal design solution, while also providing new insights into the non-linear sensitivities between façade design parameters and resilience metrics.

1.3.2 Societal / professional relevance

The aging building stock across the Netherlands and Europe presents a significant vulnerability as climate extremes intensify. Because retrofit decisions are both long-lived and capital-intensive, a “business-as-usual" approach to energy renovation—one that ignores climate adaptation—risks locking buildings into 30 to 50 years of escalating climate risk.

Public and private stakeholders, including municipalities, housing associations, and designers, urgently need evidence-based tools to justify costly retrofit choices under conditions of uncertainty. This research provides a data-driven workflow that helps these stakeholders prioritize retrofit measures. By revealing robust, balanced façade solutions that perform well across multiple hazards, this work supports the development of more resilient design guidelines, ensuring that the European "Renovation Wave" results in a building stock that is not only decarbonized but truly survivable.

1.4 Objective and motivation

1.4.1 General Objective

The primary objective of this thesis is to develop and test a data-driven Multi-Objective Optimization (MOO) workflow that relates façade design parameters to wind and thermal resilience metrics, enabling designers to generate and evaluate design options that balance complex multi-hazard trade-offs.

1.4.2 Sub-objectives

- Resilience Quantification: To define and map thermal and wind resilience metrics suitable for optimization.
- Sensitivity Analysis: To identify which façade design parameters have the strongest individual and combined influence on resilience.
- Computational Acceleration: To train an ML surrogate model capable of providing rapid resilience predictions, bypassing computational simulation.
- Multi-Objective Optimization: To generate Pareto-optimal design sets that visualize the trade-offs between maximizing thermal and wind resilience.

1.4.3 Motivation

The motivation for this study is to bridge the gap between high-level EU climate policy and the practical, day-to-day tools used in architectural practice. By embedding resilience into a generative workflow, we ensure that "adaptation" becomes a measurable performance standard in every renovation project.

1.5 Research and/or design questions

The main research question is:

“How can multi-objective optimization approach be used to relate façade design parameters to wind and thermal resilience metrics and to generate design options that support designers in balancing trade-offs between multiple hazards?”

To advance the research further, several sub-questions have been formulated below:

1. How can thermal and wind resilience be quantified in a way that is suitable for modelling and optimization?
2. How do variations in façade design parameters affect wind and thermal resilience metrics across the sampled design space?
3. What trade-offs and synergies between wind and thermal resilience emerge when different façade design strategies are explored using multi-objective optimization (MOO)?
4. How can Pareto-optimal solutions from the MOO process support designers in making informed façade design decisions that balance wind and heat hazards?

1.6 Scope

The scope of this research is limited to (proposed case study) building façades undergoing renovation. The environmental stressors are restricted to extreme heat events (heatwaves) and severe windstorms, utilizing climatic data relevant to the Netherlands.

A critical technical boundary of this study concerns the quantification of wind resilience. In structural engineering and wind science, resilience is often evaluated using probabilistic methods such as the Mean Annual Frequency of Exceedance (MAFE), which calculates the likelihood of a building component failing over a specific return period. While MAFE offers a high-fidelity assessment of risk, its implementation requires complex stochastic modelling and external structural solvers that are difficult to integrate into an iterative, early-stage design loop.

To maintain a seamless, data-driven workflow entirely within the Grasshopper/Rhino environment, this thesis intentionally moves away from MAFE-based probabilistic modelling in favour of a KPI (Key Performance Indicator) - based quantification method. By focusing on Key Performance Indicators (such as peak surface pressures, maximum deflections, or inter-story drift) that can be simulated directly within Grasshopper, the wind resilience scoring is kept technically consistent with the KPI-based approach used for thermal resilience (e.g., Standard Effective Temperature or overheating hours).

This simplification ensures that both hazards can be processed simultaneously by the Machine Learning surrogate model and the Multi-Objective Optimization (MOO) algorithm. This approach prioritizes the speed, automation, and design-support capabilities of the workflow, providing designers with rapid feedback on trade-offs rather than exhaustive probabilistic failure analysis.

2 Approach

2.1 Methodology

This thesis aims to develop and test a data driven multi-objective optimization workflow for façade design under two hazards (windstorm and heatwave). This digital workflow development consists of several steps shown in Figure 1.

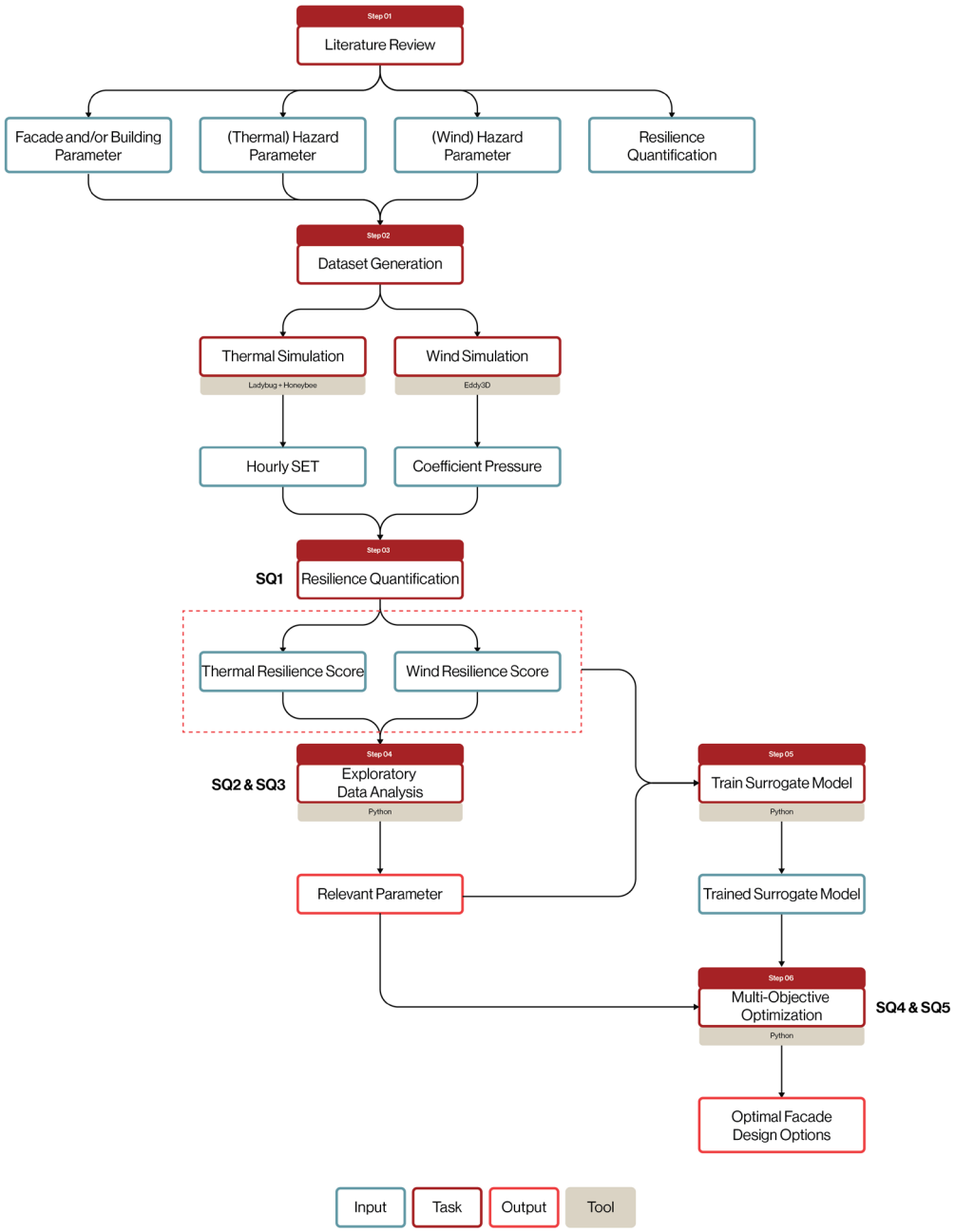

Figure 1. Graphical representation of overall workflow (Author)

2.1.1 Literature Review

The research starts with a comprehensive literature review to establish the study's theoretical domain. This initial step focuses on three main topics: defining façade resilience, understanding heatwaves and windstorms, and evaluating existing resilience quantification methodologies. Within the context of façade resilience, the review analyzes various façade design systems and types to identify the design parameters most critical to the building envelope's performance. This analysis ensures that the selection of design parameters is grounded in their ability to maintain structural and thermal integrity under the extreme events.

The review simultaneously defines heatwaves and windstorms by outlining their specific stressors, the impacts, the KPIs and the metrics used to measure resilience. Establishing these hazards parameters is important in defining the thresholds for extreme events, which subsequently serve as inputs for the next phase. Finally, a comparative evaluation of existing resilience quantification methods is conducted to select the most robust metric for the study. Ultimately, this literature review defines a framework for the proposed resilience assessment.

2.1.2 Dataset Generation

This part is where computational simulations are conducted based on the two hazards to generate the key performance indicators that will be used in the resilience quantification. Each hazard has different simulation methods and tools in order to obtain the key performance indicators. Using the selected design parameters of the façade system, it will be varied systematically to achieve different results. Each simulation result will be recorded and documented in the dataset. The output of this dataset generation is a set of Independent variables which are the design parameters, and a set of dependent variables which are the key performance indicators for each hazard.

2.1.3 Resilience Quantification

This section explains how the selected resilience quantification methods are implemented within the thesis. Building on the literature review, the chosen indicators and scoring system are mapped onto the KPIs produced by the thermal and wind simulations.

2.1.4 Exploratory Data Analysis

This part aims to understand the nonlinear relationship between the design parameters and both hazards' resilience score. Descriptive statistics and visualizations (correlation matrix, pairwise scatterplots) will be conducted in this part to identify the influential and redundant façade parameters. Furthermore, this part will reveal basic patterns such as distributions, correlations, and possible interactions.

2.1.5 Surrogate Model Training

In preparation before the final step, a surrogate model training is applied to further sped up the Multi-Objective Optimization process. With the selected design parameters that are only relevant, it is treated as the input in the machine learning model. The output is the thermal and wind resilience score. This dataset is split into train and test sets. A multi-output regression algorithm is trained on the dataset and

subsequently validated against the test set to assess its accuracy in replicating the computational simulations. The output of this step is a trained model that is able to predict the resilience score.

2.1.6 Multi-Objective Optimization

The final step is to run the multi-objective optimization. The objectives defined in this step are maximizing thermal resilience and maximizing wind resilience. Any other objective can be added by the user of this workflow. For example, minimizing cost. The design variables used in this part is the relevant design parameters. Combined with the trained surrogate model and generative algorithm, this step will generate a pareto set of façade designs showing different trade-offs between the objectives.

2.2 Theoretical Framework

2.2.1 Façade Resilience

The concept of resilience in the built environment has shifted from mere hazard prevention to the preparation for, and acceptance of, inevitable climate uncertainties (Kim et al., 2024). Resilience is now widely defined by a system's ability to "bounce back" or "bounce forward" to a new equilibrium following a disturbance (Attia et al., 2021). This capacity is traditionally structured around the "4 R's": Robustness (the ability to endure without loss of functionality), Redundancy (the presence of backup options or adaptive capacity), Resourcefulness (the mobilization of resources during emergencies), and Rapidity (the rate of recovery) (Bianchi et al., 2025). Applied specifically to building envelopes, frameworks divide resilience into distinct chronological stages: vulnerability assessment, resistance to the initial shock, robustness to absorb failure without catastrophic consequences, and recoverability(Attia et al., 2021). For instance, in the face of extreme heat or power outages, a resilient façade must ensure "passive survivability" by maintaining liveable indoor temperatures—or delaying the onset of dangerous conditions—when mechanical cooling is unavailable (Krelling et al., 2024). Thus, the façade is no longer viewed just as a static barrier, but as a dynamic system that dictates the building's capacity to protect human life and rapidly restore operational normality.

Facades function as complex filters between the building’s interior and the external environment, controlling heat transfer, mass, acoustics, and light, while simultaneously resisting structural actions like wind, impact, and seismic loads (Bianchi et al., 2024). Because of these overlapping roles, recent research emphasizes that resilience cannot be evaluated through a single-domain lens. Instead, it must be treated as a multi-domain construct encompassing physical/structural, social, economic, and environmental responses (Bianchi et al., 2025). When a facade is subjected to a disruptive event, its performance represents a time-varying integration of these interdependent domains (Ouyang & Spence, 2019). For example, evaluating wind resilience requires tracking how dynamic wind pressures and structural drift interact to create progressive damage states, which in turn dictate secondary consequences like rainwater ingress and interior economic losses (Ouyang & Spence, 2020). Because enhancing one aspect of the envelope (e.g., thermal insulation) can sometimes compromise another (e.g., trapping heat during summer or increasing structural mass), decision-making frameworks must integrate these conflicting performance criteria to identify holistic, multi-hazard trade-offs

To transition from qualitative goals to measurable engineering outcomes, modern resilience frameworks explicitly link specific design variables to quantifiable performance indicators. The geometry and detailing of a façade—such as window-to-wall ratios, balcony depths, insulation

thickness, and shading devices—directly influence the intensity of hazard impacts. For instance, multi-objective optimization studies demonstrate that carefully tuning Solar Heat Gain Coefficients (SHGC) and façade absorptance can significantly reduce maximum operative temperatures () and the required recovery time () after a heatwave (Caieiro Da Costa et al., 2026). To quantify this resilience mathematically, researchers utilize specific demand parameters and fragility curves. Structural and wind resilience are measured by the probability of exceeding specific damage states (e.g., gasket seal failure, glass cracking, or panel blowout) given a certain inter-story drift or net wind pressure (Ouyang & Spence, 2020) (Ouyang & Spence, 2019). These damage states are then translated into economic metrics, such as the ratio of repair costs to replacement costs, to define a "Resilience Loss" function over time (Bianchi et al., 2024). Conversely, thermal resilience is measured through social and environmental metrics, such as Cumulative Degree Hours of "unmet" Standard Effective Temperature (SET), which track how long the indoor environment deviates from safe comfort thresholds (Kim et al., 2024). By utilizing these hazard-specific metrics, they are adopted as the objective functions within the multi-objective optimisation workflow, providing a consistent quantitative basis for comparing how different façade design configurations perform under heatwave and windstorm conditions.

2.2.2 Multi-hazard Framework

Table 1 maps how recent façade-focused multi-hazard studies define resilience across different hazards and data structures. The studies cover a wide methodological spread, from multi-criteria scoring techniques and weighted aggregations to regression-based and probabilistic risk approaches, but they share a common feature: in all cases, the resilience score is generated as a post-processed evaluation of a small set of pre-selected façade configurations rather than as a directly optimisable design objective.

Hazard Type	Resilience Dimension	Resilience Phase	Resilience Criteria
Heatwave	Social	Resistance	Time to reach first time SET critical [h]
	Social	Robustness	Cumulative degree hours above SET critical [°h]
	Social	Recovery	Time to return to SET critical [h]
Earthquake, Wind, Flood	Technical	Response	Mean Annual Frequency of Exceedance of Damage State [1/years]
	Technical	Recovery	Downtime [months]
	Economic	Recovery	Repair Cost [cost/m2]
	Environmental	Recovery	Carbon emissions [kg CO2e]

Figure 2. Resilience criteria for facade and components (Navarro et al., 2024)

The first group of studies uses multi-criteria methods to combine hazard-specific scores into a single performance index. (Sadaphal, 2024) generated three façade systems with different properties (single, double, and triple glazing) and combined them into a total resilience score using a weighted-factor aggregation, in which each hazard-specific score is multiplied by an importance weight and the products are summed to yield a single value. The MULTICARE project (Navarro et al., 2024) takes a more structured approach and organises the resilience score along several dimensions, as shown in Figure 2 : a heatwave is placed under the social dimension because of its effects on human occupants, while earthquakes, wind, and flood fall under the technical, economic, and environmental dimensions respectively. The scores across these dimensions are then aggregated into a single performance index using TOPSIS (Technique for Order of Preference by Similarity to Ideal Solution), a multi-criteria decision-making method that ranks alternatives by their relative geometric distance to a positive and a

negative ideal solution. Bianchi (Bianchi, 2023) uses the Analytic Hierarchy Process (AHP**)** weighting method, a pairwise-comparison technique that combines hazard, vulnerability, and exposure indicators into a single weighted risk index (Gacu et al., 2025), to generate maps that describe seismic and energy losses with zones based on building class. (Kim et al., 2024) extends the multi-criteria family with a scoring approach that summarises four resilience metrics in a radar-style chart to compare different façade system options at a glance.

A second group introduces statistical and regression-based methods to capture non-linear relationships within the resilience response. (Kim et al., 2025) applies segmented multivariate regression, in which the response is partitioned into ranges and fitted with separate regression models per segment, across 200 design variations to identify non-linear interactions between façade design parameters and two resilience scores. This statistical analysis is used to derive insights into conflicting hazards and to identify the best-performing solutions among the sampled configurations.

A third group adopts probabilistic risk approaches based on Monte Carlo simulation. (Qin et al., 2026) applies Monte Carlo simulation to the cladding and interior of a building exposed to wind and rain, computing the expected recovery time as the central resilience indicator. (Yu et al., 2025) uses Monte Carlo simulation on a 12-storey reinforced-concrete frame structure exposed to earthquake and wind, with the annual failure probability as the output of interest. (Ouyang & Spence, 2019) extends this probabilistic line of work to a 45-storey steel building under combined wind and rain hazards, deriving fragility relationships for damaged envelope components and the corresponding rainwater ingress. These three studies build a robust probabilistic foundation for façade risk assessment, but their outputs remain descriptive performance indicators evaluated on a small number of fixed building configurations rather than design variables that are optimised in their own right.

Taken together, the studies reviewed in Table 1 cover a broad methodological landscape, but in all cases the resilience score is treated as a post-processed evaluation rather than as a directly optimisable objective. By treating resilience as an outcome to be measured rather than a quantity to be maximised, these frameworks offer limited support for systematically navigating trade-offs between hazards or for generating alternative design solutions during early-stage design. Positioning resilience metrics as explicit objective functions in a multi-objective optimisation workflow therefore represents a key novelty of this thesis: it turns multi-hazard assessment from a static evaluation step into a generative, Pareto-based design engine that can propose façade design options and make cross-hazard trade-offs visible to designers in real time.

Table 1. Multi-Hazard Resilient Façade Framework (Author)

Literature	Hazard	Samples Tested	Method	Data Type	Based on
(Sadaphal, 2024)	Heatwave	3 Façade System	Weighted Multi-Criteria Evaluation	Table	Total Resilience Loss
	Flood				
(Kim et al., 2025)	Heatwave	200 design variations	Segmented multivariate regression	Graph	Unmet SET
	Earthquake			Plots	Damage
(Navarro et al., 2024)	Heatwaves	4 Façade System	Multi-Criteria Decision Making: TOPSIS	Table	Social Resilience
	Earthquake				Technical Resilience
	Wind				Environmental
	Flood				Economic
(Bianchi, 2023)	Heatwave	6 Façade System	AHP weighting	Map	Seismic Loss
	Earthquake				Energy Loss
					Class
(Kim et al., 2024)	Heatwave	8 Façade System	Multi-Criteria Scoring	Radar Chart	Seismic Resilience Loss
	Earthquake				Seismic Economic Loss
					Thermal Resilience Loss
					Thermal Economic Loss
(Qin et al., 2026)	Wind	Cladding and Interior	Monte Carlo Simulation		Recovery Time
	Rain				
(Yu et al., 2025)	Earthquake	12-story concrete frame structure	Monte Carlo Simulation		Annual Failure Probability
	Wind				
(Ouyang & Spence, 2019)	Wind	45-story steel building	Monte Carlo Simulation		Damaged envelope component
	Rain				Rainwater Ingress

2.2.3 Quantitative Resilience Assessment

The primary purpose of the literature synthesis was to identify measurable KPIs that could serve as objective functions in a Multi-Objective Optimization (MOO) workflow. The review in Table 2 reveals a clear consensus on thermal resilience quantification; for instance, Kim defines the Standard Effective Temperature (SET) as the primary indicator to quantify resilience loss in hours of discomfort (Kim et al., 2025), while Sadaphal focuses on the increase in cooling energy consumption as the basis for a resilience score (Sadaphal, 2024). These thermal metrics are inherently suited for the proposed workflow because they can be extracted directly from dynamic thermal simulations within the Grasshopper environment.

In contrast, the quantification of wind resilience reveals a consistent reliance on probabilistic, hazard-based metrics rather than direct, geometry-driven KPIs. Studies on typhoon and hurricane impact on high-rise façades, such as (Qin et al., 2025), (Tokgoz & Gheorghe, 2013), and (Ouyang & Spence, 2020), typically express wind performance through Mean Annual Frequency of Exceedance (MAFE) of damage states, repair cost, or water ingress, embedding resilience in risk curves instead of simulation outputs that designers can access during early-stage modeling.

Recent façade-focused wind reviews and evaluation studies, including (Eissa et al., 2025) and (Dias, 2025), reinforce this pattern by framing façade performance in terms of exceedance probabilities or fragility rather than deterministic response indicators. While this probabilistic perspective is essential for risk assessment, it leaves “empty cells” in a KPI-based, design-space matrix because MAFE values are not directly retrievable from Grasshopper-based CFD or structural simulations, and therefore cannot be optimized alongside thermal KPIs in real time. This thesis addresses that methodological gap by interpreting insights from the probabilistic literature and recasting wind performance into simulation-friendly KPIs. So that wind and thermal resilience can be evaluated within a unified, data-driven multi-objective optimization workflow for façade design.

Table 2. Key Performance Indicators Identified in Literature (Author)

Literature	Hazard	Key Performance Indicator	Unit	Resilience Domain	Resilience Phase
(Sadaphal, 2024)	Heatwave	Cooling Energy Demand	[kwh/m2]	Economic	Response + Recovery
(Kim et al., 2025)	Heatwave	Cumulative Degree hours above SET critical	[◦Ch]	Social	Response
(Navarro et al., 2024)	Heatwave	Time to reach first time SET critical	[h]	Social	Response
		Cumulative Degree hours above SET critical	[◦Ch]	Social	Response
		Time to return to SET critical	[h]	Social	Recovery
	Wind	Mean Annual Frequency of Exceedance of Damage State	[1/years]	Physical	Response
		Downtime	[months]	Physical	Recovery
		Repair Cost	[cost/m2]	Economic	Recovery
		Carbon Emission	[kg/CO2eq]	Environmental	Recovery
(Bianchi, 2023)	Heatwave	Energy Cost	[€]	Economic	Response + Recovery
		Carbon Emission	[kg/CO2eq]	Environmental	Recovery
(Kim et al., 2024)	Heatwave	Energy Cost	[€]	Economic	Response + Recovery
		Unmet SET	[◦Ch]	Social	Response + Recovery
(Tokgoz & Gheorghe, 2013)	Wind - Hurricane	Loss Ratio for each Damage State	-	Economic	Response
		Recovery Time	-	Economic	Recovery
(Ouyang & Spence, 2020)	Wind	Mean Annual Frequency of Exceedance of Repair Cost	[1/years]	Economic	Response
		Mean Annual Frequency of Exceedance of Ingress Water Volume	[1/years]	Physical	Response
(Qin et al., 2025)	Wind	Recovery Time	-	Economic	Recovery
(Eissa et al., 2025)	Wind	Deformations (via experiment)			
(Dias, 2025)	Wind	Wind-Induced Vibrations			

2.2.4 Thermal Resilience Quantification

Thermal comfort in buildings is increasingly challenged by climate change, which intensifies heatwave events in the Netherlands and extends periods of overheating in poorly adapted building envelopes. The façade is the primary mediator between the outdoor thermal environment and the indoor occupant experience. It governs solar heat gain through glazing, convective heat exchange through the envelope and natural ventilation through operable openings. Façade design decisions therefore have direct and lasting consequences for the thermal quality of the indoor environment over the building's lifetime.

Existing practice evaluates thermal performance through static metrics. Heating and cooling energy demand, peak indoor temperature, or compliance with adaptive comfort standards. These metrics are adequate for energy certification and code compliance but are inadequate for resilience assessment, which requires understanding of how the building performs over time under dynamic conditions, and how severely and for how long occupants were exposed to uncomfortable or unsafe thermal conditions.

The thermal resilience component developed in this research quantifies the capacity of the building's thermal environment to maintain occupant functionality under realistic annual weather conditions. It follows the resilience framework established by (Bruneau & Reinhorn, 2006), which defines resilience as the integral of a quality function over a reference time period. Applied at the building-interior level, this framework produces a scalar thermal resilience score R_thermal bounded between 0 and 1, where 1.0 represents a thermally comfortable environment throughout the entire occupied period and 0.0 represents an environment that is never thermally acceptable.

The component is implemented as a GHPython script within the Grasshopper parametric environment, receiving the hourly Standard Effective Temperature (SET) time series from Honeybee EnergyPlus simulation and computing R_thermal in real time as façade parameters are varied. The following sections describe each stage of the calculation.

Standard Effective Temperature

Standard Effective Temperature (SET), adopted in ASHRAE Standard 55 (ASHRAE, 2020), is selected for this framework. SET is defined as the equivalent of a standard environment — air temperature equal to mean radiant temperature, relative humidity 50%, air speed 0.1 m/s — that would produce the same skin wettedness and mean skin temperature as the actual environment for a person performing light activity (1.0 met) in standard clothing (0.6 clo.) SET therefore integrates the combined thermal effect of air temperature, radiant temperature, humidity, and air speed into a single equivalent temperature, making it a more complete representation of occupant thermal experience than operative temperature alone.

SET is the comfort index used internally by the Honeybee thermal comfort components and is therefore directly available in the Grasshopper workflow without any added post-processing. Two threshold values define the boundaries of the quality function:

- SET_comf (comfort threshold) is the SET value at or below which the occupant is considered fully comfortable, and the environment is fully functional. A value of 24°C is recommended for office occupancy based on ASHRAE 55 Standard 55 (2020), which places the upper limit of the acceptable range for light sedentary activity at this level.

- SET_alert (alert threshold) is the SET value at or above which the environment is considered fully non-functional. A value of 30 °C is adopted, aligning with the threshold used by the Royal Netherlands Meteorological Institute (KNMI) to define a *"tropical day"* (*tropische dag*), and which also forms one of the constituent criteria of a Dutch heatwave .

Both thresholds are user-defined inputs, allowing the designer to adjust them for different building types, occupancy profiles, or climate scenarios. The difference (SET_alert – SET_comf) defines the transition zone width — a wider transition zone produces a more gradual quality function, while a narrow zone produces a sharper transition.

Thermal Resilience Score

As mentioned earlier in the methodology, the definition of resilience used in this study is expressed as an integral of functionality (Bruneau et al., 2003). Thermal resilience refers to a building's ability to maintain a comfortable and/or safe indoor thermal environment for occupants. This scoring has three steps: Quality function, resilience loss, and resilience score.

Quality Function

The quality function Q(t) quantifies the thermal functionality of the indoor environment at each time step. It is a dimensionless scalar bounded between 0 and 1, following the resilience framework of (Bucking et al., 2022). It is defined as:

$$Q(t) = \begin{cases} 1 & if\ SET(t) \leq SET_{comf} \\ 0 & if\ SET(t) \geq SET_{alert} \\ \dfrac{SET_{alert} - SET(t)}{SET_{alert} - SET_{comf}} & otherwise \end{cases}$$

With this definition, the linear function has three definitions:

- Fully functional (Q = 1.0): when SET is at or below the comfort threshold, the environment provides full functionality. No resilience loss is incurred.
- Partial functionality (0 < Q < 1): when SET is in the transition zone between the comfort alert thresholds, the environment provides reduced functionality. The quality degrades linearly from 1.0 at SET_comf to 0.0 at SET_alert. This linear degradation reflects the progressive nature of heat stress — discomfort increases gradually as temperature increases, rather than switching abruptly from acceptable to unacceptable.
- Non-functional (Q = 0.0): when SET is at or above the alert threshold, the environment is considered fully non-functional. Maximum resilience loss is incurred for every hour spent at this state.

Thermal Resilience Loss

The resilience loss adopted in this study follow the formulation of (Kim et al., 2024), originally adapted from (Bucking et al., 2022), which itself an application of the (Bruneau et al., 2003) resilience-loss integral. The cumulative thermal-resilience loss over the simulation period is the area between the perfect comfort line (Q=1) and the actual Q(t) curve:

$$L_{thermal} = \int_{t_0}^{t_N} [1 - Q(t)]dt$$

For simulation with N timesteps of duration Δt, the integral becomes a sum:

$$L_{thermal} = \sum_{k=1}^{N} [1 - Q_k]\,\Delta t$$

Where Q_k is the value of Q at the k-th timestep.

Maximum Possible Loss

If the building were in full alert for the entire simulation (Q=0 for all k), the loss would reach its theoretical maximum:

$$L_{max} = N \cdot \Delta t$$

Thermal Resilience Score

Finally the thermal resilience score is the normalized complement of the loss:

$$R_{thermal} = 1 - \frac{L_{thermal}}{L_{max}}$$

By construction, $R_{thermal}$ lies between 0 and 1: a value of 1 indicates that the building stayed within comfort for the entire simulated period. While a value of 0 indicates that It was in alert conditions throughout. In other words, the thermal resilience score is simply the time-averaged quality factor across all timesteps of the simulation.

2.2.5 Wind Resilience Quantification

Wind represents one of the primary lateral load sources acting on building facades. The wind resilience of a façade system describes its capacity to withstand wind-induced pressure demands without failure of its elements: the glazing panels and the external shading devices.

In this research, wind resilience is assessed at the early design stage using a parametric computational component implemented in Grasshopper. The component take building geometry, site conditions, façade configuration, and glass properties as inputs, and returns a continuous resilience score R_wind ranging from zero to one. Rather than producing a binary pass/fail result, the framework employs a probabilistic demand-capacity fragility approach that expresses resilience as the probability that the façade system survives under the design wind loading condition.

The wind load determination follows the Dutch National Annex to Eurocode 1 for wind actions, NEN-EN 1991-1-4 NB:2019+C2:2023. The glazing capacity is derived in accordance with NEN-EN 16612:2019, the European standard for determining the lateral load resistance of glass panes by calculation. The fragility model follows the lognormal methodology established in FEMA P-58 for performance-based engineering assessment.

Wind Event Identification

In order to simulate the extreme wind event, a literature review is done to define the definition and the hazard intensity of an extreme wind event in different context as a comparison and in The Netherlands (Table 3).

Table 3. Wind Hazard Intensity from various sources (Author)

Source	Definition	Symbol	Wind Speed	Unit/Context	Location
(Ouyang & Spence, 2019)	Target return period	V_H	46 m/s	Site-specific mean hourly, 50-year MRI	Florida, the US
			66.77 m/s	Site-specific mean hourly, 3000-year MRI	
(Ouyang & Spence, 2021)	Hurricane Category 5 (Saffir-Simpson)		67.7 m/s	Maximum mean hourly	Florida, the US
(Tokgoz & Gheorghe, 2013)	Saffir-Simpson Damage Potential Scale		74-95 mph	Category 1	
			96-110 mph	Category 2	
			111-130 mph	Category 3	
			131-155 mph	Category 4	
			>155 mph	Category 5	
(Lima-Castillo et al., 2018)	Test range for turbulent wind loads on glass facades	-	41-63 m/s	Mean	
(Yu et al., 2025b)	Damage threshold (Beaufort Scale, Level 11)		30 m/s	-	California, Kanto Region, Santiago, Hualien, and Dali and Kashi
			42.96 m/s	Average wind speed over 600s	Florida
(*NEN-EN 1991-1-4+A1+C2/NB+C2*, 1991)	Basic Wind Speed, Zone I	$V_{b,0}$	29.5 m/s		The Netherlands
	Basic Wind Speed, Zone II	$V_{b,0}$	27.0 m/s		The Netherlands
	Basic Wind Speed, Zone III	$V_{b,0}$	24.5 m/s		The Netherlands
(Geurts et al., 2004)	Standard design wind speed for wind-tunnel calibration		25 m/s	Example value for façade pressure	The Netherlands

(Fonseca Cerda et al., 2025)	Baseline Damage Threshold		15 m/s		The Netherlands
	Significant Loss Threshold		22 m/s		The Netherlands
Historical Extreme (Storm Daria, 1990)	Recorded Mean		29 m/s		The Netherlands

The literature offers a wide range of wind-speed values used in façade resilience studies, but most of these are not directly transferable to the present case. International references such as (Ouyang & Spence, 2019, 2021) and (Tokgoz & Gheorghe, 2013) develop their thresholds in the context of hurricane-prone regions, where the wind hazard is dominated by tropical cyclones with maximum mean hourly speeds well above 60 m/s. Similarly, the test ranges reported by (Lima-Castillo et al., 2018) and the Beaufort-based threshold of (Yu et al., 2025b) describe extreme events that are not representative of the wind climate experienced in the Netherlands. The Dutch building code (*NEN-EN 1991-1-4+A1+C2/NB+C2*, 1991) and the wind-tunnel reference values reported by (Geurts et al., 2004) provide locally calibrated basic wind speeds in the range of 25 to 30 m/s, but these correspond to design-level values intended for structural verification rather than to thresholds at which façade resilience begins to degrade.

For this thesis, the wind hazard is defined using the threshold reported by (Fonseca Cerda et al., 2025), whose study empirically links observed windstorm losses across the Netherlands to meteorological wind-speed data. Rather than deriving thresholds from structural design assumptions or from extreme-event categories, the authors analyze a large body of reported damage events — drawn from insurance claims and recorded property losses across Dutch buildings — and identify the wind-speed ranges at which losses begin to occur and at which they become significant. From this empirical linkage between actual damage observations and meteorological records, the authors identify a baseline damage threshold of 15 m/s and a significant loss threshold of 22 m/s for the Dutch wind climate.

The 15 m/s baseline value is adopted as the principal wind-hazard input for this study because it represents the wind speed at which façade damage begins to be observed in practice within the Dutch context, rather than the speed at which structural failure occurs under design-level loading. This empirical grounding makes the threshold well-suited to a resilience-oriented analysis whose aim is to capture the onset and propagation of damage rather than the structural collapse limit, and it ensures that the hazard input is consistent with the climatic and building-stock context of the Amsterdam demonstrator (Section 3.1). The 22 m/s significant-loss threshold is retained as a reference upper bound for the discussion of results.

Wind Pressure Calculation

The wind pressure demand on the façade is computed in two steps: the determination of the peak velocity pressure q_p from the Dutch national annex, and the multiplication of q_p by the Eddy3D-derived pressure coefficient on the relevant surface.

The peak velocity pressure q_p is read from Table NB.5 of (*NEN-EN 1991-1-4+A1+C2/NB+C2*, 1991), which tabulates values of q_p as a function of the wind zone (1, 2, or 3), the terrain category (0 — coastal,

1 — open countryside, 2 — built-up area), and the height above grade. The component evaluates q_p at the height *h = floor_number × floor_height*, applying linear interpolation between the tabulated heights. The selected height therefore corresponds to the floor being simulated, which allows the resilience score to be computed floor-by-floor and compared across the building.

The net pressure demand on the wall on each orientation *i ∈ {N, E, S, W}* is then evaluated as

$$w_{\mathrm{wall},i} = q_p \cdot | C_{p,i} |$$

where $C_{p,i}$ is the area-weighted mean pressure coefficient on façade *i* obtained from the Eddy3D RANS simulation. Internal pressure is assumed to be zero (C_{pi} *= 0*), consistent with the sealed-façade assumption appropriate to the modern curtain-wall construction of the demonstrator. Multiplying the mean Cp obtained from the RANS simulation by the peak velocity pressure produces a conservative estimate of the wall demand, which is explicitly retained as a design-safety margin. The face with the highest absolute demand is identified as the governing wall orientation.

Shading Element Demand

The shading element demand is computed analogously to the wall demand, using the Eddy3D pressure coefficient on the overhang surface:

$$w_{\mathrm{shad},i} = q_p \cdot | C_{p,\mathrm{shad},i} |$$

A limitation of the current implementation is that the Eddy3D model captures the pressure coefficient on a single surface of the overhang. The geometry of the shading element is represented with zero thickness in the Honeybee model, so the sheltered underside of the overhang is not separately probed. The single-surface Cp therefore approximates the net force on the element from above only, which is a lower-bound estimate of the true net demand acting on the cantilevered shading. The component is structured to allow a straightforward upgrade in future work: when both the top and bottom Cp distributions are available, the demand expression becomes

$$w_{\mathrm{shad},i} = q_p \cdot | C_{p,\mathrm{top},i} - C_{p,\mathrm{bot},i} |$$

The face with the highest absolute shading demand is recorded as the governing shading orientation. The shading overhang depth itself is retained as a reference input but does not directly enter the demand computation, as the geometric effect of overhang depth is already embedded in the Eddy3D Cp values.

Glazing Capacity

The Capacity of the wall glazing is determined in accordance with NEN-EN 16612:2019 Glass in building: Determination of the lateral load resistance of glass panes by calculation. This standard provides a complete method to compute the design bending strength of a glass pane and through geometrically nonlinear plate bending theory, the maximum wind pressure a panel of given dimensions and thickness can sustain before the design bending strength is exceeded.

Design Bending Strength

The design bending strength $f_{g;d}$ is the maximum allowable tensile bending stress in the glass surface under design loading conditions. It incorporates the characteristic glass strength, material partial safety factors, and modification factors for load duration, surface condition, and edge stress.

For annealed glass, the equation is taken from formula 4 of (NEN-EN 16612, 2019):

$$f_{g;d} = \frac{k_e \cdot k_{mod} \cdot k_{sp} \cdot f_{g;k}}{\gamma M; A} \quad [N/mm^2]$$

For prestressed glass such as thermally toughened or heat-strengthened is taken from formula 6 of (NEN-EN 16612, 2019):

$$f_{g;d} = \frac{k_{mod} \cdot k_{sp} \cdot f_{g;k}}{\gamma M; A} + \frac{k_v \cdot (f_{b;k} - f_{g;k})}{\gamma M; v} \quad [N/mm^2]$$

The second term in Equation above represents the additional strength contribution from the compressive surface prestress induced during the toughening or heat-strengthening process. The parameters are assigned as follows:

Table 4. Glazing Design Bending Strength Parameters (Various Sources)

Parameter	Symbol	Value	Source
Characteristic bending strength, Annealed Glass	$f_{g;k}$	45 N/mm^2	NEN-EN 572-1
Material partial factor, annealed glass	$\gamma M; A$	1.8	Table 1, NEN-EN 16612:2019
Material partial factor, surface prestress	$\gamma M; v$	1.2	Table 1, NEN-EN 16612:2019
Surface profile factor, float glass as-produced	k_{sp}	1.0	Table 4, NEN-EN 16612:2019
Edge strength factor,all four edges supported	k_e	1.0	Section 8.1.2, NEN-EN 16612:2019
Load duration factor, wind gust < 5 s	k_{mod}	1.0	Table 5, NEN-EN 16612:2019
Characteristic bending strength, toughened	$f_{b;k}$	120 N/mm^2	Table 6, NEN-EN 16612:2019
Characteristic bending strength, heat-strengthened	$f_{b;k}$	70 N/mm^2	Table 6, NEN-EN 16612:2019
Strengthening factor, horizontal toughening	k_v	1.0	Table 7, NEN-EN 16612:2019
Strengthening factor, vertical toughening	k_v	0.6	Table 7, NEN-EN 16612:2019

Plate Bending Theory

The relationship between applied wind pressure and maximum bending stress in the glass panel is governed by plate bending theory. For a rectangular glass pane simply supported on all four edges and subjected to a uniform lateral pressure, the maximum tensile bending stress occurs at the center of the panel.

Annex B of NEN-EN 16612:2019 provides calculation formula or both geometrically linear and nonlinear plate bending. In the linear case, which is adopted here as a conservative approximation appropriate for early-stage design, the maximum stress is:

$$\sigma_{max} = k_1 \cdot \frac{a^2}{h^2} \cdot F_d \quad [N/mm^2]$$

Where:
a = the shorter panel dimension $[m]$
h = the glass thickness $[m]$
F_d = the applied wind pressure $[Pa = N/m^2]$
k_1 = the dimensionless stress coefficient dependent on aspect ratio $\lambda = a/b$

The capacity is determined by rearranging this expression for F_d at the limit σ_{max} = $f_{g;d}$:

$$C_{wall,i} = \frac{f_{g;d} \cdot h^2}{k_1 \cdot a^2} \quad [Pa]$$

The deflection under wind pressure is given by Formula B.2 of NEN-EN 16612:2019:

$$w_{max} = k_4 \cdot \frac{a^4}{h^3} \cdot \frac{F_d}{E} \quad [m]$$

Where $E = 70{,}000\ N/mm^2$ is the Young's modulus of glass (Section 6.2, NEN-EN 16612:2019).

Stress and Deflection Coefficients

The coefficients k_1 and k_4 are taken from Tables B.1 and B.2 of Annex B, NEN-EN 16612:2019, evaluated at p*=0 (linear plate bending theory). They depend on the panel aspect ratio $\lambda = a/b$, where a is always shorter dimension, giving $\lambda \leq 1.0$:

Table 5. Coefficient k1 and k4 for calculation of the maximum stress (NEN 16612, 2019)

$\lambda = a/b,$	$k_1(p* = 0)$	$k_4(p* = 0)$
0.1	0.750	0.1480
0.2	0.747	0.1474
0.3	0.724	0.1421
0.4	0.671	0.1303
0.5	0.600	0.1148

0.6	0.524	0.0984
0.7	0.449	0.0826
0.8	0.380	0.0683
0.9	0.319	0.0559
1.0	0.268	0.0461

Linear interpolation is applied between tabulated values. k_1 decreases as λ increases toward 1.0, meaning that square panels experience lower stress than elongated panels of the same shorter dimension due to the evenly distributed load in both directions.

Panel Capacity

The panel capacity F_{cap} is computed per orientation because each orientation may have a different WWR, which produces different panel dimensions through the window geometry derivation described in section 4.2.1. The following steps are performed for each of the four orientations:

1. Compute the glazing area per floor per window using the WWR, façade width, floor height, and the number of windows per floor.
2. Derive the window width from glazing area and fixed window height.
3. Set $a = min(h_{win}, w_{win}), \quad b = max(h_{win}, w_{win})$ per Annex B convention
4. Compute the aspect ratio $\lambda = a/b$ and interpolate k_1 and k_4 from Table. 15.
5. Compute F_{cap} using the equation:

$$F_{cap} = \frac{f_{g;d} \cdot h^2}{k_1 \cdot a^2} \quad [Pa]$$

The governing wall face for the fragility assessment is the orientation with the highest demand-to-capacity ratio D/C, not the orientation with the highest absolute demand:

$$\text{gov_face} = \arg\max \text{ f} \in \{\text{N}, \text{S}, \text{E}, \text{W}\} \left(\frac{w_{net,f}}{F_{cap,f}} \right) \qquad \text{(X.X)}$$

This is an important distinction since a face with high demand but also high capacity (small panels from low WWR) may have a lower D/C ratio than a face with moderate demand but very low capacity (large panels from high WWR). The governing face correctly identifies the weakest link in the glazing system.

A direct consequence of this approach is that WWR affects wind resilience through the capacity pathway. Higher WWR produces larger glazing panels, which have lower capacity because capacity scales with the inverse square of the panel dimension a. This creates a genuine design trade-off: higher WWR improves daylight availability and may improve thermal performance, but simultaneously reduces glazing capacity and lowers R-wind. This trade-off is one of the central tensions in the multi-objective fitness landscape of this research.

Deflection Limit Check

As a secondary verification, the maximum deflection under the design wind pressure demand is checked against the limit prescribed in Section 9.1.4 of NEN-EN 16612:2019. In the absence of a specific requirement, deflections are limited to:

$$w_{limit} = \min\left(\frac{a}{65}, 50\ mm\right)$$

Where a is the shorter panel dimension. The checking equation is:

$$w_{max} \leq w_{limit}$$

The deflection check is reported as a supplementary indicator. It does not directly enter the fragility calculation but provides a warning If the panel is excessively flexible under the design load.

Shading Element Capacity

The shading element capacity C_{shad} represents the design resistance of the bracket fixing system that connects the shading device to the building structure. Unlike glazing capacity, this value cannot be derived from NEN-EN 16612:2019, which covers only glass panes. Shading bracket resistance depends on product specific geometry, material, and fixing details that are outside the scope of any single general standard.

In the current implementation, C_{shad} is therefore a user-defined input in Pascals, representing the bracket design resistance as specified in the manufacturer's technical datasheet or determined through separate structural calculation. The user is responsible for selecting a value appropriate to the shading system under consideration.

Typical references values from façade engineering practice are:

Shading system Type	Typical C_{shad} [Pa]
Lightweight aluminum louvre, small projection (≤0.3 m)	1000 - 2000
Medium aluminum fin, projection 0.5 – 1.0 m	600 – 1200
Deep horizontal canopy, projection 1.0 – 2.0 m	300 – 700
Heavy steel bracket system	1300 - 3500

This is acknowledged as a limitation of the current framework. Future development could integrate bracket resistance calculations based on cantilever bending theory, replacing the user input with a computed value derived from bracket geometry and material specification.

Demand-Capacity Fragility Model

A deterministic demand-capacity check of the form D/C ≤ 1.0 produces a binary outcome, the element either passes or fails at the nominal design level. While this is sufficient for code-compliance verification, it is inadequate for resilience assessment, which requires understanding of how performance degrades

continuously as loading increases beyond the nominal design level and how uncertainty in both demand and capacity affects the likelihood of failure.

Both wind demand and element capacity are subject to uncertainty. Wind pressure varies from the deterministic design value due to turbulence, gusting, and the inherent variability of meteorological events. Glass strength varies from panel to panel due to the statistical distribution of surface flaws. Bracket resistance varies due to manufacturing tolerances and installation quality. A probabilistic approach captures these uncertainties explicitly through a dispersion parameter and produces a continuous resilience metric that can be compared meaningfully across design variants.

The FEMA P-58 Fragility Function

The probability of failure of a structural component under a given demand level is expressed using a lognormal fragility function, following the performance-based engineering framework established in FEMA P-58 and the methodology of (FEMA P-58-1, 2018). The fragility function takes the form:

$$F_i(D) = \Phi\left(\frac{ln(D/\theta_i)}{\beta_i}\right)$$

Where:

D is the wind pressure demand [Pa]
θ_i is the median capacity, the demand level at which the probability of failure equals exactly 50%
β_i is the logarithmic standard deviation, also called the dispersion parameter
Φ is the standard normal CDF

The fragility function produces an S-shaped curve rising from 0 to 1 as demand increases. At $D = 0$, P_{fail} approaches zero. At $D = \theta_i$, $P_{fail} = \Phi(0) = 0.5$. at $D > \theta_i$, P_{fail} approaches 1.0. The dispersion parameter β controls the steepness. Small β gives a steep transition, large β gives a gradual slope.

In the full FEMA P-58 framework, θ_i and β_i are determined from physical fragility testing of many specimens. The total dispersion combines three components:

$$\beta_{total} = \sqrt{\beta_{DR}^2 + \beta_{DS}^2 + \beta_C^2}$$

Where β_{DR} reflects component-to-component variability, β_{DS} reflects uncertainty in the damage state definition, and β_C reflect modelling uncertainty.

Analytical Fragility Approach

The present implementation adopts an analytical fragility approach, which is a recognized alternative when component-level test data is unavailable. Experimentally calibrated pressure-based fragility functions for glass panels do exist in literature, notably the normally distributed functions derived from the experimental data of (Behr et al., 1991), with mean capacities of 5.29 kPa and 11.37 kPa for inner and outer panels of insulating glass units respectively. However, these functions cannot be directly applied in the present study for three reasons: they are calibrated for insulating glass units rather than the monolithic panels modelled here; the demand parameter P-60 (60-second equivalent pressure) is not directly comparable to the peak gust pressure q_p from NEN-EN 1991-1-4; and the mean capacity

values are substantially higher than the capacities computed for the panel geometries in the parametric design space. The analytical approach is therefore the most appropriate method for this application.

In the analytical approach, the median capacity θ_i is taken equal to the deterministic design capacity C:

$$\theta_i = C$$

The fragility function becomes:

$$P_{fail} = \Phi\left(\frac{ln(D/C)}{\beta}\right)$$

This substitution is conservative: because C from NEN-EN 16612:2019 already incorporates $\gamma M; A$, the actual median failure pressure of physical panels is likely higher than C. The fragility curves therefore overpredict the failure probability relative to experimentally calibrated curves. For the comparative purpose of ranking design variants in a fitness landscape, this conservatism is consistent across all options and the relative ordering is preserved.

The dispersion parameter β is set by the user and reflects combined uncertainty in wind demand modelling, glass strength variability, and capacity calculation simplifications. A single β is applied to both façade elements.

Two Fragility Curves

The framework generates two independent fragility curves, one for the wall glazing and one for the shading element, plotted together on a single chart.
Wall glazing fragility:

$$P_{fail,wall} = \Phi\left(\frac{ln(w_{wall,max}/F_{cap})}{\beta}\right)$$

Where $w_{wall,max}$ is the net wall pressure at the governing orientation (highest D/C ratio).
Shading element fragility:

$$P_{fail,shad} = \Phi\left(\frac{ln(w_{shad,max}/C_{shad})}{\beta}\right)$$

Where $w_{shad,max}$ is the maximum average shading demand across all four orientations.

Both curves rise from 0% at zero demand to 100% at a very high demand. The 50% crossover point coincides with the respective element capacity. The horizontal position of the two curves reveals which element is more vulnerable, the curve crossing 50% at a lower pressure is the more critical element.

Interactive Hazard Intensity Slider

The HTML visualization includes an interactive slider that moves a vertical reference line across the fragility chart. As the slider is moved, four readout values update in real time. $P_{fail,wall}$, $P_{fail,shad}$, $P_{fail,system}$, and R_{wind} at the selected pressure level. This allows exploration of performance across the full range from zero demand to three times the design pressure. Four fixed vertical reference lines are also drawn: slider position (black dashed), design demand (red dashed) wall capacity (blue dashed), and shading capacity (orange dashed).

System Fragility

The façade system fails if either the wall glazing or the shading element fails. A series reliability model. Assuming statistical independence between the two failure modes:

$$P_{fail,system} = 1 - (1 - P_{fail,wall}) \cdot (1 - P_{fail,shad})$$

The system wind resilience score is:

$$R_{wind} = 1 - P_{fail,system}$$

R_{wind} is bounded between 0 and 1 and enters the multi-objective fitness landscape alongside $R_{thermal}$

Governing Element

The governing element is the one with the higher demand-to-capacity ratio:

$$governing = \begin{cases} shading & if\ (D/C)_{shad} \geq (D/C)_{wall} \\ glazing & if\ (D/C)_{wall} > (D/C)_{shad} \end{cases}$$

The governing element indicates where design effort should be focused to most efficiently improve the R_{wind}. However both elements always contribute to R_{wind} simultaneously through the series system formula.

2.2.6 Multi-Objective Optimization

General Concept

Most real engineering problems involve more than one criterion that the designer wants to optimise at the same time, and these criteria are frequently in conflict. In the field of building and façade design, energy demand, thermal comfort, daylight provision, structural capacity, and cost rarely move in the same direction when a design variable is changed: improving one often degrades another (Alsukkar et al., 2026; Duan et al., 2026). When several objectives must be optimised simultaneously, the problem is referred to as a multi-objective optimisation problem (Sayyaadi, 2021).

A multi-objective optimisation problem can be expressed in the general form (Sayyaadi, 2021):

$$Minimize/Maximize f_m(X); m = 1,2,\dots,M$$
$$s.t.:$$
$$g_j(X) \leq 0; j = 1,2,\dots,J$$
$$h_k(X) = 0; k = 1,2,\dots,K$$
$$X = [x_1\, x_2 \dots x_n]^T$$

A single combination of decision variables can almost never optimise all objectives at the same time, and the result of the optimisation is therefore not a unique optimum but a set of compromise solutions that represent the best achievable trade-offs in the objective-function space (Sayyaadi, 2021).

To compare candidate solutions in a multi-dimensional objective space, the concept of *dominance* is introduced. A solution D is said to dominate a solution S if it is at least as good as S in all objectives and strictly better in at least one. The set of solutions that are not dominated by any other in the feasible region forms the **Pareto optimal front**, on which all members are mutually non-dominated and therefore equivalent from an optimisation perspective: moving along the front improves one objective at the expense of another (Sayyaadi, 2021). The Pareto front is the natural output of a multi-objective optimisation, because it visualises the design trade-offs explicitly and allows the decision maker to select a final solution on the basis of secondary criteria once the trade-off boundary is known.

Among the metaheuristic methods that can return the full Pareto front in a single run of the algorithm, the Non-dominated Sorting Genetic Algorithm II (NSGA-II) is the most widely used in energy- and building-related applications (Caieiro Da Costa et al., 2026; Duan et al., 2026; Omidian & Khaji, 2022; Sayyaadi, 2021). At each generation, NSGA-II sorts the population into successive non-dominated layers based on the Pareto-dominance criterion, assigns each individual a rank equal to its layer number and a crowding distance that measures its isolation from neighbours along the same layer, and uses both quantities in a tournament selection that drives the genetic operations toward solutions of low rank and well-spread distribution (Sayyaadi, 2021). The algorithm terminates once a maximum number of generations or a stagnation criterion is reached.

Multi-objective optimization in building and façade design

Multi-objective optimisation has become an established tool in building-performance research, in particular when conflicting performance metrics or hazard responses need to be balanced from the earliest design stages.

In the thermal and energy domain, (Caieiro Da Costa et al., 2026) used NSGA-II to enhance the thermal resilience of a multifamily housing typology in São Paulo under historical and projected heatwave conditions, simultaneously minimising the cooling load and the maximum operative temperature while constraining the recovery time. (Alsukkar et al., 2026) reviewed the use of multi-objective optimisation for daylighting and shading systems and reported that NSGA-II combined with Pareto-frontier analysis can balance energy savings, glare reduction, and thermal-visual comfort metrics that would otherwise be impossible to satisfy individually. (Duan et al., 2026) applied NSGA-II together with machine-learning surrogates to optimise window and PV-louver geometry on south-facing office façades in cold regions, generating 193 Pareto-optimal solutions that simultaneously improve useful daylight illuminance, net energy use intensity, and thermal discomfort percentage.

In the structural and seismic domain, (Omidian & Khaji, 2022) used NSGA-II to select retrofit patterns for typical reinforced-concrete buildings, optimising simultaneously the seismic resilience index and the cost of retrofit, and reported that the Pareto-optimal solutions allow decision makers to choose retrofit strategies that achieve a target resilience level at minimum cost.

In the multi-hazard and community-resilience domain, (Gupta et al., 2024) proposed a multi-objective optimisation model to determine optimal building-retrofitting strategies for the community of Seaside, Oregon, under combined earthquake and tsunami hazards, reducing overall economic loss, population dislocation, and building repair times in a single framework. (Javanroodi et al., 2020) used a multi-objective framework to design climate-resilient building forms in urban areas, simultaneously optimising the energy performance and the thermal comfort across three thirty-year climate projection periods, reporting up to 34 % improvement in energy performance. In the urban microclimate and pedestrian-comfort domain, (Guo et al., 2026) combined CFD simulation, surrogate modelling, and a human-AI collaborative optimisation workflow to improve the pedestrian-level wind environment around football stadiums in high-density urban blocks, achieving up to 38 % improvement in wind-environment quality without reducing land-use efficiency. (Abdallah et al., 2025) used a multi-objective optimisation method to enhance outdoor environmental quality in university courtyards in hot arid climates, jointly optimising thermal comfort (UTCI), CO2 concentration, and wind velocity.

Taken together, these studies illustrate that multi-objective optimisation has evolved into a generative design instrument across a range of building-performance domains, from façade components to building forms and to the wider urban microclimate. Façade design specifically has been identified as a discipline in which a paradigm shift is needed: rather than designing on the basis of historical climate data and treating performance as a verification step, façade systems must be designed for uncertainty and change, and they must do so while balancing multiple competing demands placed on the building envelope by climate change, occupant comfort, and structural integrity (Patterson, 2022). Multi-objective optimisation provides the technical means to support this paradigm shift, because it converts performance trade-offs from after-the-fact diagnoses into design objectives that actively shape the geometry and material composition of the envelope.

3 Case Study

3.1 Building Selection

The case study selected for this thesis is De Centrale IJburg, a residential redevelopment located in Block 30 of the IJburg district in Amsterdam, the Netherlands. The project is led by a developer-investor Midvast and designed by VURB Architects, with construction planned between late 2021 and early 2023. The site occupied the footprint of the former KPN telecommunications central exchange building. The building has a footprint of approximately 32 x 20 m and a height of approximately 20 m (Figure 3).

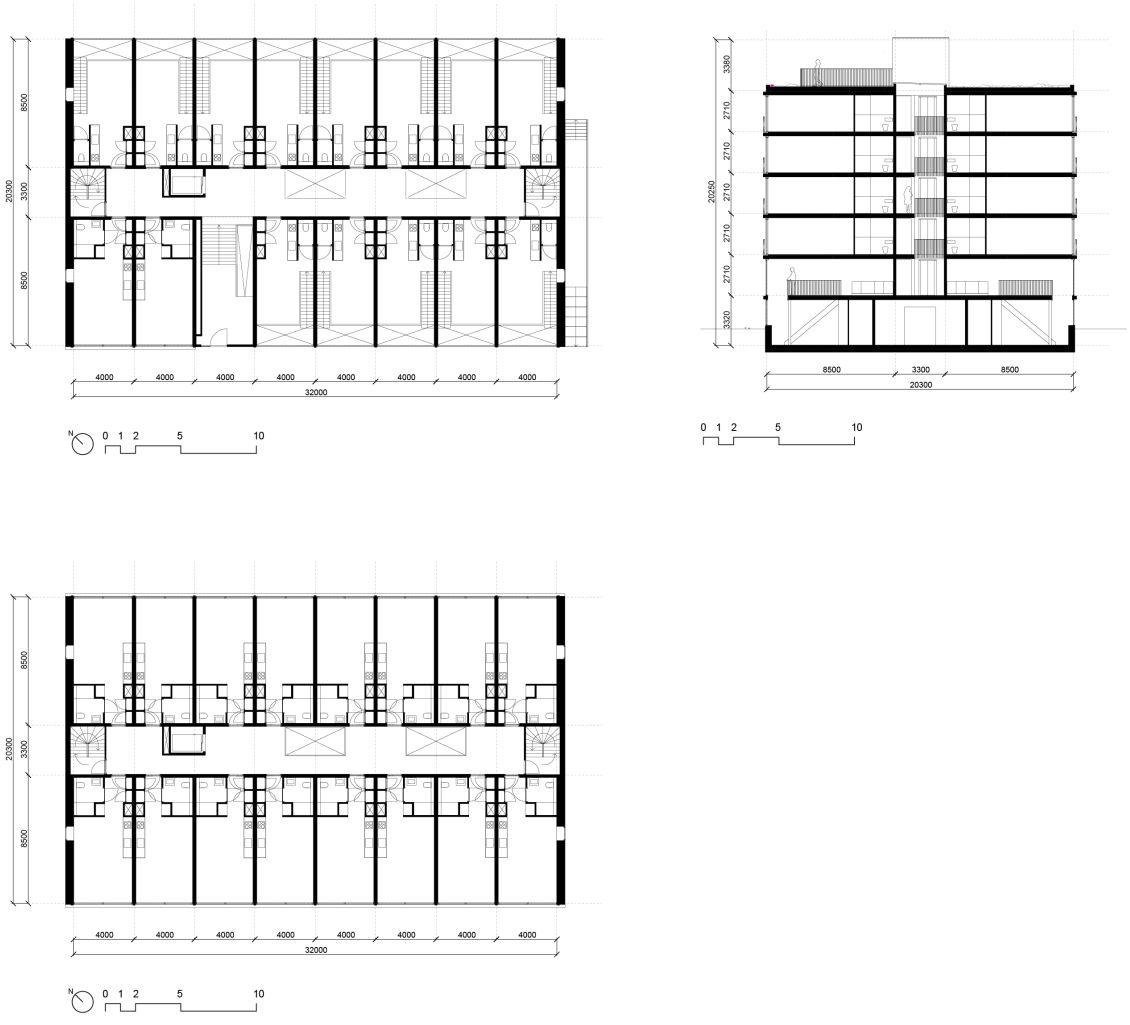

Figure 3. De Centrale IJburg Floor Plan and Section (vurbarchitects, 2020)

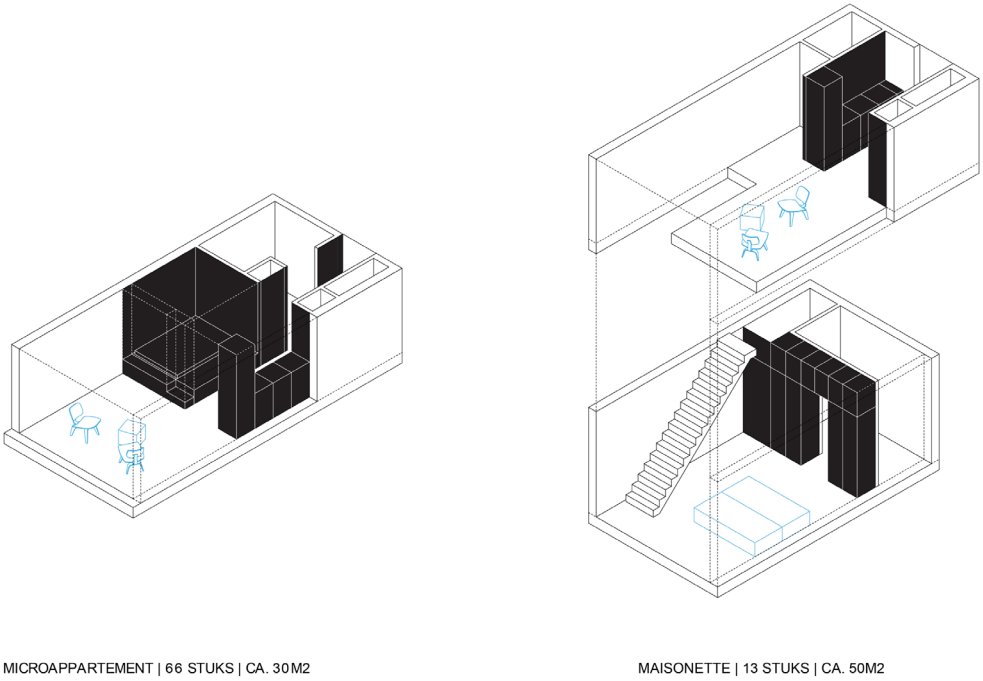

Figure 4. Type of apartments in De Centrale IJburg (vurbarchitects, 2020)

The redeveloped building accommodates 79 serviced rental apartments in two typologies (Figure 4): 66 micro-studies of approximately 30 m² for one person and 13 maisonette apartments of approximately 50 m² for up to two person. The target user group consists of expatriates and international professionals based in Amsterdam on short-stay contracts of minimum seven nights to six months. Collective spaces include a main entrance and a lobby, a central atrium connecting the floors vertically, a shared roof terrace, and a ground-level inner courtyard with a communal vegetable garden. The souterrain accommodates bicycle parking and a technical service spaces. The building sits within a mixed-use urban block that also includes the Olympus primary school, the Partou after-school care facility, sports facilities, and a public picnic space.

De Centrale IJburg was selected as the case study for this thesis because it serves as the Netherlands demonstration site of the MULTICARE (Horizon Europe grant agreement no. 101123467), a European research and innovation project that develops a multi-criteria decision-making framework for resilient and low-carbon façade systems. MULTICARE addresses the growing exposure of the building stock to climate-change-driven hazards — including heatwaves, heavy rainfalls, strong winds, and seismic activity — through modular, hazard-proof, and reversible façade technologies. The project is demonstrated in three European countries (Italy, the Netherlands, and Romania) with the Maria Austriastraat building representing the Dutch context.

3.2 Façade Parameter Space

The façade parameter space defined for this thesis is structured to capture the geometric and material choices that strongly influence both thermal and wind resilience, while remaining compact enough to support dataset generation and surrogate-model training. The parameter space is layered on top of the MULTICARE base envelope specified for the Amsterdam demonstrator — a prefabricated composite system combining cross-laminated timber (CLT) panels with a standardized unitized profile, mineral-

wool insulation, a ventilated cavity, and an outer cladding layer. The opaque construction, insulation specification, frame profile, and overall panel modulation defined by MULTICARE work package 11 are treated as a fixed boundary conditions throughout the parametric analysis. The variable parameters operate only on those façade attributes that a designer would tune when adapting the MULTICARE system to a specific site, orientation, and climatic exposure.

In total, eleven independent design variables describe the parametric façade. They are organized into three groups: orientation specific aperture ratios, orientation specific shading depths, and building-wide window and glass parameters.

The first group, aperture ratios, defines the window-to-wall ratio on each of the four cardinal orientations (north, east, south, west) independently. Orientation-specific treatment is essential because thermal and wind resilience both behave asymmetrically with respect to orientation: solar gains differ strongly between south and north exposures, while wind pressure coefficients vary with prevailing wind direction and façade exposure. Allowing each orientation to vary independently exposes the workflow to the full asymmetry of the design space rather than collapsing it into a single global ratio.

The second group, shading depths, defines the projection length of a continuous external horizontal overhang above the glazing on each of the four cardinal orientations independently. The same orientation argument applies: deeper southern shading is typically beneficial for overheating mitigation, while east and west orientations require different shading strategies to address low-angle solar radiation. From a wind perspective, the depth of a horizontal projection governs both the wind load that the element itself must resist and the leverage it exerts on its fixings under extreme conditions — both of which are relevant to the MULTICARE design intent of producing hazard-proof and reversible façade components.

The third group consists of building-wide window and glass parameters that act on the window unit itself withing each window panel. The horizontal separation ratio controls the relative width of solid wall between adjacent window panels along the façade, determining whether the glazing reads as a continuous ribbon or as a discrete openings. The window height ratio controls the vertical proportion of the glazed area within each storey, given the fixed 2.7 m floor-to-ceiling height of the demonstrator. Together these two parameters describe the subdivision of the glazed surface and affect both thermal performance and wind performance. The glass thickness parameter selects between 3 mm and 6 mm of the outer layer of an Insulated Glass Unit (IGU), primarily influencing wind resilience through resistance to wind-borne debris impact and pressure-induced bending, with a secondary effect on the thermal U-value of the glazing unit.

The parameter set is intentionally orientation-aware for the dominant geometric variables (aperture and shading) while keeping window subdivision and glass specification consistent across the building. The parametric space therefore probes the most influential and design-controlled dimensions of resilience performance, while remaining fully compatible with the base assembly and its modular construction logic.

3.3 Design Variable Ranges

The eleven design variables defined in Section 3.2 and their sampling ranges are summarized in Table 6. The ranges have been selected to encompass the architecturally realistic span of choices that a designer would consider when configuring the façade system on a mid-rise residential building of this typology.

Table 6. Independent Variables used in the study (Author)

Group	Variable	Symbol	Range	Units
Aperture Ratio	North	aperture_N	0.1 – 0.9	-
	East	aperture_E	0.1 – 0.9	-
	South	aperture_S	0.1 – 0.9	-
	West	aperture_W	0.1 – 0.9	-
Shading Depth	North	shading_N	0.1 – 1.0	m
	East	shading_E	0.1 – 1.0	m
	South	shading_S	0.1 – 1.0	m
	West	shading_W	0.1 – 1.0	m
Window subdivision	Horizontal Separation Ratio	horiz_separ_ratio	0.2 – 1.0	-
	Window Height Ratio	window_height_ratio	0.2 – 1.0	-
Glazing	Glass Thickness (discrete: 3 mm or 6 mm)	glass_thickness	1-2	Index

The aperture ratio range of 0.1 to 0.9 were selected to span the full architecturally meaningful design space rather than to reflect a specific construction constraint. For dataset generation, a wide range is desirable because it produces a more uniformly distributed set of training samples, which in turn improves the generalization capacity and predictive accuracy of the surrogate model trained on the resulting data. A narrower range would over-represent typical contemporary practice and reduce the model's ability to capture non-linear behaviour at the extremes. The lower bound of 0.1 was adopted at the author's discretion to reflect the minimum aperture below which a habitable space would no longer receive adequate natural light for residential use. While Dutch building regulations do not specify a single numerical minimum for the window-to-wall ratio, the value of 0.1 was selected as a practical architectural floor that keeps the sampled configurations within the range of plausibly habitable residential dwellings and that simultaneously provides a useful sampling boundary for the surrogate model.

The shading depth range of 0.1 to 1.0 m reflects the realistic projection length of an external horizontal overhang at a storey level for a mid-rise residential building. Shorter projections of 0.1 m approximate near-flush or decorative shading elements, while the upper bound of 1.0 m is selected because it corresponds to the typical depth of balconies and continuous horizontal overhangs commonly found on mid-rise apartment buildings. Deeper projections would move the element into territory more

characteristic of loggias or terraces, which carry different structural, occupancy, and detailing implications and therefore fall outside the scope of this study.

The horizontal separation ratio and window height ratio are both rounded between 0.2 and 1.0 to describe the geometric subdivision of the glazed area along the façade. A value of 1.0 corresponds to continuous glazing in the relevant dimension, while a value of 0.2 corresponds to strongly subdivided, punched-opening configurations. Given the demonstrator's 2.7 m floor-to-ceiling height, the window height ratio operates over a practical glazed-surface range of approximately 0.54 to 2.7 m per storey.

The glass thickness parameter refers specifically to the outer pane of an insulating glazing unit (IGU), as the window of the demonstrator are configured as double-glazing assemblies. The variable is treated as a discrete two-level variable indexed by the values 1 and 2, corresponding to the monolithic outer panes of 3 mm and 6 mm respectively. The choice of these two thicknesses is motivated by (Behr et al., 1991) Which provide validated probability-of-failure relationships for outer and inner glass panes. The variable therefore captures the practical resilience-relevant decision faced by a designer choosing between a thinner, cheaper, lighter outer pane and a thicker, more debris-resistant alternative.

3.4 Latin Hypercube Sampling

The eleven-dimensional design spaced defined in 3.3 is sampled using Latin Hypercube Sampling (LHS) to generate the dataset that supports the descriptive statistical analysis, surrogate-model training, and multi-objective optimization presented in the subsequent chapters. The whole workflow can be seen in Figure 5. LHS is selected over simple random sampling because it ensures that each variable's range is stratified into equiprobable intervals and that exactly one sample is drawn from each interval. This produces a space-filling design that achieves better coverage of high-dimensional spaces with fewer samples than a random or grid-based approaches, which is a critical property given the computational cost of the underlying thermal and wind simulations.

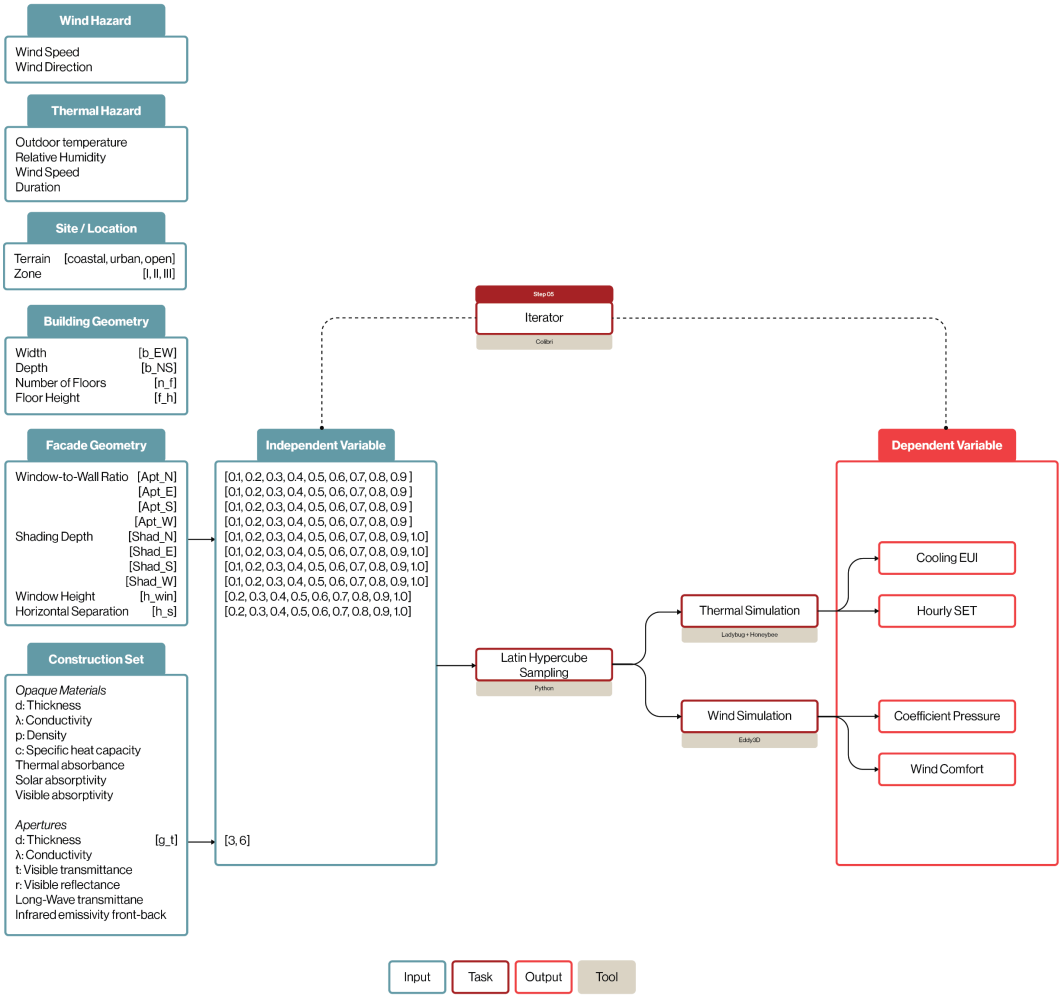

Figure 5. Dataset Generation Workflow (Author)

The continuous variables — the four aperture ratios, the four shading depths, the horizontal separation ratio, and the window height ratio — are sampled directly over their respective bounded ranges defined in the Table 3. The glass thickness variable, although technically discrete with only two admissible values (3 mm and 6 mm), is sampled in a continuous form as a slider index between 1.0 and 2.0 and subsequently snapped to the nearest discrete option before the simulation is run. This treatment allows the LHS algorithm to operate uniformly on a continuous hypercube, while preserving the discrete physical meaning of the variable in the simulation pipeline.

The sample size N is set to 500 design points. This value balances three competing considerations: the need for sufficient coverage of an eleven-dimensional space, the desire to obtain a dataset large enough to support stable surrogate-model training and validation, and the computational budget imposed by the per-sample simulation cost for both the thermal and wind simulation workflows described in the following chapter. A fixed random seed is used so that the sample set is reproducible across runs. The resulting sample matrix is exported from SALib in Python and passed to the Grasshopper parametric model, which generates a unique geometric configuration of the demonstrator's façade for each sample. Each configuration is then evaluated through the simulation workflows described in the following chapter.

4 Thermal Resilience Quantification

4.1 Thermal Simulation

4.1.1 Heatwave Identification

The heatwave definition used in this study is CTX90pct, developed by (Perkins & Alexander, 2013) that describes a heatwave as a period when the maximum daily temperature exceeds the 90th percentile for at least three consecutive days. Based on this definition and the location of the case study, an hourly climate observation from De Bilt, NL were used to identify the heatwave events. By using the historical weather data from 1901-2025 (NOAA, 2019), a graph of historical heatwave event is generated with a python script (Appendix B).

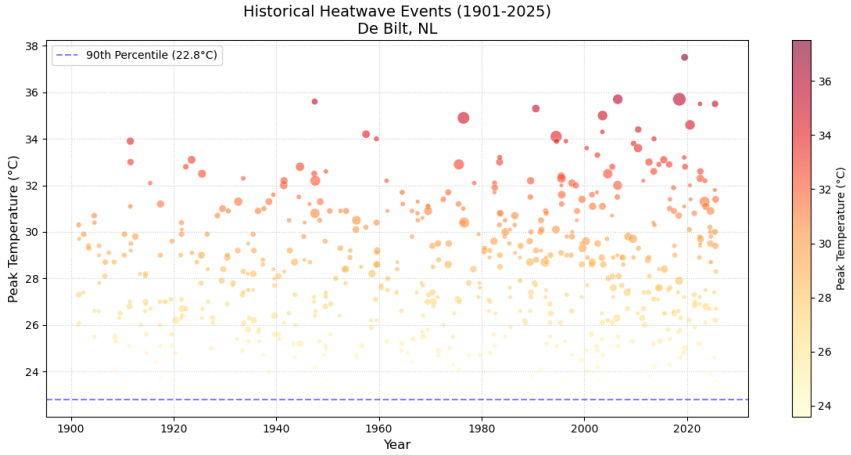

Figure 6. Historical Heatwave Events from 1901-2025 (Author)

It can be seen in Figure 5 that there are several heatwave events that has happened throughout the year, therefore, the most extreme one is selected as a use case in this study. The heatwave event that has occurred during 22-30th of July 2019 has the highest maximum daily temperature of 35.9°C. The hourly temperature can be seen in Figure 7, it is shown that using the 90th percentile - 23°C, a heatwave event occurs within more than three days with a peak of 35.9°C.

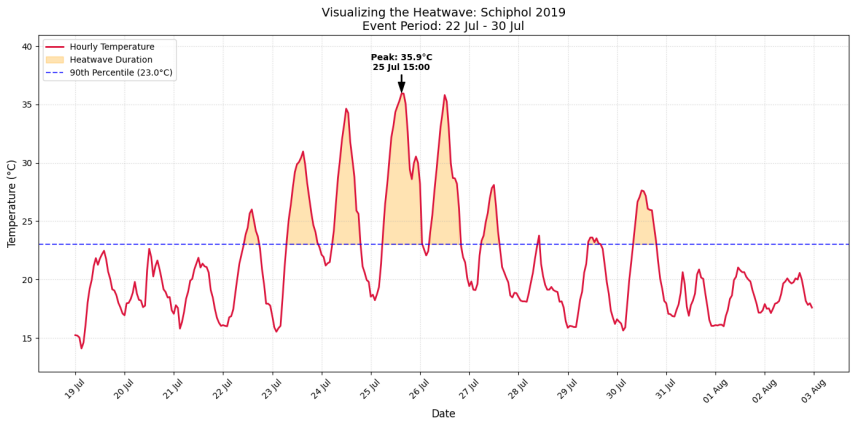

Figure 7. Most Intense Heatwave Recorded (Author)

4.1.2 Thermal Simulation Setup

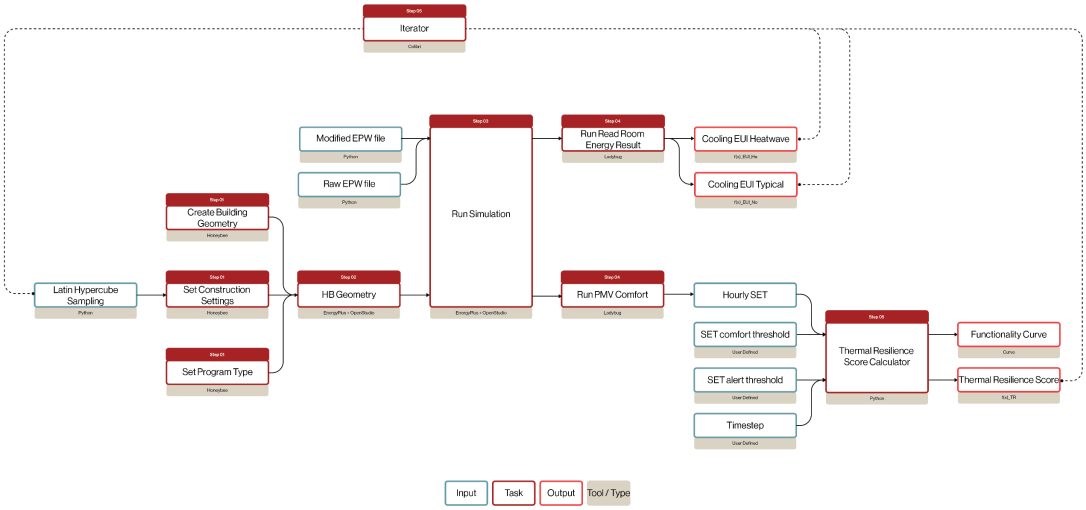

Figure 8. Graphical Representation of Thermal Simulation Workflow (Author)

The thermal simulation workflow is organized into five steps (Figure 8). The pipeline begins with the independent variable dataset generated through Latin Hypercube Sampling. In Step 1, this dataset is combined with the building geometry, construction settings, and program type, and the resulting configuration is passed into HB geometry. Two additional environmental inputs are introduced at this stage: the raw EPW file and a modified EPW file in which a heatwave event has been embedded. With these inputs in place, the model is ready to be executed using the EnergyPlus + OpenStudio plugin.

The simulation output is then fed into the next step. "Run Read Room Energy Result" produces two performance outputs: the cooling Energy-Use-Intensity (EUI) during the heatwave period and the cooling EUI during the typical period. "Run PMV Comfort", in parallel, requires further user-defined inputs, namely the SET comfort and alert thresholds, which are treated as context-dependent and therefore specified by the user rather than fixed. The final input to the workflow is the timestep, expressed in hours and typically set to 1. The final output are cooling EUI during heatwave, cooling EUI at typical, functionality curve, and thermal resilience score.

4.1.3 Example Use on Case Study

The developed workflow of the thermal simulation and thermal resilience quantification is put to the case study in this chapter. In Figure 9, it can be seen that it starts with modelling the basic geometry of the building, setting the program type, and then putting in the independent design parameters that was generated with the LHS sampling. In this example, the design parameters are shown in Table 7.

Table 7. Design Parameter of Selected Iteration

id	Apt_N	Apt_E	Apt_S	Apt_W	Sha_N	Sha_E	Sha_S	Sha_W	h_win	h_s	G_t
0	0.3	0.3	0.5	0.7	1	1	0.7	1	1	0.5	3

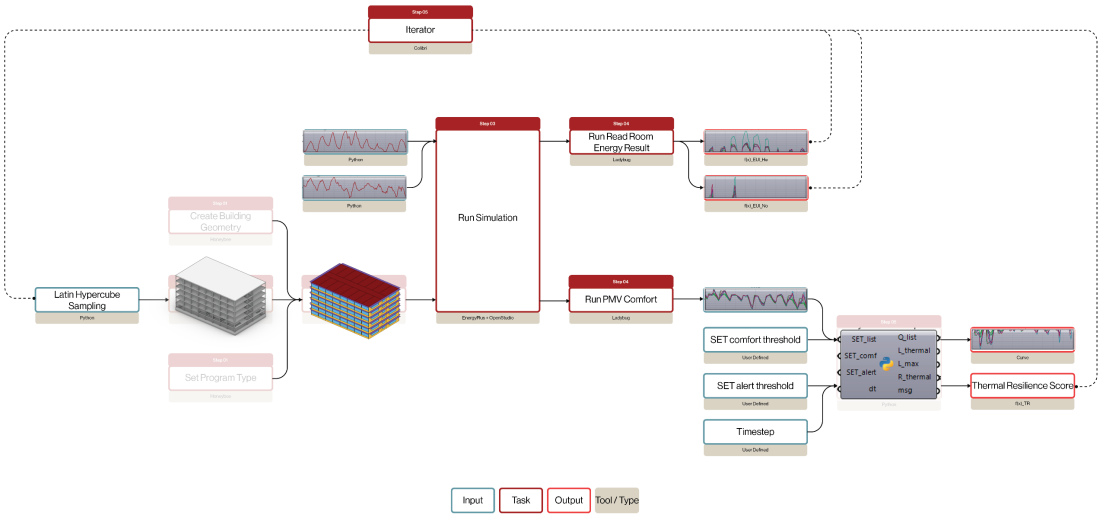

Figure 9. Thermal Resilience Workflow Application on Case Study (Author)

After running the simulation, there are four outputs. The first two are the cooling EUI during the heatwave with the modified EPW and the typical with a historical weather data. It can be seen that in Figure 10 the cooling rises up at certain time when the temperature inside the building increases. Meanwhile in Figure 11, the amount of peak is less compared to when the heatwave happens.

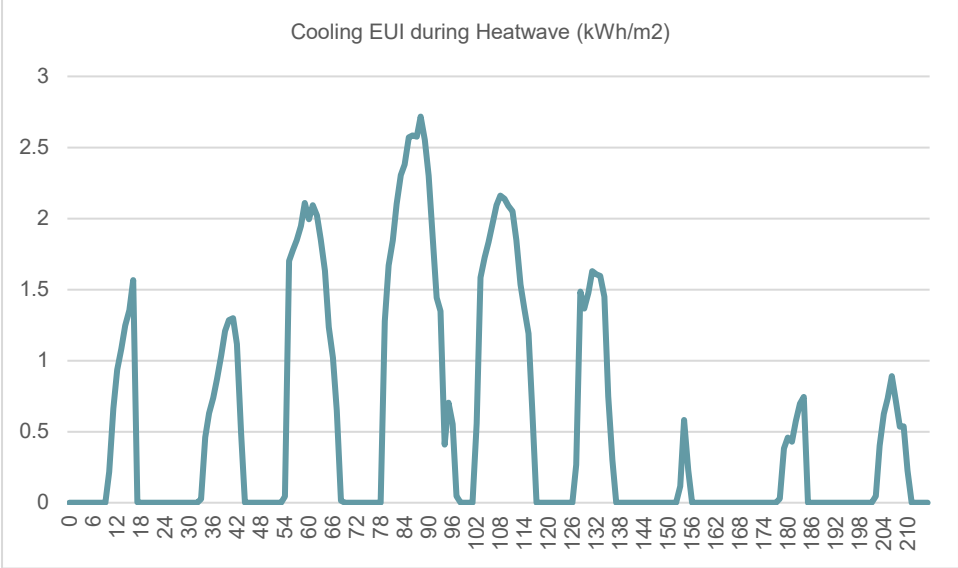

Figure 10. Cooling EUI during Heatwave (Author)

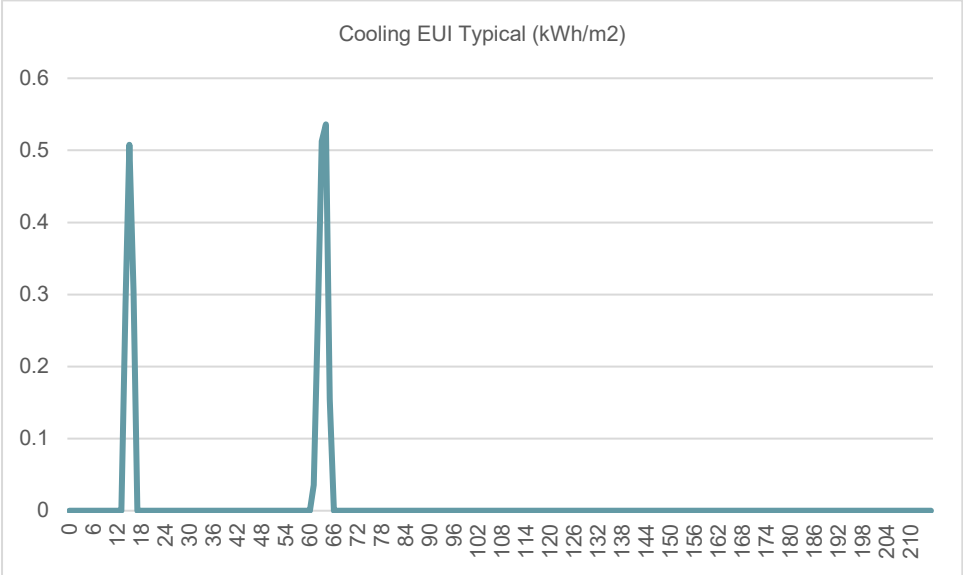

Figure 11. Cooling EUI Typical (Author)

The other two outputs are the SET during heatwave and the functionality curve. The SET in this case (Figure 12) has a peak of 23.9°C and a hit its lowest at 17.7°C. Every time it almost reaches the SET alert threshold, the functionality is also affected. It hits it lowest at timeframe 40. When the SET reach 23.9°C, the functionality curve goes down into 0.75 (Figure 13).

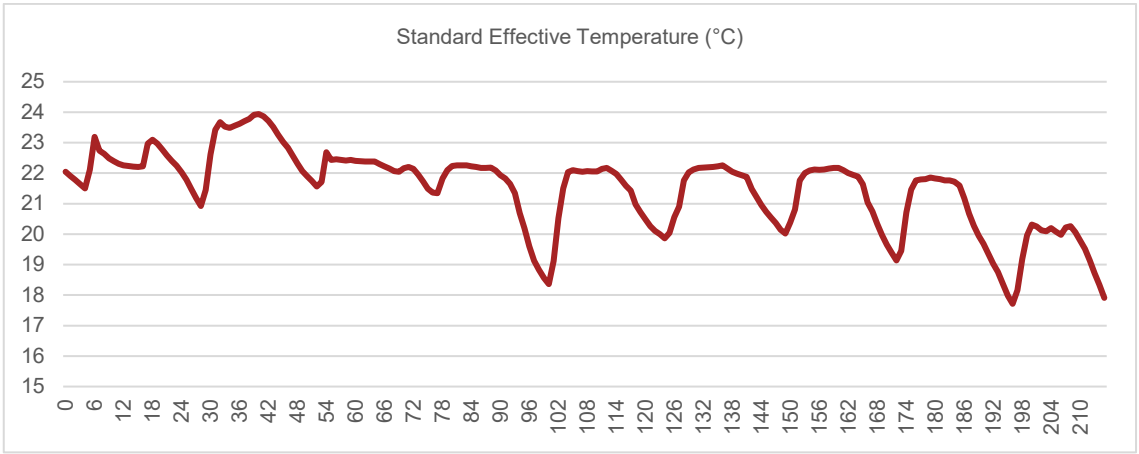

Figure 12. Example of Thermal Resilience Workflow Output - SET (Author)

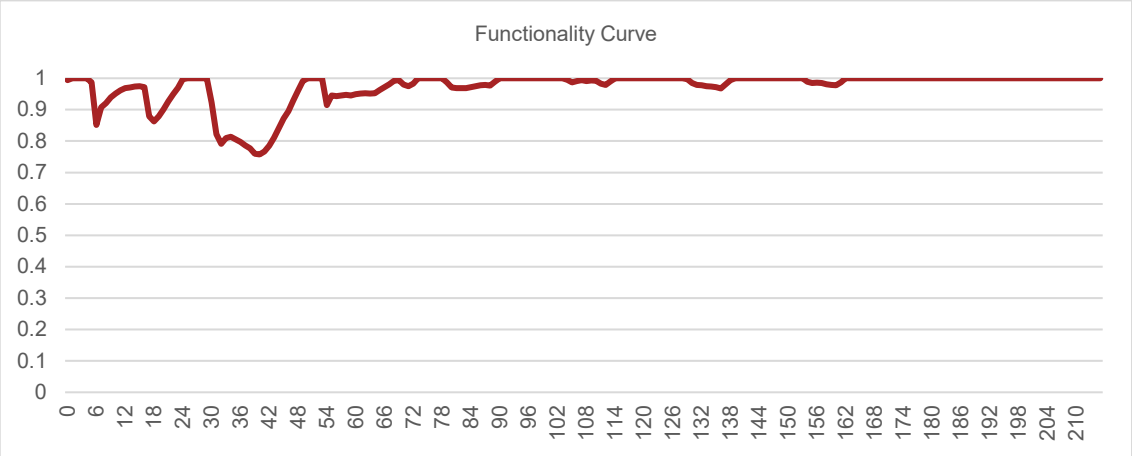

Figure 13. Example of Thermal Resilience Workflow Output - Functionality Curve (Author)

All of the mention outputs are available for each rooms. This data can be shown per room, per floor, or in this thesis, the average value of all the rooms is used to simplify the final output that is going to be put as objective in the multi-objective optimization.

4.2 Thermal Resilience Score Calculator

4.2.1 Grasshopper Python Component

The thermal resilience quantification explained in section 4.3.2 is then applied to a custom grasshopper python component. The full script can be found in Appendix B. The component has 4 inputs and 5 outputs (Figure 14) with input and output explained in Table 8 and Table 9.

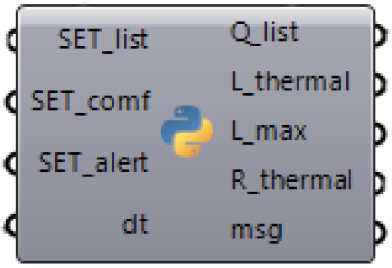

Figure 14. Thermal Resilience Calculator Grasshopper Component (Author)

Table 8. Thermal Resilience Score Calculator Grasshopper Component Input (Author)

Input	Symbol	Unit	Description
SET_list	SET(t)	°C	Hourly Standard Effective Temperature time series from EnergyPlus simulation via Honeybee. One value per hour of the annual simulation period. One value per hour for the heatwave simulation period. For multi-

			room assessments, a list of lists is accepted — one inner list per room.
SET_comf	SET_c	°C	Upper comfort threshold. At or below this temperature the occupant is considered fully comfortable and Q(t) = 1.0.
SET_alert	SET_a	°C	Alert threshold. At or above this temperature the environment is fully non-functional and Q(t) = 0.0.
dt	t	h	Time step of the simulation output. Typically, 1.0 for hourly EnergyPlus output.

Table 9. Thermal Resilience Score Calculator Grasshopper Component Output (Author)

Input	Symbol	Unit	Description
Q_list	Q(t)	-	List of quality function values, one per timestep. Bounded between 0 and 1. For multi-room assessments, a list of lists is returned, one inner list per room.
L_thermal	L	h	Cumulative thermal resilience loss, computed as the sum of [1 − Q(t)] · Δt across all timesteps.
L_max	L_max	h	Maximum possible loss, equal to N · Δt, representing the worst case where Q(t) = 0 throughout the simulation..
R_thermal	R	-	Normalised thermal resilience score on [0, 1], computed as 1 − (L_thermal / L_max). A value of 1 indicates full comfort throughout the simulation.
msg	-	-	Diagnostic status message, reporting the computed R_thermal value or an error if inputs are invalid.

4.3 Heatwaves Surrogate Model Training

Running a full dynamic thermal simulation for every candidate façade design during the optimization process would be prohibitively expensive, as each simulation requires the execution of EnergyPlus over an annual weather file with an embedded heatwave event, followed by post-processing through the PMV Comfort and Read Room Energy Result components. To remove this computational bottleneck, a surrogate modelling stage is incorporated into the workflow. The surrogate is trained on the dataset generated from the Latin Hypercube sample of design configurations and learns the mapping between the eleven design variables and the thermal resilience score, allowing predictions to be returned in fractions of a second rather than minutes per evaluation. This makes it feasible to embed the surrogate inside the multi-objective optimization routine, where many thousands of candidate designs must be evaluated.

The surrogate modelling stage is structured around three analyses, each serving a distinct purpose. The first is a correlation analysis, which provides an initial descriptive view of the dataset by quantifying the strength and direction of the statistical association between each design variable and the simulated thermal resilience score. This step functions as an exploratory data analysis and as a first-pass screening of which inputs exert the strongest monotonic influence on the output. The second is a random forest regression, an ensemble machine-learning method that fits multiple decision trees to bootstrapped subsets of the data and aggregates their predictions. Random forest is selected as the surrogate model because it captures non-linear relationships and interaction effects between design variables that a purely correlation-based view cannot detect, and because it remains robust to hyperparameter choices and to the presence of noisy or weakly informative inputs.

The trained random forest is the component that replaces the expensive thermal simulation inside the multi-objective optimization routine described in the following section. The third is a Sobol sensitivity analysis, which decomposes the predicted variance of the thermal resilience score into contributions from each design variable individually and from their interactions. While the correlation analysis identifies linear associations and the random forest acts as a fast predictor, Sobol indices serve a different role: they identify which design variables act as the strongest drivers of the resilience response, including non-linear and interaction-driven effects that the correlation analysis would miss. Together, the three analyses provide a complementary view of the dataset — descriptive screening, predictive surrogate, and driver identification.

4.3.1 Correlation Analysis

This chapter starts with correlation analysis to better understand the relationship between different façade design parameters and the building's thermal performance. There are eleven inputs and eighteen outputs. The inputs are already mentioned in Chapter 3.4. The outputs are grouped in sets of three, since each floor produces three types of output and the demonstrator has six floors in total. Within each floor, two types of room are evaluated separately: the corridor and the living units.

To allow a detailed reading of the results, the outputs are disaggregated by floor, room type, and performance metric. The naming convention used throughout the heatmaps follows the format f(x)_metric_period_zone, where f(x) identifies the floor number (x running from 0 for the ground floor to 5 for the top floor); metric is either EUI (cooling energy use intensity in kWh/m²) or TR (thermal resilience score as defined in Section 4.3); period distinguishes the He (heatwave) period from the No (typical)

period and applies only to EUI outputs; and zone is either Co (corridor) or Li (living area, where the _avg suffix indicates averaging across multiple living spaces on the same floor). For example, the column header *f2_EUI_He_Co* refers to the cooling EUI of the corridor on the second floor during the heatwave period, while *f4_TR_Li_avg* refers to the thermal resilience score averaged across the living areas on the fourth floor.

The four charts presented below progressively zoom out from zone-specific to building-level views and conclude with a feature-importance ranking. Together, they identify which design variables exert the strongest statistical influence on the thermal response of the demonstrator.

In Figure 15 reports the Pearson correlation between each design variable and eighteen corridor outputs (six floors x three metrics: EUI_He, EUI_No, and TR). Two design variables stand out. Aperture N shows a near-perfect positive correlation with the fourth-floor corridor heatwave EUI (r = +0.98) and an equally strong negative correlation with the fourth-floor corridor thermal resilience score (r = -0.96), indicating that the corridor is highly exposed to north-facing aperture variation. Aperture E demonstrates consistently strong correlations across most corridor outputs, with values ranging from r = +0.96 (f2_EUI_He_Co) and r = +0.87 to r = −0.95 (f2_EUI_No_Co) and r = −0.84 across multiple floors. The remaining variables, including the south and west apertures, all shading depths, window subdivision parameters, and glass thickness, show only weak correlations (|r| < 0.4) with corridor outputs. This pattern suggests that corridor thermal performance is dominated by the apertures on the orientations that physically bound the corridor (north and east in this configuration), while other variables exert little direct influence on corridor conditions.

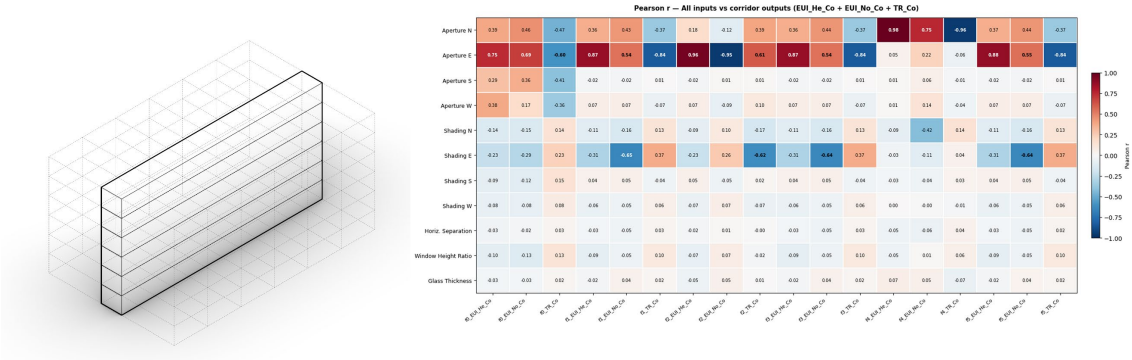

Figure 15. Correlation Analysis of Thermal Resilience of Corridor Rooms (Author)

The second heatmap (Figure 16) presents the same correlation analysis but evaluated against the living-area outputs (Li_avg) on each floor. Here, the pattern shifts considerably. Aperture S emerges as the most consistently influential variable, with moderate-to-strong correlations between r = +0.49 and r = +0.63 for heatwave EUI outputs and between r = −0.55 and r = −0.69 for thermal resilience outputs across floors. Aperture N also shows a meaningful effect, with correlations in the range of r = +0.56 to +0.65 for heatwave EUI and r = −0.51 to −0.57 for thermal resilience. Shading S shows a localized but notable correlation with the second-floor living-area thermal resilience (r = −0.63), suggesting a floor-specific shading-resilience relationship. Other variables, including all east and west shading parameters, window subdivision, and glass thickness, remain near-zero. This indicates that the living areas are primarily driven by north and south aperture choices, the orientations along which most living spaces are exposed.

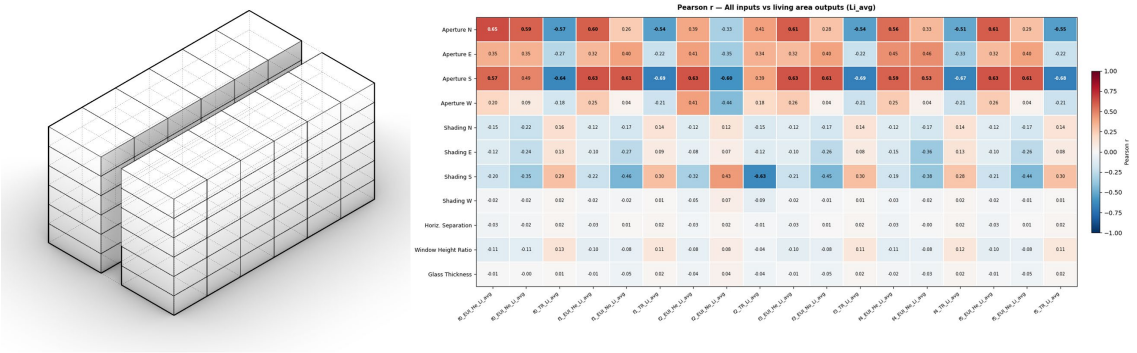

Figure 16. Correlation Analysis of Thermal Resilience of Living Area (Author)

The third heatmap in Figure 17 aggregates the outputs to floor-level averages, removing the corridor/living-area distinction. The dominant drivers become clearer at this scale. Aperture S shows a stable and strong influence across all floors and metrics, with correlations consistently between r = +0.55 and r = +0.64 for heatwave EUI and r = −0.55 to r = −0.64 for thermal resilience. Aperture N behaves similarly, with correlations in the range of r = +0.60 to +0.64 for heatwave EUI and r = −0.55 to r = −0.56 for thermal resilience. Aperture E contributes a more moderate effect (r ≈ +0.44 for EUI_He, r ≈ −0.32 for TR), while Aperture W shows weaker but still discernible influence (|r| ≈ 0.2 to 0.4). Shading S is the only shading variable with a non-trivial floor-averaged contribution (r ≈ +0.27 to +0.38 for thermal resilience). Window subdivision parameters (horizontal separation ratio and window height ratio) and glass thickness remain near-zero across all outputs.

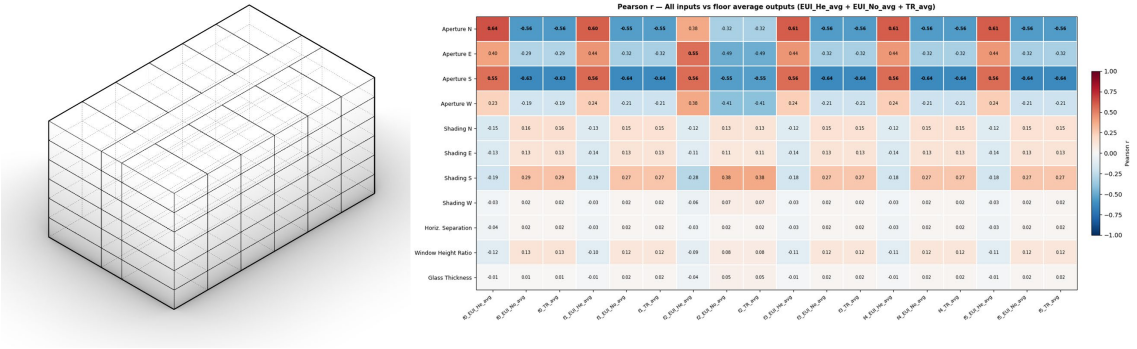

Figure 17. Correlation Analysis of Thermal Resilience of the Whole Building (Author)

Figure 18 summarize the feature-importance picture by reporting, for each design variable, the strongest absolute Pearson correlation observed across all outputs, annotated with the specific output column that produced it. The ranking confirms the pattern emerging from the previous heatmaps. Aperture N (|r| = 0.98) and Aperture E (|r| = 0.96) appear as the two strongest drivers, both peaking on the fourth-floor corridor heatwave EUI. Aperture S (|r| = 0.69), Shading E (|r| = 0.65), and Shading S (|r| = 0.63) form a second tier of moderately strong drivers, each associated with floor- or zone-specific resilience and EUI outputs. Aperture W (|r| = 0.44) and Shading N (|r| = 0.42) show modest influence. The remaining four variables — Shading W, Horizontal Separation, Window Height Ratio, and Glass Thickness — exhibit maximum absolute correlations below 0.15, indicating that, at the linear-association level, they exert little measurable influence on the thermal performance of the demonstrator. These weak correlations do not necessarily mean these variables are unimportant: their effects may

be non-linear or only emerge in interaction with other variables, both of which will be tested in the subsequent random forest regression and Sobol sensitivity analysis.

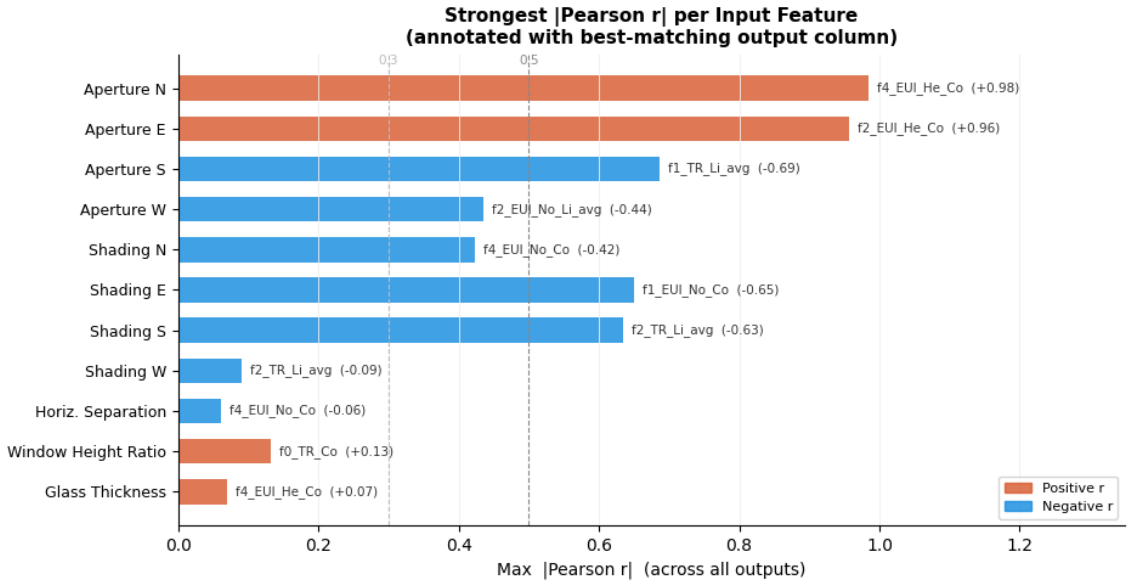

Figure 18. Strongest per Input Feature (Author)

4.3.2 Random Forest Regression

Building on the correlation analysis, the random forest regression is trained to serve two purposes: (i) to act as the surrogate model that replaces the dynamic thermal simulation inside the multi-objective optimisation routine, and (ii) to provide an interaction-aware view of feature importance that complements the linear-association picture given by Pearson correlation. A separate random forest model is trained for each of the three floor-averaged target outputs introduced in the previous section: the cooling EUI during the heatwave period (EUI_He_avg), the cooling EUI during the typical period (EUI_No_avg), and the thermal resilience score (TR_avg). Each model is trained on the eleven design variables and validated using cross-validation, with out-of-bag (OOB) error monitoring used to confirm convergence. The four charts below summarise the dataset distribution, the model convergence behaviour, the resulting feature importance ranking, and the predictive accuracy of each trained model.

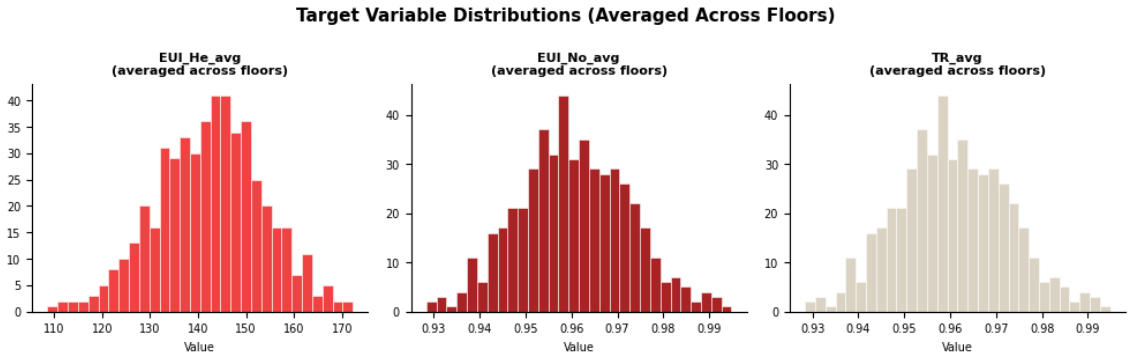

Figure 19. Target Variable Distributions for EUI and Thermal Resilience (Author)

In Figure 18 is displayed the distributions of the three target variables averaged across all floors. EUI_He_avg ranges from approximately 110 to 170 kWh/m² and exhibits an approximately normal distribution centred near 145 kWh/m². EUI_No_avg ranges from approximately 0.93 to 1.00 (normalised) and is similarly bell-shaped, centred near 0.96. TR_avg spans the same range from 0.93 to 1.00, also approximately normal and centred near 0.96. The bell-shaped, well-spread distributions confirm that the Latin Hypercube sample produces an output dataset suitable for surrogate model training: each target covers a meaningful range without strong skew or clustering, providing the model with sufficient variation across the design space to learn the underlying input–output mapping.

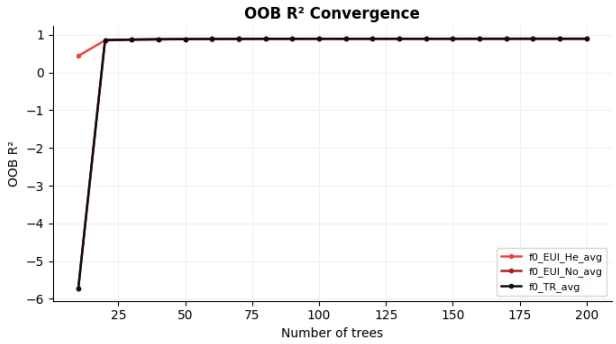

Figure 20. OOB Convergence for Thermal Resilience (Author)

Figure 20 shows the convergence of the out-of-bag (OOB) coefficient of determination as a function of the number of trees in the forest, for each of the three target variables. At small forest sizes (around 10 trees), the OOB R² is unstable, with one target showing a strongly negative value of approximately −6, indicating that very small forests overfit the bootstrap samples and generalise poorly. From approximately 25 trees onward, all three targets converge sharply to OOB R² values of approximately 0.85–0.90 and remain stable up to 200 trees. This convergence behaviour confirms that a forest size of around 100 trees is sufficient to obtain stable predictions, with no measurable benefit from further increasing the ensemble size. This value is therefore adopted for the final surrogate models embedded in the optimization routine.

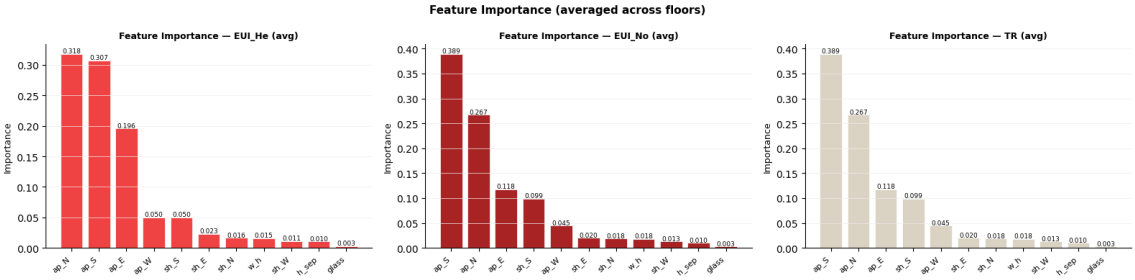

Figure 21. Feature Importance Averaged Across Floors for Thermal Resilience (Author)

Figure 21 reports the mean-decrease-in-impurity feature importance for each design variable, for the three floor-averaged targets. The ranking is broadly consistent across the three outputs but with informative differences. For EUI_He_avg (heatwave EUI), the dominant drivers are Aperture N (0.318) and Aperture S (0.307), followed by Aperture E (0.196). The remaining variables contribute very little, with Aperture W and Shading S each accounting for approximately 0.050 of the importance, and all other variables below 0.025. For EUI_No_avg (typical-period EUI) and TR_avg (thermal resilience), the ranking shifts so that Aperture S becomes the single most important driver (0.389), followed by Aperture N (0.267), Aperture E (0.118), and Shading S (0.099). The identical pattern between EUI_No_avg and

TR_avg reflects the strong inverse relationship between cooling energy demand and resilience under typical conditions. In all three cases, window subdivision parameters (horizontal separation and window height ratio) and glass thickness consistently appear at the bottom of the ranking, contributing less than 0.02 of the total importance.

Compared with the Pearson correlation results in the previous section, the random forest analysis confirms the same top-tier drivers (Aperture N, Aperture S, Aperture E) but introduces a more pronounced role for Shading S, which the Pearson analysis only flagged on a floor-specific basis. This is consistent with the expected behaviour of random forest: it captures non-linear and interaction-driven contributions that pairwise linear correlation cannot detect.

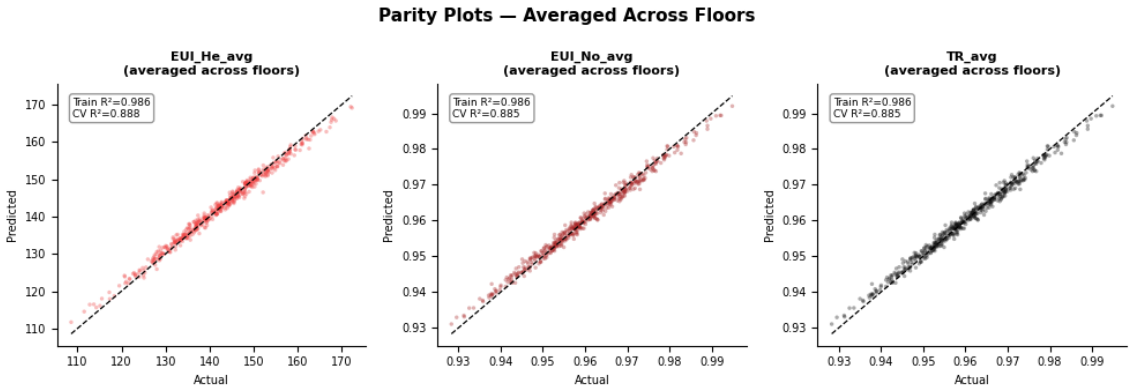

Figure 22. Parity Plots Averaged Across Floors for Thermal Resilience (Author)

The fourth chart (Figure 22) reports parity plots of predicted versus actual values for each of the three target outputs, with the dashed diagonal representing perfect prediction. All three plots show points tightly clustered along the diagonal, with reported training $R^2 = 0.986$ and cross-validation $R^2 \approx 0.885$–0.888 for all three targets. The close agreement between training and cross-validation R^2 indicates that the model generalizes well to unseen samples and is not significantly overfitted, which is a critical property given that the surrogate will be used to evaluate design configurations not present in the training set during the optimization. The small dispersion observed at the tails of the EUI_He_avg distribution is consistent with the expected behavior of random forest at the extremes of the training data and does not affect the validity of the model for use within the explored design space.

4.3.3 Sobol Sensitivity Analysis

While the correlation analysis and the random forest regression provide complementary views of the input–output relationship, neither method directly quantifies how much of the total variability in the thermal response can be attributed to each design variable, nor whether that contribution arises from the variable acting alone or in combination with others. To address this, a Sobol sensitivity analysis is conducted on the trained surrogate model. Sobol is a variance-based global sensitivity method that decomposes the total variance of the output into additive contributions from each input and from their interactions, producing two complementary indices: the first-order index (S_1), which captures the variance attributable to each input acting independently, and the total-order index (ST), which captures the variance attributable to each input including all of its interactions with other variables. The difference between ST and S_1 for a given variable therefore quantifies the strength of its interaction effects with the remaining variables. The analysis is performed across the three floor-averaged targets, and the

chart below reports the indices averaged across the three targets to produce an overall ranking of input sensitivity.

The Sobol indices confirm and sharpen the picture suggested by the previous two analyses (Figure 18). Aperture S emerges as the dominant driver, with a total-order index of ST = 0.503 (σ = 0.088), meaning that this single variable accounts for approximately half of the variance in the thermal response of the demonstrator. Aperture N is the second strongest driver (ST = 0.309, σ = 0.115), followed by Aperture E (ST = 0.142, σ = 0.093). Shading S contributes a moderate but non-negligible effect (ST = 0.062, σ = 0.045), and Aperture W appears in fifth place with a small contribution (ST = 0.026, σ = 0.035). Together, the top five variables account for over 95 % of the total-order variance attributable to the eleven design variables.

The remaining six variables — Shading E (ST = 0.004), Window Height ratio (ST = 0.002), Shading N (ST = 0.002), Shading W (ST = 0.001), Horizontal Separation (ST ≈ 0.000), and Glass Thickness (ST ≈ 0.000) — all exhibit total-order indices at or below 0.005, confirming that they exert no measurable influence on the thermal response of the demonstrator over the design space considered.

A notable feature of the ranking is the comparatively large gap between the first-order and total-order indices for Aperture E and Shading S. This gap indicates that part of the influence of these variables emerges through interactions with other design variables rather than through their independent effect, which explains why Shading S appeared more strongly in the random forest feature importance than in the linear Pearson correlation. For the dominant variables (Aperture S, Aperture N), the first-order and total-order indices are close, meaning that their effect is largely independent and additive rather than interaction-driven. The relatively large standard deviations associated with the top three drivers (σ between 0.088 and 0.115) reflect the variability of the sensitivity contribution across the three target outputs (EUI_He_avg, EUI_No_avg, TR_avg) rather than instability in the Sobol estimator itself.

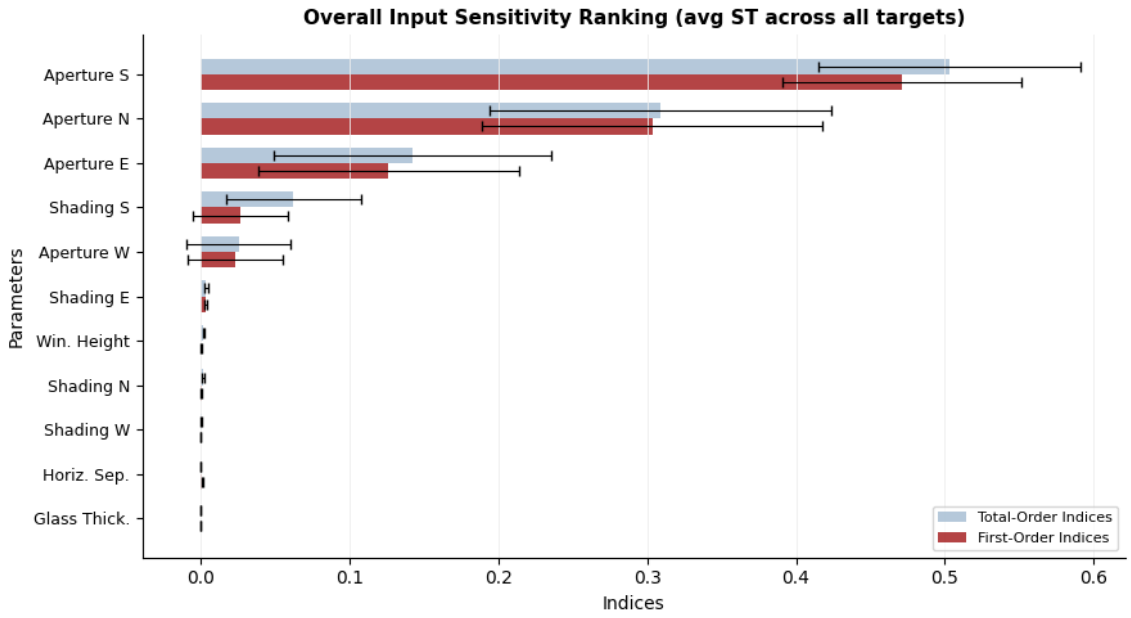

Figure 23. Overall Input Sensitivity for Thermal Resilience (Author)

4.3.4 Key Findings and Implications

Across the three complementary analyses conducted in this chapter, Pearson correlation, random forest feature importance, and Sobol sensitivity analysis, a consistent picture emerges of the thermal response of the demonstrator. The dataset generated through Latin Hypercube Sampling covers the eleven-dimensional design space with sufficient spread to support reliable model training, and the resulting input–output relationships are well-defined and dominated by a relatively small subset of the design variables. The main findings of the analysis can be summarised as follows.

- **Three orientation-specific apertures dominate the thermal response.** Aperture S, Aperture N, and Aperture E consistently appear as the three strongest drivers across all three analyses, jointly accounting for the majority of the variance in cooling EUI and thermal resilience. Aperture S alone accounts for approximately half of the variance attributed to the eleven design variables.

- **Shading S contributes a moderate, interaction-driven secondary effect.** Its influence is more visible in the random forest and Sobol analyses than in the Pearson correlation, indicating that part of its effect emerges through interactions with other design variables rather than through a direct linear association.

- **Aperture W exerts a small but discernible influence**, ranking just below the three dominant apertures and Shading S in both feature importance and total-order Sobol indices.

- **Six variables exhibit negligible influence on the thermal response** within the explored design space: Shading N, Shading E, Shading W, the horizontal separation ratio, the window height ratio, and the glass thickness. Their total-order Sobol indices are below 0.01, and their feature importances are below 0.025. These variables may still play a meaningful role in the wind-resilience analysis presented in the next chapter, where geometric parameters that control glazing panel dimensions become relevant for structural capacity.

- **The random forest surrogate is trained, validated, and ready for use** as a fast predictor of the thermal resilience score. Training R^2 values of 0.986 and cross-validation R^2 values of approximately 0.885 confirm that the model generalises well to unseen design configurations and that its predictions can be relied upon within the explored design space.

These findings inform the next steps of the workflow in two ways. First, the trained random forest surrogate replaces the expensive EnergyPlus simulation inside the multi-objective optimisation routine described in Chapter 6, providing fast and accurate predictions of the thermal resilience score for any combination of the eleven design variables. Second, the sensitivity ranking provides a physical interpretation of the design space that will guide the discussion of the Pareto front: configurations that maximise thermal resilience are expected to be driven primarily by aperture choices, with the south, north, and east orientations setting the dominant trade-offs. The wind-resilience analysis in the next chapter will reveal whether the dominant drivers on the wind side overlap with these geometric levers or engage a different subset of the design space, and the comparison between the two will set the stage for the multi-objective optimisation.

5 Wind Resilience Quantification

5.1 Wind Simulation

5.1.1 CFD Simulation Setup

The CFD simulations were performed using Eddy3D (Kastner & Dogan, 2022), a Grasshopper plugin that couples OpenFOAM with the Rhino–Grasshopper environment for outdoor wind and microclimate analysis. The workflow shown in Figure 24 operates on the same building geometry used in the thermal simulation and is driven by the independent variables sampled through Latin Hypercube Sampling. Beyond the design variables, three additional groups of inputs are required to fully define the wind simulation.

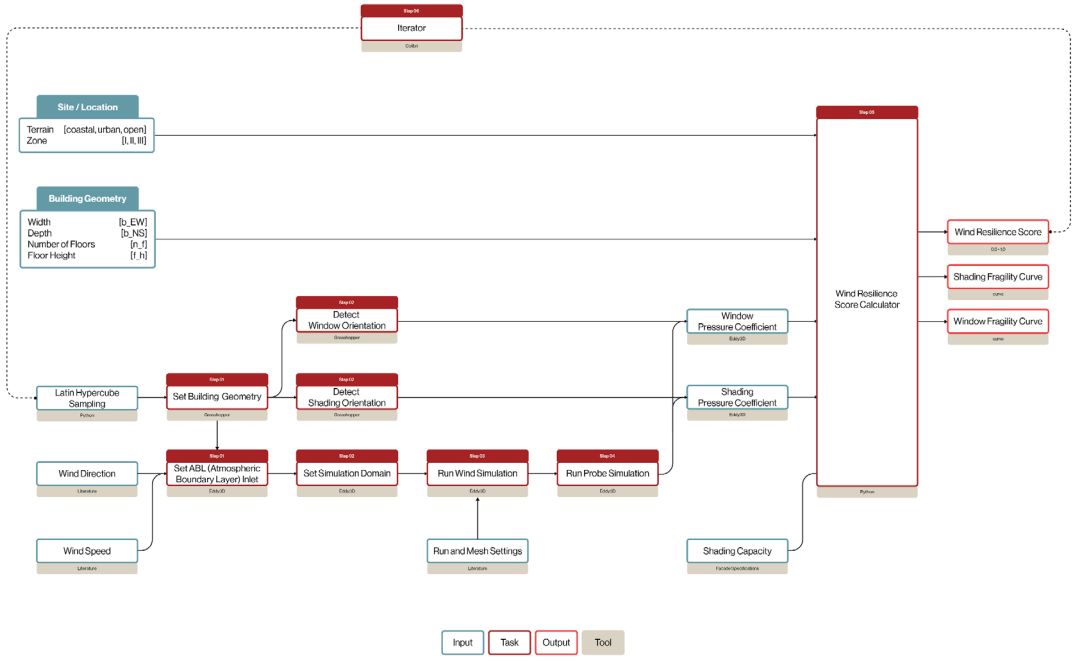

Figure 24. Graphical Representation of Wind Simulation Workflow (Author)

The first group consists of site-specific inputs, namely the wind zone and the terrain type at the location of the building, which together determine the atmospheric boundary layer profile used in the simulation. The second group consists of the hazard stressors, which describe the wind event itself: the wind direction and the wind velocity. In this case study, the wind direction is set to southwest (225°), as this represents the prevailing wind exposure across the Netherlands. (Pérez-Bella et al., 2025) report that the most wind-exposed façades throughout the year consistently face southwest across all twenty-eight Dutch weather stations analyzed, making this orientation the most representative single-direction input for a national-context analysis. The wind velocity adopted in this study is described in Section 5.2.1. Both inputs are fed into the *Set Atmospheric Boundary Layer (ABL) Inlet* component, which constructs the inflow conditions and the simulation domain. The third group consists of building-specific inputs, building width, depth, number of floors, and floor height, which are inherited directly from the parametric model already established in the thermal simulation.

Two final settings, the run settings and the mesh settings, control the resolution and computational cost of the simulation and are configured according to the available computational resources. Once all inputs are specified, the wind simulation is ready to be executed.

5.1.2 Example Use on Case Study

The developed workflow of the wind simulation and wind resilience quantification is put to the case study in this chapter. The workflow starts similarly like shown in Figure 25. It begins with the design parameters which feeds the Honeybee geometry but postprocessed into a mesh that can be read by the Eddy3D plugin. A script that separates the faces and shadings based on cardinal directions is created so the simulation can be partitioned. A set of probing points are generated to assign the simulation output based on these points. After the simulation run is done, the output, pressure coefficient C_p can be seen in each probing points (Figure 26).

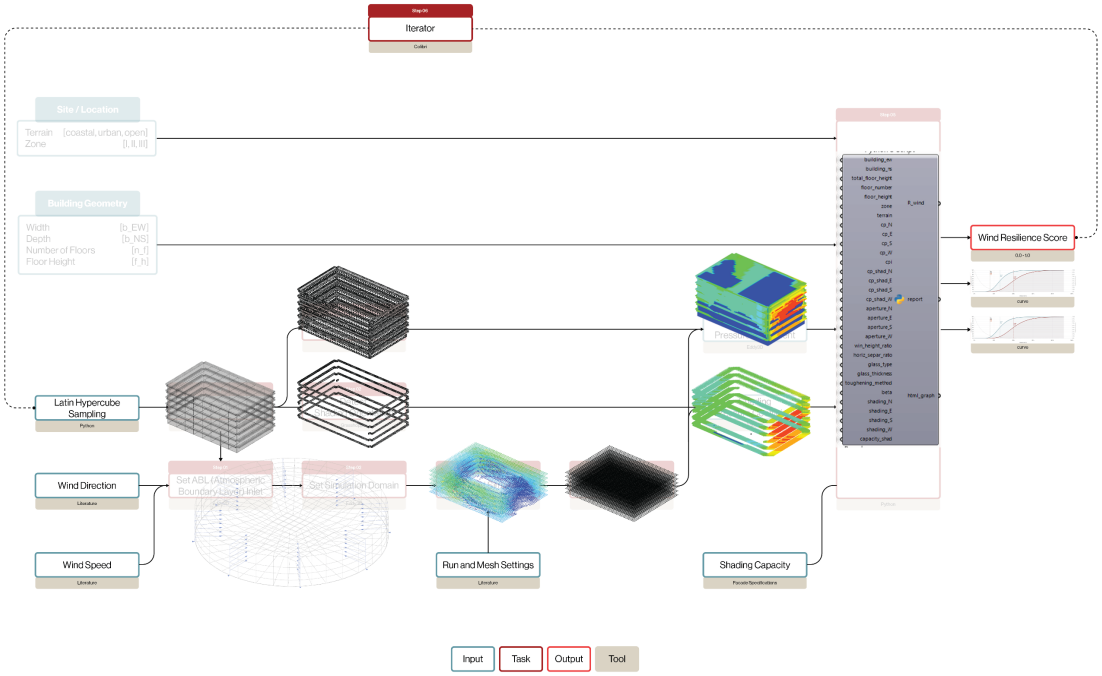

Figure 25. Wind Resilience Workflow Application on Case Study (Author)

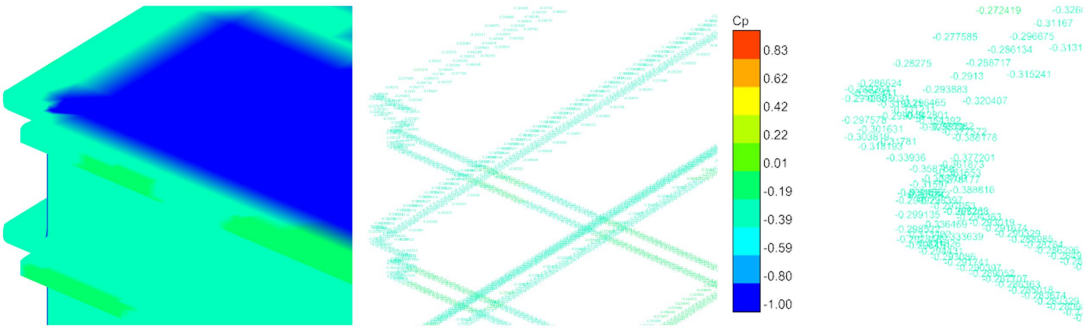

Figure 26. Pressure Coefficient on Probing Points (Author)

5.2 Wind Resilience Score Calculator

The Wind Resilience Score Calculator is implemented as a custom Grasshopper Python (GHPython) component that processes the CFD outputs from Eddy3D together with site, geometry, and material inputs to produce a single bounded resilience score for each design configuration. The component is the wind-side counterpart of the Thermal Resilience Score Calculator described in Chapter 4 and is structured around four computational stages: (i) the determination of wind pressure demand on the wall and on the shading element, (ii) the determination of the glazing capacity according to the relevant European glass design standard, (iii) the demand–capacity fragility model used to translate demand and capacity into a probability of failure, and (iv) the aggregation of the resulting probabilities into the final wind resilience index R_wind. A built-in fragility curve viewer is generated alongside the numerical output to support inspection of the underlying probability curves.

5.2.1 Grasshopper Python Component

The Grasshopper Python component takes three groups of inputs and returns two principal outputs. The first input group consists of building geometry parameters (overall east–west and north–south dimensions, total number of floors, floor-to-floor height, and the floor number at which the simulation is evaluated). The second group consists of wind site parameters that determine the peak velocity pressure (wind zone and terrain exposure category according to NEN-EN 1991-1-4), and the Eddy3D-derived pressure coefficients (Cp) on each of the four façades and on each of the corresponding shading overhangs. The third group consists of glazing parameters (window-to-wall ratio per orientation, window-height ratio, horizontal separation ratio, glass type, glass thickness, and toughening method) together with two fragility parameters (the lognormal dispersion β and the rated capacity of the shading element).

The component returns two principal outputs. *R_wind* is a scalar resilience index bounded on [0, 1], where 1 indicates full façade integrity under the considered wind hazard and 0 indicates certain failure. In addition, the component produces a plain-text report summarizing the intermediate quantities and an HTML dashboard that renders the underlying fragility curves and demand–capacity comparison for inspection. The overall structure of the component, including the inputs, the four computational stages, and the outputs, follows the workflow illustrated in Figure 20.

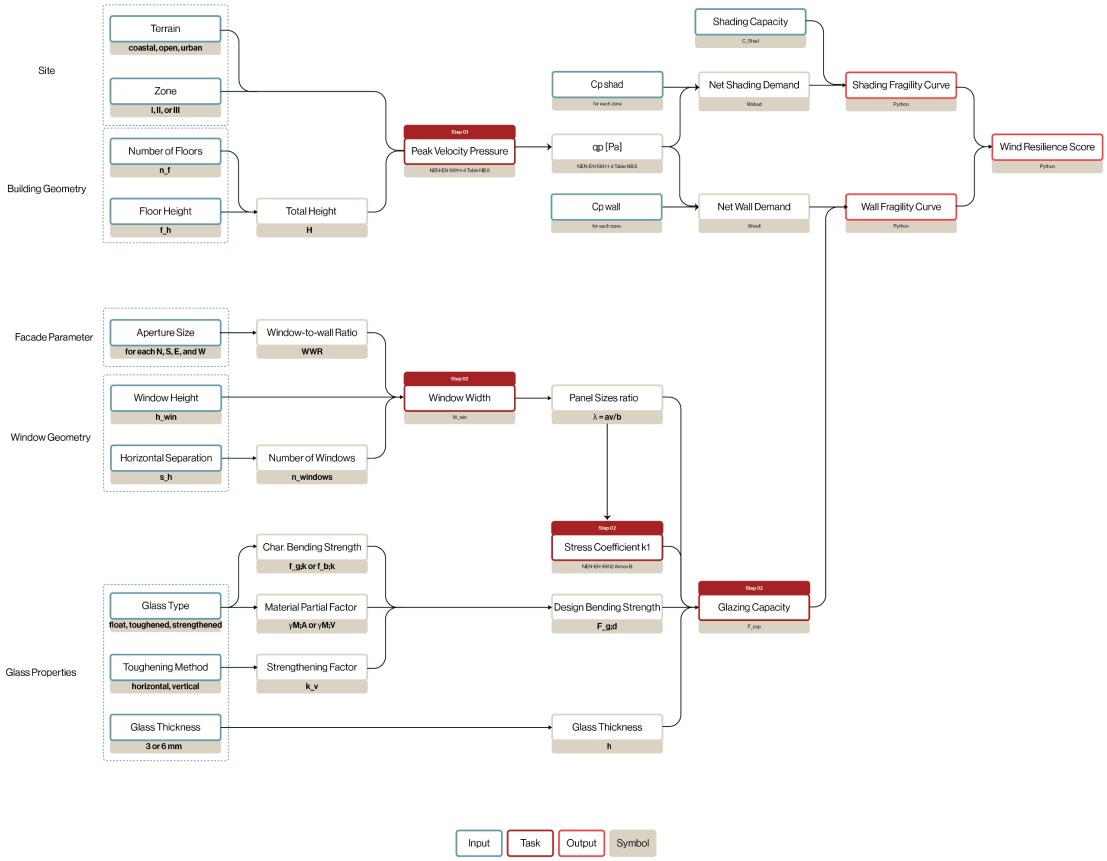

Figure 27. Graphical Representation of Wind Resilience Calculator Workflow (Author)

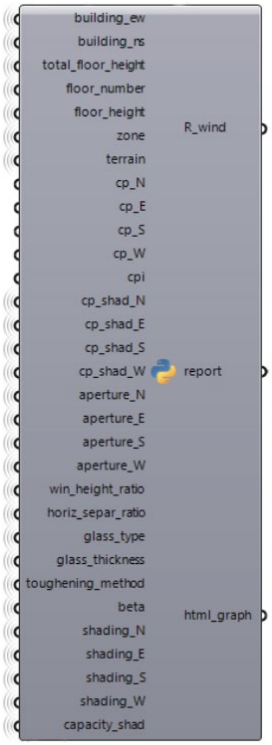

Figure 28. Wind Resilience Calculator Grasshopper Component (Author)

The component accepts the following user-defined inputs, organized by category.

Table 10. Building Geometry Input (Author)

Input	Symbol	Unit	Description	
num_floors	n_f	-	Number of storeys	
floor_height	f_h	m	Floor-to-floor height	
building_ew	b_EW	m	Building dimension in the east-west direction	
building_ns	b_NS	m	Building dimension in the north-south direction	

The total building height is computed internally as:

$$H = n_f \,.\, f_h \quad [m]$$

Table 11. Site and Wind Parameters (Author)

Input	Unit	Options
zone	-	1 = coastal ($V_{b,0}$=29.5 m/s), 2 = west Netherlands ($V_{b,0}$=27 m/s), 3 = inland ($V_{b,0}$=24.5 m/s)
terrain	-	0 = coastal, 1 = open country, 2 = urban
wind_dir	-	0 = West, 1 = South, 2 = East, 3 = North

Table 12. Facade Parameters (Author)

Input	Symbol	Unit	Description
aperture_N	WWR	0-1	Window-to-wall ratio
aperture_S	WWR	0-1	Window-to-wall ratio
aperture_E	WWR	0-1	Window-to-wall ratio
aperture_W	WWR	0-1	Window-to-wall ratio
shading_N	d_sh	m	Horizontal projection depth of shading element
shading_S	d_sh	m	Horizontal projection depth of shading element
shading_E	d_sh	m	Horizontal projection depth of shading element
shading_W	d_sh	m	Horizontal projection depth of shading element

It is noted that WWR does not affect wind demand. The internal pressure coefficient C_{pi} is fixed per Section 7.2.9 of the Dutch National Annex regardless of aperture size. However, WWR does affect glazing capacity through the panel dimensions it implies, as described in Section 4.5

Table 13. Glass Properties (Author)

Input	Unit	Options
glass_type	-	0 = annealed float glass, 1 = thermally toughened, 2 = heat strengthened
toughening_method	-	0 = horizontal toughening (k_v = 1.0), 1 = vertical toughening (k_v = 0.6)
glass_thickness	mm	Nominal glass thickness. Typical values: 6,8,10,12,15,19 mm

For the window geometry, these two inputs define individual window dimensions in a manner consistent with the Honeybee AperturesByRatio component used in the thermal simulation workflow.

Table 14. Window Geometry Parameter (Author)

Input	Symbol	Unit	Description
window_height	h_win	m	Fixed window height, matching the _win_height_ parameter in Honeybee AperturesByRatio.
horiz_separ_m	s_h	m	Horizontal separation between window centerlines in metres, matching the _horiz_separ_ parameter in Honeybee AperturesByRatio. This value is remapped from ratio slider in Grasshopper using the shortest façade dimension.

The number of windows per floor on each orientation follows the Honeybee rule:

$$n_{windows} = \begin{cases} 1, & if\ s_h \geq facade_width \\ facade_width/s_h, & otherwise \end{cases}$$

The individual window width is derived from the WWR, façade geometry, and number of windows:

$$w_{win} = \frac{WWR \cdot facade_width \cdot f_h}{h_{win} \cdot n_{windows}} \quad [m]$$

The panel dimensions for the NEN-EN 16612 capacity calculation follow the NEN-EN 16612:2019 Annex B convention that a is always the shorter side:

$$a = min(h_{win}, w_{win}), \quad b = max(h_{win}, w_{win})$$

Because different orientations have different WWR values and potentially different façade widths, each orientation produces different panel dimensions and therefore different glazing capacities..

Table 15. Shading Element Capacity (Author)

Input	Symbol	Unit	Description
capacity_shad	C_shad	Pa	Bracket design resistance of the shading element. Derived from manufacturer technical datasheet or

			separate structural calculation. Typical range: 300-3000 Pa depending on system type and projection depth.

Table 16. Fragility Parameter (Author)

Input	Symbol	Unit	Description
beta	β	-	Lognormal dipersion parameter, reflecting combined uncertainty in wind demand and element capacity. Typical range: 0.3-0.5. Source: FEMA P-58 methodology

Table 17. Wind Resilience Component Output (Author)

Output	Type	Description
R_wind	0-1	System wind resilience score. 1.0 = fully resilient, 0.0 = certain failure
report	String	Full report of all intermediate results including qp, Cpe, per face, net demands, capacity values, D/C ratios, and fragility probabilities.
html_graph	String	Interactive HTML visualization containing a fragility curve and a demand versus capacity bar chart per façade element.

5.2.2 Fragility Curve Viewer

To support the interpretation of the numerical results, the component generates a self-contained HTML dashboard alongside the plain-text report. The dashboard presents the fragility curves of the governing wall face, of each individual façade orientation, and of the shading element across a range of wind pressure demands, together with a representative annual exceedance curve as a contextual reference. A demand–capacity bar chart compares the simulated demand against the computed capacity on each orientation (Figure 30), and an interactive slider allows the reader to vary the hazard intensity and observe the corresponding probabilities of failure and resilience index in real time (Figure 29).

The fragility curves themselves are computed by evaluating the fragility expression over a range of demand values from 0 to $3 \times q_p$. This range spans well beyond the design demand and ensures that the full transition of each curve from near-zero failure probability at low demands to near-certain failure at high demands is visible. The dashboard is intended as a diagnostic and communication tool rather than as a computational element of the workflow: the R_{wind} value used in the subsequent surrogate model training and multi-objective optimization is computed exclusively from the inputs and expressions described in Sections 5.3.2 to 5.3.5.

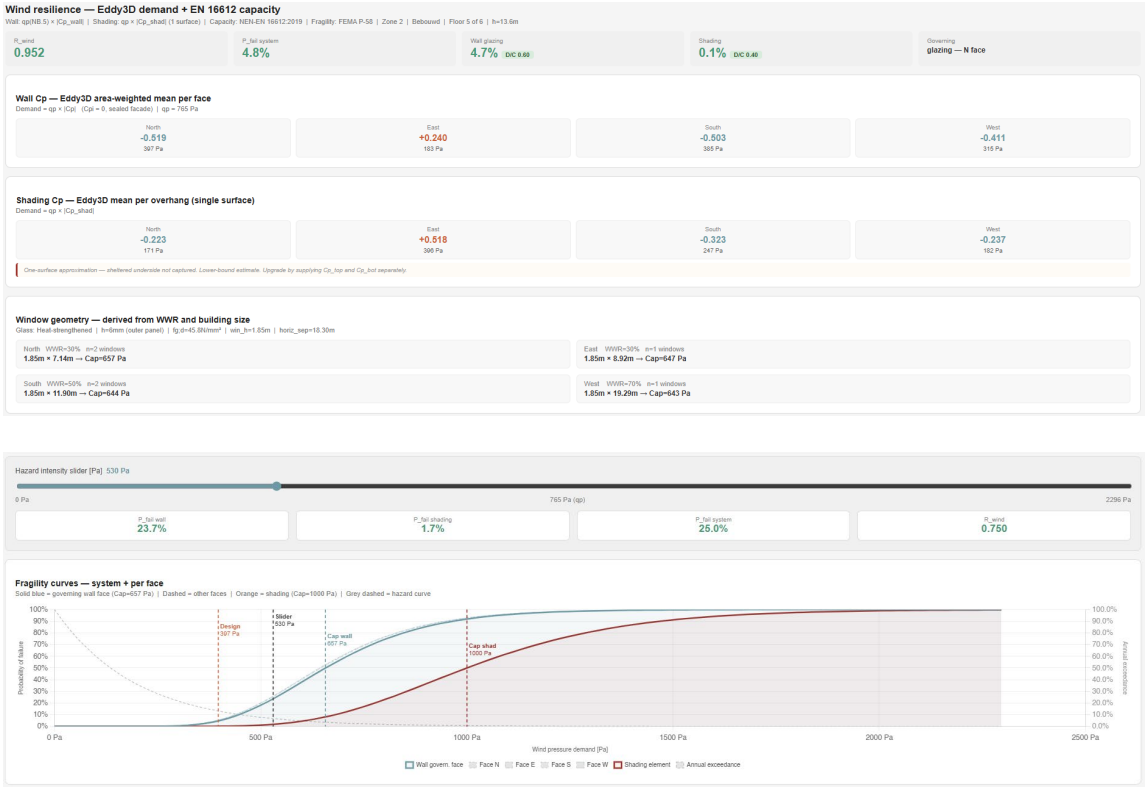

Figure 29. Fragility Curve Viewer - Interactive Hazard Intensity Slider

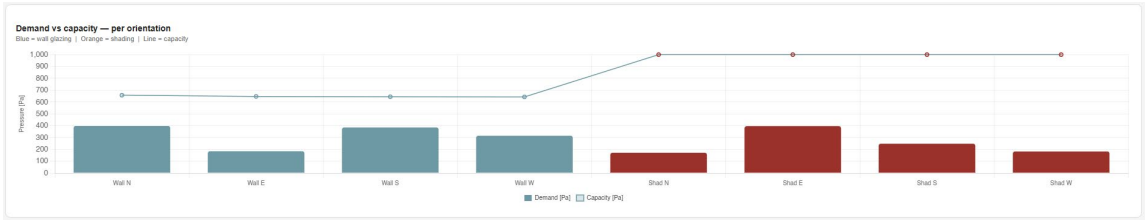

Figure 30. Fragility Curve Viewer - Demand vs Capacity per Orientation (Author)

5.3 Wind Surrogate Model Training

Running a full CFD simulation for every candidate façade design during the optimization process would be prohibitively expensive, as each simulation requires the generation of a refined mesh around the building, the RANS-based solution of the flow field in Eddy3D/OpenFOAM, the extraction of pressure coefficients from façade probes, and the subsequent post-processing through the Wind Resilience Score Calculator described in Section 5.3. To remove this computational bottleneck, a surrogate modelling stage is incorporated into the wind workflow as well. The surrogate is trained on the dataset generated from the Latin Hypercube sample of design configurations and learns the mapping between the eleven design variables and the wind resilience score, allowing predictions to be returned in fractions of a second rather than minutes per evaluation. This makes it feasible to embed the surrogate inside the multi-objective optimization routine, where many thousands of candidate designs must be evaluated.

The surrogate modelling stage is structured around three analyses, each serving a distinct purpose. The first is a correlation analysis, which provides an initial descriptive view of the dataset by quantifying the strength and direction of the statistical association between each design variable and the simulated wind resilience score. This step functions as an exploratory data analysis and as a first-pass screening of which inputs exert the strongest monotonic influence on the output. The second is a random forest regression, an ensemble machine-learning method that fits multiple decision trees to bootstrapped subsets of the data and aggregates their predictions. Random forest is selected as the surrogate model because it captures non-linear relationships and interaction effects between design variables that a purely correlation-based view cannot detect, and because it remains robust to hyperparameter choices and to the presence of noisy or weakly informative inputs.

The trained random forest is the component that replaces the expensive CFD simulation inside the multi-objective optimization routine described in the following section. The third is a Sobol sensitivity analysis, which decomposes the predicted variance of the wind resilience score into contributions from each design variable individually and from their interactions. While the correlation analysis identifies linear associations and the random forest acts as a fast predictor, Sobol indices serve a different role: they identify which design variables act as the strongest drivers of the resilience response, including non-linear and interaction-driven effects that the correlation analysis would miss. Together, the three analyses provide a complementary view of the dataset, descriptive screening, predictive surrogate, and driver identification.

5.3.1 Correlation Analysis

This chapter begins with correlation analysis to better understand the relationship between the façade design parameters and the building's wind performance. As in the thermal chapter, there are eleven design inputs (already detailed in Chapter 3.4). The wind outputs are organized into three groups: the wall Cp values on each of the four orientations, the shading Cp values on each of the four overhangs, and the wind resilience score (WR) computed by the calculator described in Section 5.3. For each Cp group, both the area-weighted mean ("avg") and the local maximum ("max") are reported per orientation, producing eight Cp columns per group. The wind resilience score is reported as both an average (WR_avg) and a maximum (WR_max) across the simulated configurations.

The Pearson correlation coefficient is selected for the same reasons established in the thermal correlation analysis (Section 4.4.1): the Latin Hypercube sample produces uniformly distributed inputs, the outputs are continuous and approximately well-behaved, and Pearson is the most widely reported correlation metric in building-performance literature, making the present results directly comparable to related studies. The known limitation that Pearson captures only linear association is again addressed in the subsequent random forest regression (Section 5.4.2) and Sobol sensitivity analysis (Section 5.4.3).

Three heatmaps are presented below. The first two examine the intermediate CFD outputs (wall Cp and shading Cp), and the third examines the final wind resilience score. Together, they trace how each design variable propagates through the wind workflow, from local aerodynamic effects on individual surfaces to the integrated resilience metric used in the optimization routine.

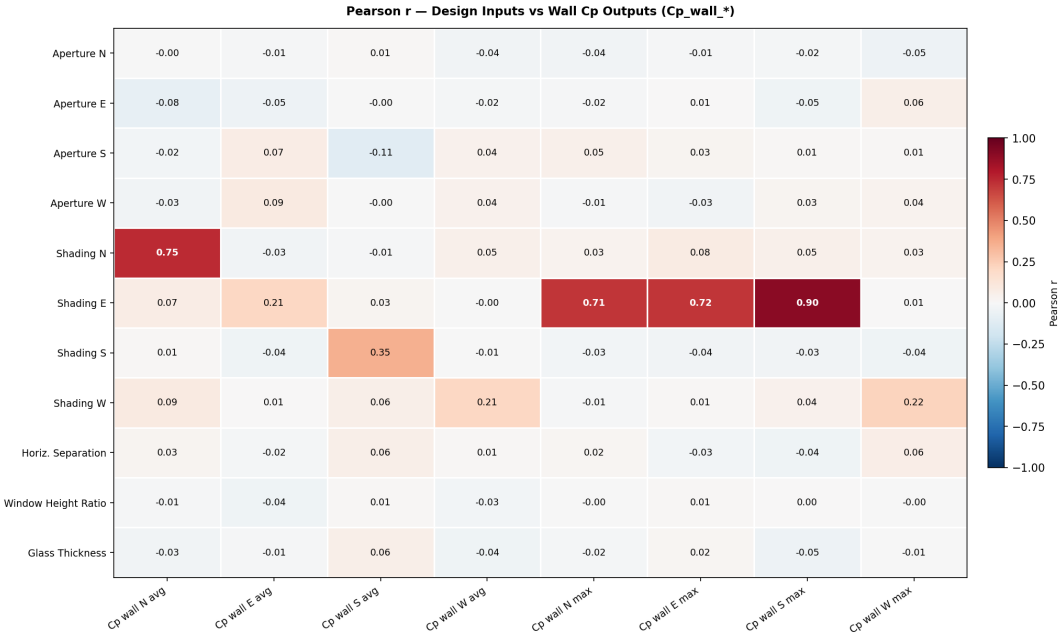

Figure 31. Correlation Analysis of Design Inputs vs Wall Cp Outputs (Author)

The first heatmap (Figure 31) reports the Pearson correlation between each design variable and the eight wall Cp outputs (mean and maximum on each of the four orientations). The dominant pattern is that the wall Cp values are not influenced by the aperture, window subdivision, or glass thickness variables: their correlations are all near zero ($|r| < 0.12$). Instead, the wall Cp values are governed by the shading depths. The strongest associations are observed between Shading E and the maximum wall Cp on multiple faces ($r = +0.71$ on the N face, $r = +0.72$ on the E face, and $r = +0.90$ on the S face), and between Shading N and the average wall Cp on the N face ($r = +0.75$). Weaker but still notable correlations are observed for Shading S with the average wall Cp on the S face ($r = +0.35$) and Shading W with the maximum wall Cp on the W face ($r = +0.22$). This pattern is physically consistent: the shading overhangs act as flow-modifying elements that locally redistribute the pressure field on the wall behind and around them, while the geometric parameters that describe the openings themselves (apertures, window subdivision) do not alter the building's external aerodynamics within the explored design space.

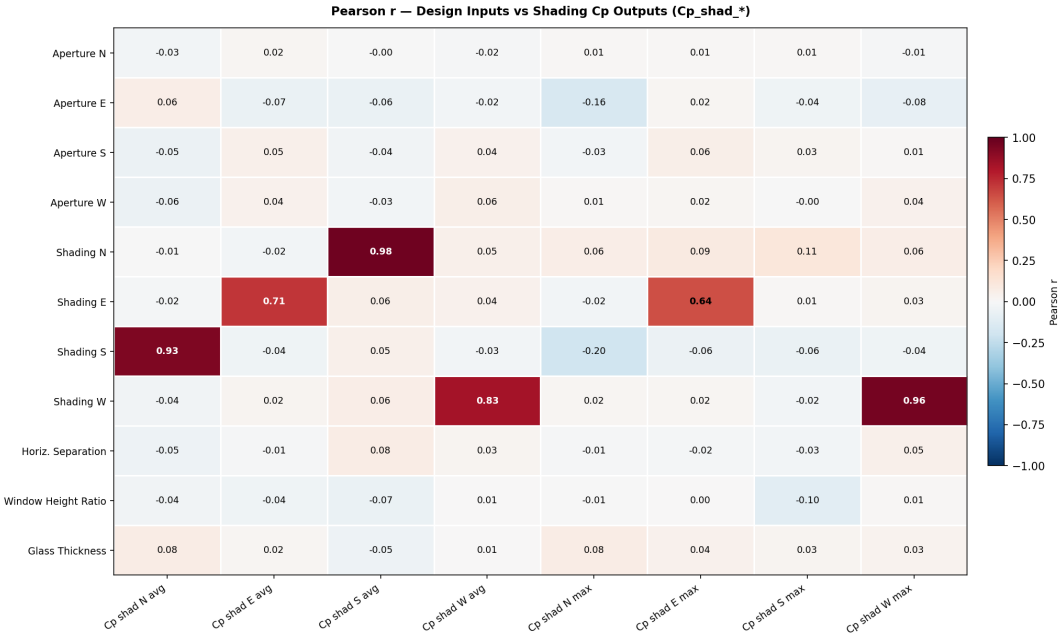

Figure 32. Correlation Analysis of Design Inputs vs Shading Cp Outputs (Author)

The second heatmap (Figure 32) reports the correlation between each design variable and the eight shading Cp outputs. As expected, the shading Cp values are essentially insensitive to aperture, window subdivision, and glass thickness variables. The dominant correlations come from the shading depths themselves, with a distinctive pattern that depends on orientation. For the east and west shadings, the correlations align with their own face: Shading E correlates with Cp_shad_E_avg (r = +0.71) and Cp_shad_E_max (r = +0.64), while Shading W correlates with Cp_shad_W_avg (r = +0.83) and Cp_shad_W_max (r = +0.96). For the north and south shadings, by contrast, the strongest correlations are observed with the opposite face: Shading N correlates with Cp_shad_S_avg (r = +0.98), and Shading S correlates with Cp_shad_N_avg (r = +0.93). This asymmetric pattern likely reflects the southwest prevailing wind direction (225°) adopted in the CFD setup, which leaves the north and south overhangs in markedly different upstream–downstream configurations: their pressure distributions interact through the global wake structure rather than locally. This behaviour deserves further inspection in the random forest and Sobol stages, where any non-linear or interaction-driven contribution can be quantified separately.

The third heatmap (Figure 33) reports the correlation between each design variable and the two aggregated wind resilience outputs, WR_avg and WR_max. The picture is fundamentally different from both Cp heatmaps and from the thermal correlation results discussed in Chapter 4. The window height ratio emerges as the single strongest driver, with a substantial negative correlation against both WR_avg (r = −0.72) and WR_max (r = −0.79). This is consistent with the underlying structural mechanics encoded in the glazing capacity expression of NEN-EN 16612: the panel capacity scales inversely with the square of the short panel dimension, so taller windows produce larger panels with lower capacity and therefore lower resilience. The horizontal separation also contributes negatively, with moderate correlations (r = −0.33 for WR_avg, r = −0.32 for WR_max), reflecting the fact that wider window panels likewise reduce capacity. All other design variables, including the four apertures, the four shading depths, and glass thickness, show only weak correlations ($|r| \leq 0.12$) with the resilience score at this linear level. The absence of a strong glass-thickness signal at the correlation stage is consistent with the discrete two-level treatment of this variable (3 mm and 6 mm) and with the fact that

its main contribution operates through the fragility model rather than through a smooth dose–response relationship; this is expected to surface more clearly in the random forest feature importance and Sobol sensitivity results.

The contrast between the strong shading-driven correlations observed in the Cp heatmaps and the absence of shading effects in the wind resilience heatmap is informative: although the shading depths strongly influence the local aerodynamic field, their effect on the system-level resilience score is moderated by the demand–capacity comparison and the FEMA P-58 fragility aggregation, in which the glazing capacity (governed by window geometry) is the dominant term. This decoupling between intermediate CFD outputs and integrated resilience outputs is one of the main reasons that a system-level resilience metric is required rather than a direct interpretation of pressure coefficients.

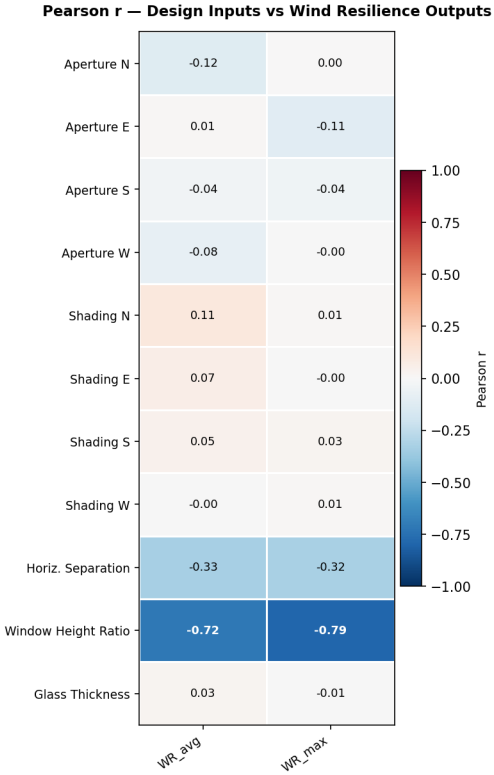

Figure 33. Correlation Analysis of Design Input vs Wind Resilience Outputs (Author)

5.3.2 Random Forest Regression

Building on the correlation analysis, the random forest regression is trained to serve two purposes: (i) to act as the surrogate model that replaces the expensive CFD simulation inside the multi-objective optimisation routine, and (ii) to provide an interaction-aware view of feature importance that complements the linear-association picture given by Pearson correlation. A separate random forest model is trained for each of the two aggregated wind resilience outputs: the average wind resilience score across the simulated configurations (WR_avg) and the maximum wind resilience score (WR_max). Each model is trained on the eleven design variables and validated using cross-validation, with out-of-bag (OOB) error monitoring used to confirm convergence. The four charts below summarise the dataset distribution, the model convergence behaviour, the resulting feature importance ranking, and the predictive accuracy of each trained model.

Figure 34 reports the distributions of the two wind resilience targets across the Latin Hypercube sample. WR_avg is strongly right-skewed: the bulk of the configurations cluster at values close to 1.0, with a count peak of approximately 195 samples near the upper bound and a long, thin tail extending down toward 0.2. This indicates that, in the average sense, the majority of design configurations achieve high wind resilience under the 15 m/s baseline hazard. WR_max displays a markedly different, bimodal distribution: one peak occurs near 1.0 (approximately 90 counts) and a second, broader peak emerges near 0.0 (approximately 40 counts), with the remaining samples distributed across the intermediate range. This bimodality reflects the worst-case behaviour captured by the maximum score: some configurations contain at least one weak orientation that drives the maximum probability of failure close to 1, while others maintain high resilience across all orientations. The two distributions together confirm that the dataset contains enough variability across the full resilience range to support the training of a meaningful surrogate model, even if the WR_avg distribution is heavily concentrated near the upper bound.

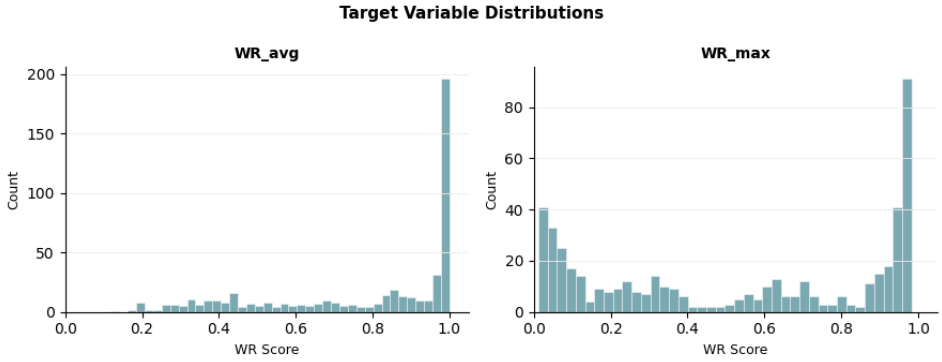

Figure 34. Target Variable Distributions for Wind Resilience Score (Author)

Figure 35 shows the convergence of the out-of-bag (OOB) coefficient of determination as a function of the number of trees in the forest, for both wind resilience targets. At small forest sizes (around 10 trees), the OOB R^2 starts at approximately 0.87 for WR_avg and 0.94 for WR_max. Both targets converge rapidly: WR_max stabilises at approximately 0.952 by 30 trees, while WR_avg climbs more gradually to approximately 0.910 by 70 trees. Beyond this point, both curves remain stable up to 200 trees, with no measurable benefit from further increasing the ensemble size. A forest size of approximately 100 trees is therefore adopted for both surrogate models, consistent with the configuration used in the thermal chapter. The fact that WR_max consistently achieves a higher OOB R^2 than WR_avg is

consistent with the structural difference between the two targets: WR_max is dominated by a single governing orientation per configuration, which the random forest can identify with relatively clean decision splits, whereas WR_avg averages across four orientations and therefore embeds more sample-to-sample noise.

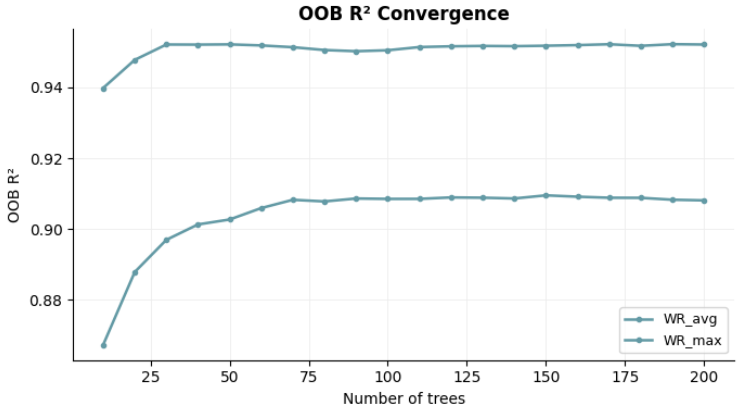

Figure 35. OOB Convergence for Wind Resilience (Author)

Figure 36 reports the mean-decrease-in-impurity feature importance for each design variable, for both WR_avg and WR_max. The picture is striking in its concentration. For WR_avg, the window height ratio alone accounts for an importance of 0.614, with the horizontal separation ratio in second place at 0.233. Together, the two window-subdivision parameters account for approximately 85 % of the total feature importance. The remaining variables follow far behind: Aperture N (0.054), Aperture W (0.032), Shading N (0.017), Aperture S (0.015), and a long tail of shading and glass-thickness variables all below 0.010. For WR_max, the same pattern is even more concentrated, with the window height ratio reaching 0.760 and horizontal separation at 0.131, jointly accounting for approximately 89 % of the importance. The four apertures contribute marginally (each below 0.05), the four shading depths are negligible, and glass thickness appears at the very bottom of both rankings with importance below 0.002.

Compared with the Pearson correlation results in the previous section, the random forest analysis confirms the same two dominant drivers (window height ratio and horizontal separation) and reinforces the picture that the wind resilience score is essentially determined by the geometric subdivision of the glazing rather than by aperture, shading, or glass-thickness choices. The exceptionally small contribution of glass thickness is consistent with the discrete two-level treatment of this variable, and may also reflect that the chosen capacity range (3 mm vs 6 mm panes) is not wide enough to materially shift the demand–capacity ratio across the design space.

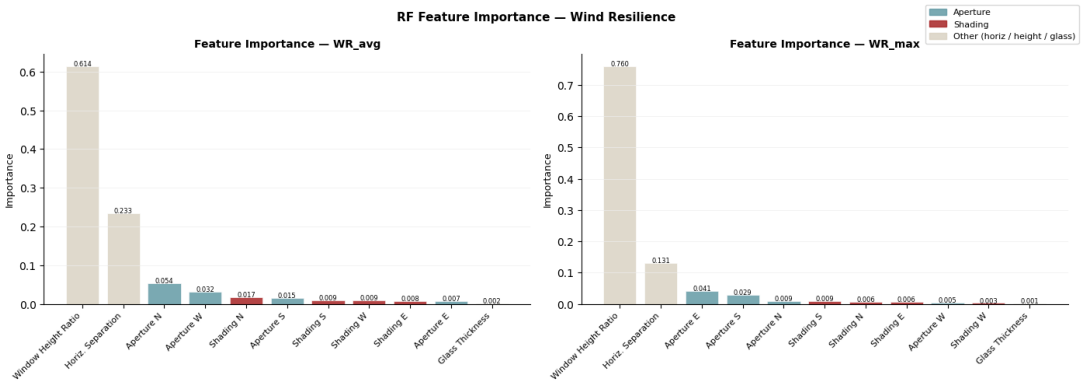

Figure 36. Feature Importance for Wind Resilience (Author)

Figure 37 reports parity plots of predicted versus actual values for both wind resilience targets, with the dashed diagonal representing perfect prediction. Both plots show points tightly clustered along the diagonal across the full target range. For WR_avg, the model reports a training R^2 of 0.987 and a cross-validation R^2 of 0.900, with the largest dispersion concentrated in the mid-range (WR between 0.4 and 0.9) where the dataset is sparsest. For WR_max, the model reports a training R^2 of 0.993 and a cross-validation R^2 of 0.937, with tight clustering throughout the full range and only slight dispersion at the lower end. The close agreement between training and cross-validation R^2 for both targets indicates that the models generalise well to unseen samples and are not significantly overfitted. The higher cross-validation R^2 achieved by the WR_max model is consistent with the convergence behaviour observed in Chart 2 and confirms that, where this thesis ultimately relies on a single integrated wind resilience indicator in the optimisation routine, both targets are sufficiently well predicted to support its use as a surrogate.

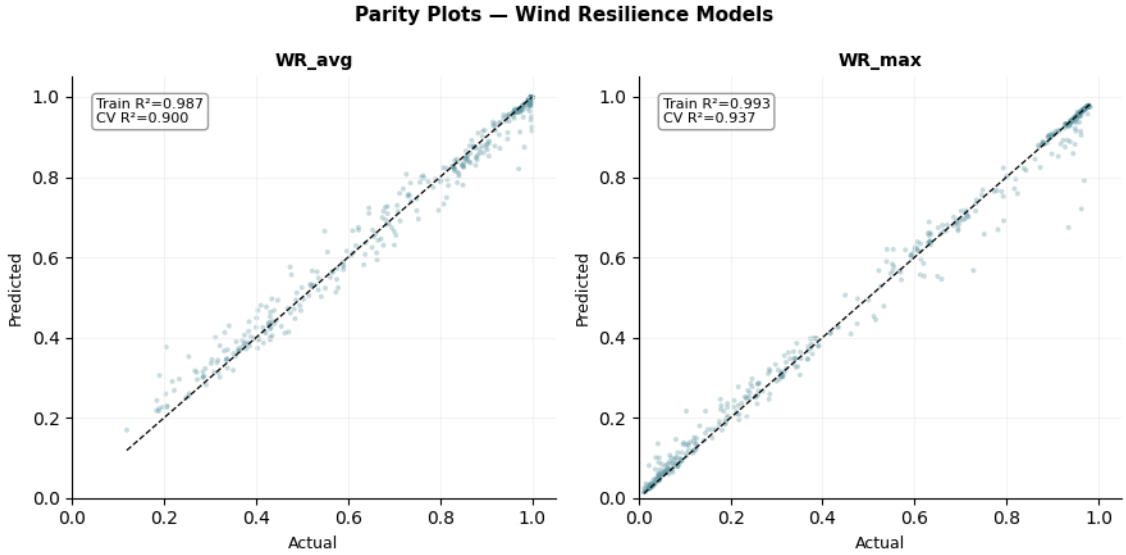

Figure 37. Parity Plots for Wind Resilience Models (Author)

5.3.3 Sobol Sensitivity Analysis

The Sobol sensitivity analysis is performed on the trained wind surrogate models following the same procedure described in Section 4.4.3, decomposing the output variance into first-order (S_1) and total-order (ST) contributions from each design variable. The indices are computed for both wind resilience targets and reported as an average across WR_avg and WR_max in Figure 38.

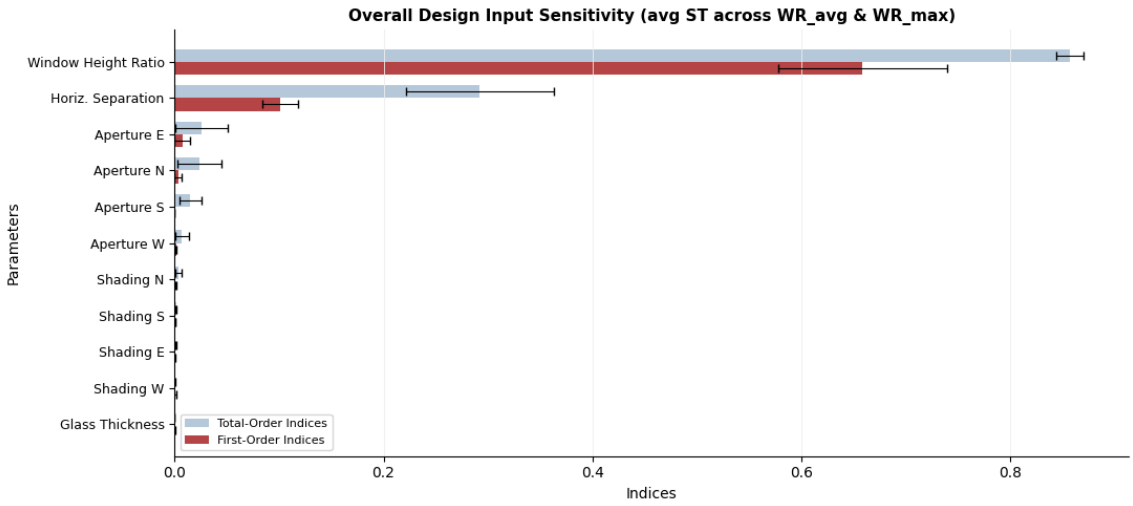

Figure 38. Overall Input Sensitivity for Wind Resilience (Author)

The Sobol indices confirm and sharpen the picture suggested by the previous two analyses. Window Height Ratio is the overwhelmingly dominant driver (ST ≈ 0.85, S_1 ≈ 0.65), accounting for the majority of the variance in the wind resilience response. Horizontal Separation appears in second place (ST ≈ 0.29, S_1 ≈ 0.10). The four apertures contribute marginal effects (ST < 0.03 each), and the four shading depths and glass thickness exhibit total-order indices at or below 0.005, confirming that they exert no measurable influence on the wind resilience response over the design space considered. Together, the top two variables account for the vast majority of the explained variance.

The most informative feature of the ranking is the large gap between first-order and total-order indices for Window Height Ratio ($\Delta ST - S_1$ ≈ 0.20) and Horizontal Separation ($\Delta ST - S_1$ ≈ 0.19). This indicates that a significant portion of their influence emerges through interaction with each other — physically expected, since both jointly determine the glass panel dimensions that control the NEN-EN 16612 capacity. The relatively large error bars on the top drivers reflect the difference between WR_avg and WR_max rather than estimator noise.

5.3.4 Key Findings and Implications

Across the three complementary analyses conducted in this chapter, Pearson correlation, random forest feature importance, and Sobol sensitivity analysis, a consistent picture emerges of the wind resilience response of the demonstrator. The dataset generated through Latin Hypercube Sampling spans the eleven-dimensional design space with sufficient variability to support reliable model training, although the wind resilience score is concentrated near the upper bound for the majority of configurations and only deteriorates meaningfully for a small subset of designs. The main findings of the analysis can be summarised as follows.

- **The window subdivision parameters dominate the wind resilience response.** The window height ratio alone accounts for approximately 85 % of the total-order Sobol variance across both WR_avg and WR_max, and the horizontal separation ratio adds a further 29 %. Together, the two parameters explain the overwhelming majority of the variability in the wind resilience score across the design space.
- **The dominant drivers act through strong mutual interactions.** The gap between the first-order and total-order Sobol indices reaches approximately 0.20 for the window height ratio and 0.19 for

the horizontal separation ratio, indicating that a substantial portion of their effect emerges through their joint contribution to the glass panel dimensions, which in turn govern the glazing capacity in the NEN-EN 16612 expression.

- **Apertures, shading depths, and glass thickness exert negligible influence on the integrated wind resilience score.** All four apertures show total-order Sobol indices below 0.03, the four shading depths and glass thickness all remain at or below 0.005. The shading depths nevertheless show strong correlations with the intermediate CFD outputs (wall Cp and shading Cp), illustrating that effects visible at the local aerodynamic level can be decoupled from effects on the system-level resilience metric.

- **The wind resilience response engages a fundamentally different subset of the design space than the thermal resilience response.** Thermal resilience was driven by the orientation-specific apertures (Chapter 4), whereas wind resilience is driven by the window subdivision parameters. These two subsets are essentially disjoint, which is precisely the condition under which a multi-objective optimisation produces a non-trivial Pareto front.

- **The random forest surrogates are trained, validated, and ready for use** as fast predictors of both wind resilience targets. Training R^2 values of 0.987 and 0.993 with cross-validation R^2 values of 0.900 and 0.937 (for WR_avg and WR_max respectively) confirm that the models generalise well to unseen design configurations and can be relied upon within the explored design space.

These findings inform the next steps of the workflow in two ways. First, the trained random forest surrogates replace the expensive CFD simulation inside the multi-objective optimisation routine described in Chapter 6, providing fast and accurate predictions of the wind resilience score for any combination of the eleven design variables. Second, the comparison between the thermal and wind sensitivity rankings sets the stage for the optimisation: because the two hazards engage disjoint subsets of the design space, the Pareto front is expected to contain configurations in which both objectives can be jointly improved, with trade-offs becoming visible only at the extremes of the front. The next chapter introduces the optimisation setup, where the two surrogates are paired to generate the Pareto-optimal designs that balance thermal and wind resilience.

6 Multi-Objective Optimization

With the thermal and wind random forest surrogates trained and validated against the Latin Hypercube dataset, the workflow proceeds to the multi-objective optimization (MOO) stage. The objective is to identify the set of façade design configurations that jointly maximize the thermal and wind resilience scores, recognizing that the two hazards engage different subsets of the design space (as established in Chapters 4 and 5) and that the resulting trade-offs can only be made visible through a Pareto-front exploration. The optimization is performed using the NSGA-II algorithm (Non-dominated Sorting Genetic Algorithm II) implemented in the *pymoo* Python framework, which is the de facto standard for multi-objective design problems in building performance and engineering practice.

6.1 Defining Parameters

The decision variables for the optimisation are the same eleven façade design parameters defined in Section 3.3: the four orientation-specific aperture ratios, the four orientation-specific shading depths, the horizontal separation ratio, the window height ratio, and the glass thickness. The bounds applied during the optimisation are identical to those used for the LHS dataset that trained the surrogates, ensuring that the candidate designs explored by NSGA-II remain within the domain in which the surrogate predictions are valid. The continuous variables are sampled directly from their bounded ranges, while the glass thickness is treated as a discrete two-level variable (3 mm and 6 mm) by snapping the continuous slider to the nearest admissible value before evaluation, following the same convention used during dataset generation.

6.2 Defining Objectives

Two objective functions are defined, one per hazard: the average thermal resilience score TR_avg and the average wind resilience score WR_avg**,** both predicted by their respective random forest surrogates. Because *pymoo* implements minimization by default and the objectives in this study are to be maximized, both scores are negated before being passed to the algorithm and un-negated when the Pareto front is extracted for post-processing. The maximum-based companion metrics (TR_max and WR_max) are not used as separate objectives in the optimization but are reported in the post-processing of the top solutions as a sanity check.

The NSGA-II algorithm is configured with a population size of 200 and a termination criterion of 300 generations. The initial population is generated by *FloatRandomSampling*, the crossover operator is *Simulated Binary Crossover* (SBX) with a probability of 0.9 and a distribution index $\eta = 15$, and the mutation operator is *Polynomial Mutation* (PM) with $\eta = 20$. Duplicate solutions are eliminated automatically at each generation, and a fixed random seed is used to ensure reproducibility. The full evolutionary history is saved for post-hoc inspection of the convergence behaviour.

6.3 Results

It can be seen in Figure 39 that the convergence of the NSGA-II algorithm across the 300 generations. The upper panel tracks the best summed objective value (TR + WR) on the Pareto front at each generation, and the lower panel tracks the Pareto front size. The summed objective rises rapidly from approximately 1.9635 at generation 0 to approximately 1.9670 by generation 50, after which it plateaus and remains stable for the remaining 250 generations. The Pareto front size grows steadily from fewer than ten non-dominated solutions in the initial population to the population cap of 200 by generation 45, and remains saturated at 200 for the rest of the run. The combination of a stable summed objective and a saturated front size indicates that the algorithm has converged well before the 300-generation termination, and that the additional generations serve only to refine the spread along the Pareto front rather than to discover further improvement in objective value.

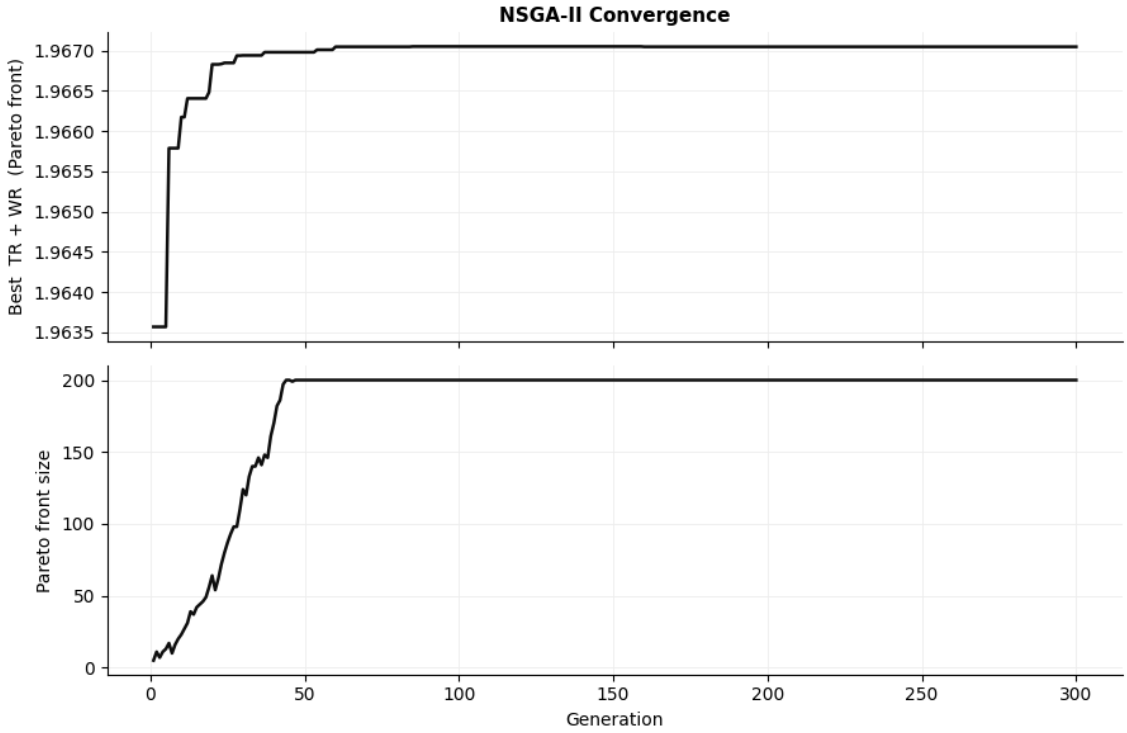

Figure 39. NSGA-II Convergence of the MOO Result (Author)

The results shown in Figure 40 is the complete optimization history (left) and a zoomed-in view of the top-five Pareto solutions (right). In the full view, the grey cloud represents all configurations evaluated across all generations, while the red points indicate the final Pareto front. The front exhibits a pronounced L-shape: a horizontal segment at WR ≈ 1.0 across a range of TR values, a vertical segment at TR ≈ 0.969 across a range of WR values, and a sharp knee region at approximately (TR_avg, WR_avg) = (0.969, 0.99). This shape indicates that the design space contains a clear "best-compromise" region in which both resilience scores are simultaneously high, beyond which further gains in one objective come at sharp expense to the other. The zoomed view (right) shows that the five highest-ranked Pareto solutions cluster very tightly inside this knee region, separated only by sub-percent differences in either objective.

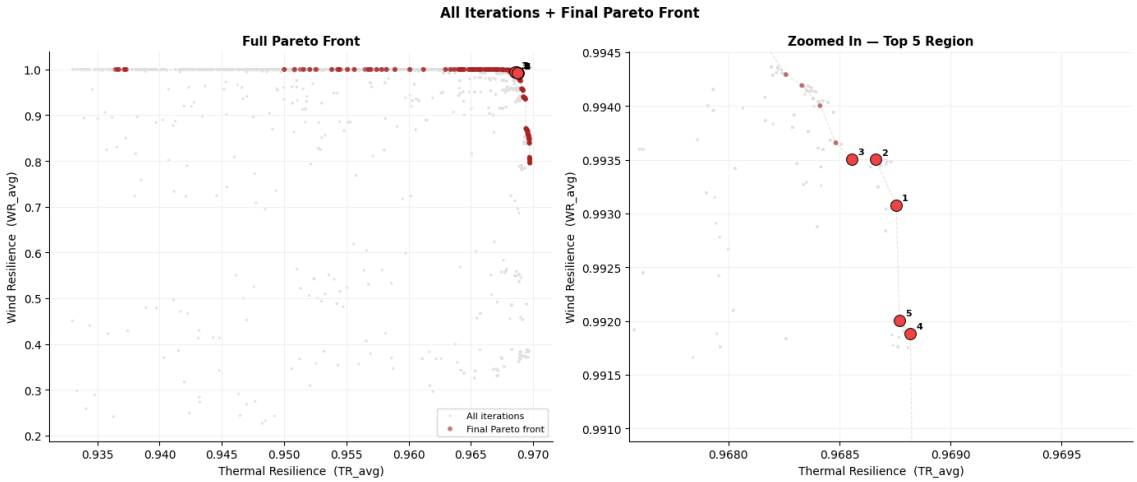

Figure 40. All iterations and Final Pareto Front Results (Author)

Figure 41 compares the TR_avg and WR_avg scores of the top five Pareto solutions. All five solutions deliver near-identical performance, with TR_avg ≈ 0.968–0.969 and WR_avg ≈ 0.991–0.994. The visual indistinguishability of the bars across the five solutions confirms what the zoomed Pareto view in Chart 2 already suggested: from a pure objective-score perspective, the top of the Pareto front represents a plateau of essentially equivalent designs, and the choice between them must be made on the basis of design preference, architectural intent, or secondary criteria not captured by the two objectives.

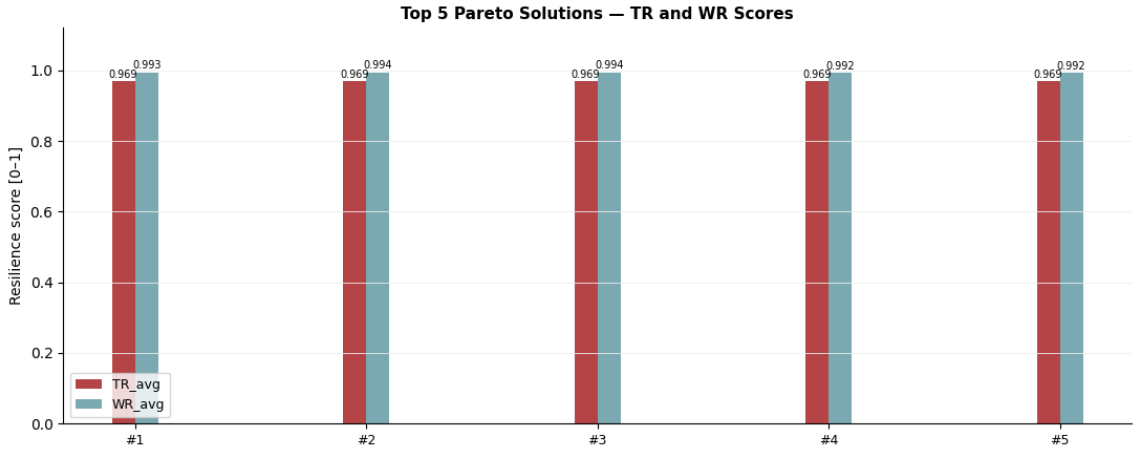

Figure 41. Top 5 Pareto Solutions with Scores (Author)

Table 18 and Table 19 report the design-variable configurations corresponding to the top five and bottom five Pareto solutions respectively with visualization shown in Figure 42. Three observations stand out.

First, the **top five solutions share a coherent design pattern**: moderate aperture ratios on all four orientations (approximately 0.40–0.45), **deep shadings on the north and east faces** (Sha_N ≈ 0.92–0.93, Sha_E ≈ 0.96–0.99), moderate shadings on the south and west faces (Sha_S ≈ 0.66–0.68, Sha_W ≈ 0.65–0.73), a **low horizontal separation ratio** (H.s.r ≈ 0.17–0.24), a **moderately high window height ratio** (W.h ≈ 0.82–0.88), and predominantly the **6 mm glass thickness** (four of five solutions). The combination of a small horizontal-separation ratio and a high window-height ratio produces narrow, tall window panels, which maximise the glazing capacity through the inverse-square dependence on the short panel dimension in the NEN-EN 16612 expression — consistent with the dominant role of window subdivision parameters identified by the wind Sobol analysis.

Second, the **bottom five solutions show a broader and noisier mix of design choices**: window height ratios as low as 0.16 (which produces short, wide window panels with lower capacity), horizontal separation ratios as high as 1.0 (large separation between windows, also reducing capacity), and inconsistent shading and aperture configurations. These solutions retain high TR_avg (≈ 0.94–0.97) but their WR_avg drops to approximately 0.80–0.89, confirming that wind resilience is the dimension on which the lower-ranked Pareto solutions fail.

Third, the **glass thickness shows a clear preference for the 6 mm option** in the top tier — consistent with its higher wind-debris resistance — even though this variable was identified as nearly negligible in the Sobol sensitivity analysis. This apparent contradiction reflects the difference between **variance contribution** (which the Sobol indices measure) and **optimal-design preference** (which the optimisation reveals): a variable can have a small global variance contribution while still being consistently set to one of its two admissible values at the optimum.

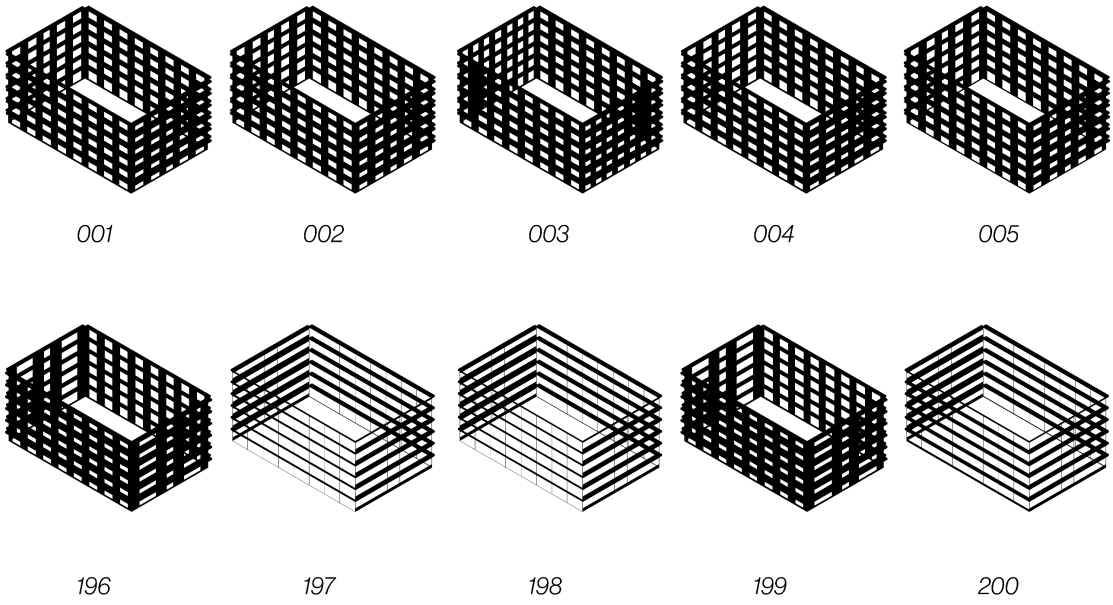

Figure 42. Top 5 and Bottom 5 Solutions Facade Geometry (Author)

Table 18. Top 5 MOO Result (Author)

Rank	TR	WR	Apt_N	Apt_E	Apt_S	Apt_W	Sha_N	Sha_E	Sha_S	Sh_W	H_s_r	W_h	G_t
1	0.968	0.993	0.427	0.413	0.440	0.420	0.924	0.994	0.656	0.728	0.237	0.84	6
2	0.968	0.993	0.431	0.411	0.440	0.401	0.931	0.956	0.660	0.651	0.231	0.849	6
3	0.968	0.993	0.418	0.406	0.426	0.401	0.919	0.990	0.675	0.721	0.168	0.841	3
4	0.968	0.993	0.404	0.446	0.440	0.415	0.925	0.999	0.660	0.651	0.242	0.836	6
5	0.968	0.991	0.440	0.407	0.438	0.409	0.919	0.964	0.663	0.721	0.221	0.884	3

Table 19. Bottom 5 MOO Result (Author)

Rank	TR	WR	Apt_N	Apt_E	Apt_S	Apt_W	Sha_N	Sha_E	Sha_S	Sh_W	H_s_r	W_h	G_t
196	0.969	0.795	0.408	0.414	0.404	0.415	0.685	0.955	0.973	0.739	0.525	0.838	6
197	0.936	0.888	0.882	0.641	0.789	0.427	0.771	0.111	0.001	0.429	0.972	0.318	3
198	0.969	0.795	0.412	0.414	0.418	0.415	0.682	0.953	0.974	0.731	0.517	0.824	6
199	0.969	0.795	0.408	0.414	0.404	0.415	0.685	0.956	0.973	0.739	0.525	0.838	6
200	0.936	0.888	0.811	0.583	0.796	0.429	0.760	0.109	0.059	0.429	0.996	0.164	3

The NSGA-II optimization converges to a stable Pareto front that contains a clear knee region in which both thermal and wind resilience scores reach approximately 0.97 and 0.99 respectively. The top-ranked solutions share a coherent geometric signature — moderate apertures, deep shading on the north and east faces, narrow-tall window panels, and the 6 mm glass option — that combines the dominant drivers identified in Chapters 4 and 5 in a complementary way. The Pareto front itself is dense and saturated, providing the designer with a continuum of essentially equivalent compromise solutions from which the final façade configuration can be selected on the basis of architectural intent or secondary considerations. The interpretation of these results, the comparison against single-objective baselines, and the implications for resilience-based design practice are discussed in Chapter 7.

7 Conclusion and Discussion

7.1 Conclusion

This thesis project has investigated the quantification of multi-hazard resilience in building façades, with the focus placed on two climate-driven stressors: heatwaves and windstorms. The central aim was to construct a data-driven methodology capable of measuring the impact of both hazards on building envelopes and translating their combined effect into a tool that supports early-stage design decisions. A targeted literature review identified clear research gaps at the intersection of resilience-based building design and façade parametric optimization, and motivated the development of a comprehensive workflow that equips façade designers with a practical means of evaluating and improving multi-hazard envelope performance.

The thermal side of the analysis began with a detailed treatment of heatwave stressors and their implications for façade behaviour and occupant comfort. A parametric Honeybee–EnergyPlus model of the Amsterdam demonstrator was developed, and the Standard Effective Temperature was adopted as the underlying comfort variable feeding a piecewise quality function Q(t), built on the formulation of Kim et al. (2024) and the resilience-loss integral originally proposed by Bruneau (2003). A Latin Hypercube sample across eleven façade design variables was generated, and random forest surrogate models were trained to predict cooling energy use intensity and the thermal resilience score. Pearson correlation, random forest feature importance, and Sobol sensitivity analyses were carried out in sequence, and all three converged on the South, North, and East apertures as the dominant geometric drivers of the thermal response.

A parallel structure was adopted for the wind side of the work. The demand–capacity ratio served as the central resilience indicator, with the wind pressure demand derived from Eddy3D CFD simulations coupled with the peak velocity pressure tabulated in the Dutch national annex to NEN-EN 1991-1-4, and the glazing capacity computed according to NEN-EN 16612:2019. The probability of failure of the wall glazing and the shading element was obtained from the FEMA P-58 analytical lognormal fragility model, and the two failure modes were combined as a series system to produce a normalized wind resilience score on the interval [0, 1]. A corresponding random forest surrogate was trained on a second Latin Hypercube dataset, and the same three sensitivity analyses identified the window height ratio and the horizontal separation ratio as the overwhelmingly dominant drivers of the wind response — a result that stands in clear contrast to the aperture-driven thermal response.

The two surrogates were then brought together in a multi-objective optimization case study based on the Amsterdam demonstrator of the MULTICARE Horizon Europe project, a serviced residential building in the Iburg district exposed to both heatwaves and windstorms in the Dutch climate. Coupling the thermal and wind surrogates inside an NSGA-II optimization produced a stable Pareto front containing a pronounced knee region where both resilience scores can be simultaneously maximized. The highest-ranked solutions shared a coherent geometric signature: moderate apertures across all four orientations, deep shading on the north and east faces, narrow-tall glazing panels driven by a low horizontal-separation ratio and a high window-height ratio, and a preference for the thicker 6 mm glass option. By formalizing hazard-specific resilience metrics, replacing expensive simulations with fast surrogates, and embedding both objectives inside a generative optimization loop, the workflow gives

designers a concrete means of identifying the design parameters that matter most and of navigating the trade-offs between hazards from the earliest project stages.

Taken as a whole, the work contributes to the advancement of resilience-based design practice by providing a robust and transferable methodology for the joint quantification and optimization of façade performance under heatwave and windstorm hazards. The insights produced here address gaps in the existing literature on multi-hazard façade design and translate directly into practical guidance for designing building envelopes that hold up against an increasingly varied and intense climatic context.

7.2 Discussion

Contribution to current design practice

Current façade design practice in the Netherlands typically addresses thermal performance and wind performance as separate verification steps. Thermal performance is checked at the very late design stage against the TO-juli overheating indicator, while wind performance is verified by a structural engineer against the prescriptive code values of NEN-EN 1991-1-4 once the geometry has been frozen. Neither workflow exposes the design team to the trade-offs between the two hazards during the geometry-setting phase, which is precisely when those trade-offs can be acted upon at no additional cost. The contribution of this thesis is therefore not the simulation methods themselves, which exist in mature form, but the integration of these methods into a single optimisation-ready loop that delivers Pareto-optimal façade configurations early in the design process. The surrogate-based formulation closes the practical gap between the available physics-based tools and the iteration speed required by an architectural workflow: a design configuration that would require minutes of CFD or EnergyPlus simulation can now be evaluated in milliseconds, and a population of two hundred configurations can be evolved across three hundred generations within the time previously required for a handful of one-off evaluations. This shifts multi-hazard resilience from a *verification* role at the end of the design process to a *generative* role at the beginning.

Scope of the parametric design space

The eleven design variables explored in this thesis are predominantly geometric: four orientation-specific aperture ratios, four orientation-specific shading depths, two window-subdivision ratios, and the outer-pane glass thickness. The last of these is the only variable that engages a material specification, and it operates almost exclusively on the wind side through the glazing capacity. The framework therefore investigates resilience as a function of façade geometry rather than as a function of façade material composition, and the dominant drivers identified in Chapters 4 and 5 should be read in that light.

This is a deliberate scoping decision rather than a methodological constraint. Keeping the design space geometric was useful for two reasons. First, geometric variables are the most direct levers available to architects during early-stage design, which aligns the workflow with the decision-making process it is intended to support. Second, restricting the variables to geometry kept the dimensionality of the design space manageable for surrogate-model training within the available computational budget.

The framework itself, however, is not limited to geometric parameters. Several material and thermophysical variables would be natural extensions of the design space if the workflow were applied to a project where these are not yet fixed. The most obvious candidates on the thermal side are the glazing U-value (number of panes, gas fill, low-emissivity coatings), the opaque-wall U-value (insulation thickness and conductivity), the solar heat gain coefficient (SHGC or g-value) of the glazing, the thermal mass of the opaque construction, and the solar absorptance of the external surface finish. On the wind side, the natural extensions are the glass type (annealed, heat-strengthened, thermally toughened, or laminated), the inner pane thickness of the IGU, and the frame and bracket strength at the connection details. Including these would broaden the resilience picture from a purely geometric one to a coupled geometric-and-material one, and would in particular allow the trade-off between glazing area and glazing performance to be navigated directly.

Adding such variables would not require any change to the workflow logic: the LHS sampler, the simulation pipeline, the surrogate model, and the NSGA-II routine all accept additional variables without modification. The practical constraint is the size of the LHS dataset required to train a reliable surrogate, which grows with the dimensionality of the design space. Future work that extends the parameter set would need to expand the LHS sample correspondingly and may benefit from screening methods (such as Morris elementary effects) to prune variables with negligible contribution before committing computational budget to the full Sobol analysis.

Limitations of the wind resilience model

Several limitations of the wind resilience formulation deserve explicit acknowledgement.
The fragility curves used in this work are constructed analytically from the NEN-EN 16612:2019 design capacities, treated as the median, rather than from physical impact or pressure tests. The absolute failure probability values should therefore not be interpreted as calibrated predictions of real-world failure rates; their purpose is to support the comparative ranking of design variants rather than to forecast absolute risk.

The design capacity itself is computed from NEN-EN 16612:2019, which incorporates material partial safety factors. Actual median failure pressures observed in physical panels are likely to be higher than the computed capacity C, which means the fragility curves overestimate the failure probability relative to experimentally calibrated curves.

A single dispersion parameter β is applied uniformly to both the wall glazing and the shading element. In reality, dispersion would differ between glass panels (where dispersion is governed by surface flaw statistics) and bracket systems (where dispersion is governed by manufacturing tolerances).
The glazing capacity is computed using the linear plate-bending theory of NEN-EN 16612 ($p^* = 0$), which is conservative for large panels where non-linear membrane action would reduce stress significantly. This conservatism reinforces the comparative rather than predictive nature of the fragility outputs.

The series-reliability model used to combine the wall and shading failure modes assumes statistical independence between the two elements. Because the wall glazing and the shading element are fixed to the same structural frame, their failures may be correlated under extreme wind events, leading to a slight underestimation of the system failure probability.

Finally, the demand–capacity calculation uses one representative panel per orientation, with panel dimensions derived from the window-to-wall ratio and window subdivision parameters. The probability that *at least one* panel fails across the full façade height is necessarily higher than the probability that any single panel fails, which means the per-orientation fragility curves underestimate the full-façade failure probability.

These limitations do not undermine the use of the model as a relative-performance tool for design exploration but should be addressed in any subsequent step that aims at absolute risk quantification or code-compliant safety verification.

Choice of average over maximum as the optimization objective

The two objectives passed to the NSGA-II algorithm are formed by averaging operations that have a different meaning on each side. For the thermal objective, the resilience score is first computed per floor; the value used by the optimization is the average across all six floors of the building, which represents the typical thermal performance of the building rather than the performance of a single critical story. For the wind objective, the pressure coefficient on each façade is first extracted from a large set of probing points generated by Eddy3D; the value used by the optimization is the area-weighted mean Cp on the surface, while the maximum represents the most extreme single probing point.

The choice of the mean rather than the maximum is motivated by the physical behavior of the system on each side. On the thermal side, averaging across floors reflects the fact that the resilience metric is intended to describe the building as a whole rather than the response of any individual story. On the wind side, averaging across the surface reflects the fact that the shading element is a continuous structural component that resists wind loads systematically, and that a single high-pressure point captured at one probing location is unlikely to cause failure of the element if the surrounding area is not similarly loaded. Using the surface mean is therefore consistent with the physical interpretation of demand on a distributed component.

The implication of these choices is that the optimisation maximises a measure of typical, system-level performance rather than worst-case behaviour at a single point or floor. A more risk-averse formulation could use the per-floor or per-point maxima as the objective instead, or could combine the mean and the maximum through a weighted sum or a min-max constraint. The maximum-based companion metrics (TR_max and WR_max) are retained as post-processing diagnostics, and inspection of the top-five Pareto solutions confirms that the maxima track the means closely in this case study.

Applicability and scalability

The workflow is intentionally parameter-agnostic and case-agnostic at the methodological level. The simulation engines (EnergyPlus and Eddy3D), the resilience quantification framework, the LHS sampling, the surrogate model, and the NSGA-II routine all operate on inputs that are not specific to the Amsterdam demonstrator. In principle, the framework can be transferred to a different building geometry, climate context, or construction system by replacing the weather file, the wind hazard

reference, the building geometry, and the code-specific capacity expression, without altering the workflow logic itself.

In practice, three caveats apply to such a transfer. First, the resilience scores depend on user-defined thresholds (the SET comfort and alert thresholds for thermal, the baseline damage threshold for wind), which should be re-selected for the new context. Second, the surrogate model must be retrained on a new LHS dataset for each new case, because the input–output mapping is geometry- and climate-specific; the trained random forest for *De Centrale IJburg* would not generalise to a high-rise in a different climate zone. Third, the dominant design drivers identified for this case study (apertures for thermal, window subdivision for wind) reflect a specific combination of building proportions, prevailing wind direction, and hazard intensity, and these drivers may shift when the workflow is applied to a substantially different building or climate. Recovering them is one of the principal outputs of the workflow itself.

Within these caveats, the workflow scales naturally. The same methodology applies whether the design space contains eleven parameters or thirty, whether the building is a mid-rise demonstrator or a high-rise tower, and whether the climate context is Dutch or otherwise. The framework's value lies precisely in providing a transferable structure within which case-specific findings can be generated.

Limited trade-off between thermal and wind resilience

A notable feature of the Pareto front produced by the multi-objective optimisation is that the conventional notion of a clear "trade-off curve" between thermal and wind resilience does not appear over most of the design space. The front exhibits a pronounced L-shape with a sharp knee region in which both resilience scores reach near-optimal values, and the actual exchange between the two objectives is only visible at the extreme tails of the front. This shape reflects four reinforcing factors in this case study. First, as established in Chapter 4 and Chapter 5, thermal and wind resilience are governed by disjoint subsets of the design space: the thermal response is driven by the orientation-specific apertures, whereas the wind response is driven by the window subdivision parameters. Because the two hazards engage independent design levers, the two objectives do not need to compete directly in most of the feasible region. Second, the distribution of the wind resilience score itself is heavily right-skewed in the sampled dataset, with the majority of configurations reaching WR_avg values close to one under the 15 m/s baseline hazard. This concentration means that wind resilience saturates quickly across a broad portion of the design space and does not act as a binding constraint until extreme configurations are reached. Third, the wind resilience score is built on a fragility model that only begins to deteriorate meaningfully once the demand-to-capacity ratio approaches one, so configurations within a relatively wide envelope of design choices yield similar near-maximum wind resilience values.

Fourth, the thermal resilience score may itself be artificially concentrated near the upper bound because of the SET threshold settings used in the quality function. The alert threshold of 30 °C, taken from the KNMI tropical-day definition, is set such that the indoor SET in the simulated demonstrator only rarely exceeds it, and the gap between the comfort threshold (24 °C) and the alert threshold (30 °C) keeps Q(t) high across most of the simulated period. As a result, the thermal resilience score is biased toward values close to one, with relatively few configurations exhibiting genuinely low TR_avg. This has two consequences for the optimisation. On the data side, the random forest surrogate is trained on a dataset in which the low-resilience region is under-represented, which means the model is less reliable when

extrapolating to extreme thermal configurations than when interpolating within the well-sampled high-resilience region. On the optimisation side, the apparent flatness of the Pareto front in the high-TR region partly reflects this score concentration rather than a true insensitivity of the building to design choices. A tighter alert threshold (for example 28 °C, closer to the upper end of adaptive thermal comfort) or an explicit redefinition of the linear ramp between comfort and alert would broaden the distribution of TR_avg, populate the lower end of the score range more uniformly, and likely sharpen the trade-off curve observed in the Pareto front.

The practical implication of this finding is positive for design: in the context of the Amsterdam demonstrator and the Dutch climate, a designer does not need to sacrifice thermal performance to obtain wind resilience or vice versa, and a continuum of essentially equivalent compromise solutions exists at the top of the Pareto front. The methodological implication is more nuanced. The absence of a strong trade-off should not be read as a general property of multi-hazard façade design; it is a property of this specific combination of building geometry, hazard intensity, parametric scope, and threshold choices. A more aggressive wind-hazard threshold (for example the 22 m/s significant-loss value of Fonseca Cerda et al., 2025 rather than the 15 m/s baseline), a tighter SET alert threshold for the thermal side, a different climate context with more frequent extreme heat, or an expanded design space that introduces variables which couple the two hazards (such as glazing U-value, SHGC, or frame strength) could produce a Pareto front with a much sharper visible trade-off. The current result therefore confirms the workflow's ability to produce a Pareto front and to identify joint optima, but the qualitative shape of the front should be re-examined whenever the workflow is applied to a different case or threshold configuration.

7.3 Answer to research questions

The main research question is:

“How can multi-objective optimization approach be used to relate façade design parameters to wind and thermal resilience metrics and to generate design options that support designers in balancing trade-offs between multiple hazards?”

The thesis answers this question by proposing and validating a five-stage data-driven workflow — hazard-specific simulation, resilience quantification, dataset generation through Latin Hypercube Sampling, surrogate model training, and NSGA-II multi-objective optimisation — that makes the relationship between façade design parameters and multi-hazard resilience both quantifiable and operationally usable. The optimisation produces a Pareto-optimal set of design configurations that explicitly visualises the trade-offs between thermal and wind resilience, allowing the designer to select among compromise solutions rather than committing to a single hazard-specific optimum. The five sub-questions are addressed in turn below.

(1) How can thermal and wind resilience be quantified in a way that is suitable for modelling and optimization?

Thermal resilience is quantified through a quality function Q(t) that maps the Standard Effective Temperature (SET) onto a normalized comfort score, integrated over the heatwave period into a thermal resilience loss following the Bruneau (2003) formulation and adapted from Kim et al. (2024).

The loss is then normalized by the maximum possible loss to produce a bounded score on [0, 1]. Wind resilience is quantified through a demand–capacity fragility model in which the wind pressure demand is computed from the Eddy3D-derived pressure coefficients and the peak velocity pressure from NEN-EN 1991-1-4 NB:2019, the glazing capacity is derived from NEN-EN 16612:2019, and the probability of failure is evaluated using the FEMA P-58 analytical lognormal fragility expression. The wall and shading failures are combined as a series system, and the resulting wind resilience score is also bounded on [0, 1]. Both metrics are therefore continuous, bounded, comparable across designs, and directly usable as objective functions in the optimization.

(2) How do variations in façade design parameters affect wind and thermal resilience metrics across the sampled design space?

The Latin Hypercube exploration of the eleven-dimensional design space revealed that the two resilience metrics respond to design changes in very different ways. **Thermal resilience** is influenced by a relatively broad set of parameters: the four orientation-specific apertures all contribute, with the South, North, and East apertures producing the largest swings (Pearson correlations of $|r| \approx 0.55–0.69$ against the floor-averaged thermal resilience score), and the South shading depth adding a moderate secondary effect ($|r| \approx 0.27–0.38$). Together, varying these five parameters across their bounded ranges shifts the thermal resilience score by approximately 0.06 absolute units (from roughly 0.93 to 0.99 at the floor-averaged level), with the remaining six variables — the other shading depths, window subdivision parameters, and glass thickness — producing essentially no measurable change in the thermal response.

Wind resilience behaves differently. The score is concentrated near the upper bound (the majority of sampled configurations achieve $WR_avg \geq 0.95$ under the 15 m/s baseline hazard), but a meaningful subset of configurations drops down to $WR_avg \approx 0.2$, indicating that some design changes are capable of degrading the response substantially. The variation is driven almost entirely by the **window height ratio** ($|r| \approx 0.72–0.79$) and the **horizontal separation ratio** ($|r| \approx 0.32–0.33$), both of which control the dimensions of the individual glazed panels and therefore the glazing capacity under wind load. The four apertures, the four shading depths, and the glass thickness produce only marginal changes in WR_avg across the explored range, despite the strong influence of the shading depths on the **intermediate CFD outputs** (the wall and shading pressure coefficients). The decoupling between the strong shading effect on Cp and the weak shading effect on WR_avg indicates that the resilience score, as defined here through the demand–capacity fragility, is moderated more by the structural geometry of the panels than by the local aerodynamic field.

In short, the sampled design space produces a clear bifurcation between two groups of parameters: **apertures (with secondary shading)** dominate the thermal metric, while **window subdivision parameters** dominate the wind metric. Glass thickness, despite being the only material-resistance variable in the parameter set, produces negligible variation in either metric at the bounded ranges considered. The relative magnitudes and the specific ranking of the individual drivers within each group are addressed in detail in sub-question 3.

(3) What trade-offs and synergies between wind and thermal resilience emerge when different façade design strategies are explored using MOO?

The NSGA-II optimization reveals that thermal and wind resilience engage **disjoint subsets of the design space**: apertures dominate the thermal response, while window subdivision dominates the wind response. Because these subsets do not directly conflict, the resulting Pareto front exhibits a pronounced L-shape with a sharp knee region in which both objectives can be jointly maximized. The top-ranked Pareto solutions combine moderate apertures (≈ 0.40–0.45) with narrow-tall window panels (low horizontal separation, high window height ratio) and deep shading on the north and east orientations. The trade-off becomes visible only at the extremes of the Pareto front, where pushing one objective beyond its knee value produces sharp degradation in the other. The optimization therefore reveals more **synergy** than competition between the two hazards, a finding that would not have been visible without the joint formulation.

(4) How can Pareto-optimal solutions support designers in making informed façade design decisions that balance wind and heat hazards?

The Pareto front produced by the workflow gives designers a continuum of objectively non-dominated façade configurations from which to select the final design. Because the top of the Pareto front contains a dense plateau of essentially equivalent solutions (TR_avg ≈ 0.968–0.969, WR_avg ≈ 0.991–0.994), the designer retains substantial architectural freedom in selecting the final configuration on the basis of secondary criteria — aesthetic preference, daylight performance, cost, constructability — without compromising on resilience performance. Conversely, the tail of the Pareto front identifies configurations that should be avoided, namely those with wide-short window panels and high horizontal separation, which sacrifice wind resilience without commensurate gain. The workflow therefore supports informed decision-making both by revealing what is achievable and by mapping the trade-off boundary explicitly.

7.4 Further development

Several extensions of this thesis are envisaged for future work.
The first natural extension is to upscale the analysis from a single building to the urban scale. The present workflow treats the demonstrator as an isolated object in its own CFD domain and its own thermal model. A more realistic representation would embed the building within its surrounding urban context to capture the urban heat island effect in the thermal simulation and the urban canyon effects in the wind simulation. This would allow the workflow to assess how the resilience of a façade depends not only on its own design but also on the configuration of the neighbouring buildings, which is increasingly relevant as cities densify and adapt to climate change.
A second extension is to apply the workflow to high-rise buildings. The fundamental aerodynamics of high-rises differs substantially from that of the mid-rise demonstrator considered here: wind pressures vary more strongly with height, leeward suction is more pronounced, and the consequences of glazing failure are more severe in terms of debris-fall risk. The same surrogate-based workflow could be re-trained on a high-rise sample to investigate whether the dominant drivers identified in this thesis (apertures for thermal, window subdivision for wind) generalise, or whether the high-rise context introduces new dominant parameters such as orientation-specific glass specifications or façade-zoning strategies.

A third extension is to integrate pedestrian-level wind and thermal comfort as additional objectives in the optimisation. The CFD output already contains the ground-level flow field, and the thermal simulation could be coupled with outdoor microclimate metrics. Adding pedestrian comfort as a third or

fourth objective would transform the workflow from a building-scale tool into a comprehensive **multi-**hazard, multi-scale design support tool that captures the consequences of façade design choices on the surrounding public space.

Further refinements include broadening the parametric space to incorporate currently fixed variables (glazing U-value, frame specification, opaque-wall properties), exploring different climatic contexts beyond the Netherlands, comparing the random forest surrogate against alternative ML methods (gradient boosting, neural networks), and validating the surrogate-predicted Pareto front against full-simulation evaluations at a few representative Pareto points to quantify the residual prediction error introduced by the surrogate. The methodology is intentionally parameter-agnostic and the workflow itself transfers without modification to any of these extensions.

References

Abdallah, A. S. H., Mahmoud, R. M. A., Ragab, A., & Gomaa, M. M. (2025). A Multi-Objective Optimization Method for Enhancing Outdoor Environmental Quality in University Courtyards in Hot Arid Climates. *Buildings*, *15*(17), 3140. https://doi.org/10.3390/buildings15173140

Alsukkar, M., Ibrahim, A., & Eltaweel, A. (2026). Multi-objective optimization of daylighting systems for energy efficiency and thermal-visual comfort in buildings: A review. *Building and Environment*, *288*, 113921. https://doi.org/10.1016/j.buildenv.2025.113921

ASHRAE. (2020). *ANSI/ASHRAE Standard 55-2020: Thermal Environmental Conditions for Human Occupancy*.

Attia, S., Levinson, R., Ndongo, E., Holzer, P., Berk Kazanci, O., Homaei, S., Zhang, C., Olesen, B. W., Qi, D., Hamdy, M., & Heiselberg, P. (2021). Resilient cooling of buildings to protect against heat waves and power outages: Key concepts and definition. *Energy and Buildings*, *239*, 110869. https://doi.org/10.1016/j.enbuild.2021.110869

Behr, R. A., Karson, M. J., & Minor, J. E. (1991). Reliability analysis of window glass failure pressure data. *Structural Safety*, *11*(1), 43–58. https://doi.org/10.1016/0167-4730(91)90026-6

Bianchi, S. (2023). Integrating resilience in the multi-hazard sustainable design of buildings. *Disaster Prevention and Resilience*, *2*(3). https://doi.org/10.20517/dpr.2023.16

Bianchi, S., Andriotis, C., Klein, T., & Overend, M. (2024). Multi-criteria design methods in façade engineering: State-of-the-art and future trends. *Building and Environment*, *250*, 111184. https://doi.org/10.1016/j.buildenv.2024.111184

Bianchi, S., Kim, K., Matteoni, M., Koniari, A. M., Koning, K., Costache, R.-D., Ciobotaru, N., Luna-Navarro, A., Peng, Z., Ciurlanti, J., Shahriari, H., Mittal, D., Stavridou, E., Silva, A., Petrini, F., Palmieri, M., Pampanin, S., & Overend, M. (2025). *Resilience Readiness Levels for Buildings: Establishing Multi-Hazard Resilience Metrics and Rating Systems*. SSRN. https://doi.org/10.2139/ssrn.5177406

Bruneau, M., Asce, F., Barbato, M., Asce, M., Padgett, J. E., Asce, A. M., Zaghi, A. E., Asce, M., Mitrani-Reiser, J., Asce, A. M., Li, Y., & Asce, M. (2017). *State of the Art of Multihazard Design*.

Bruneau, M., Chang, S. E., Eguchi, R. T., Lee, G. C., O'Rourke, T. D., Reinhorn, A. M., Shinozuka, M., Tierney, K., Wallace, W. A., & Von Winterfeldt, D. (2003). A Framework to Quantitatively Assess and Enhance the Seismic Resilience of Communities. *Earthquake Spectra*, *19*(4), 733–752. https://doi.org/10.1193/1.1623497

Bruneau, M., & Reinhorn, A. (2006). Overview of the Resilience Concept. *Proceedings of the 8th U.S. National Conference on Earthquake Engineering*.

Bucking, S., Rostami, M., Reinhart, J., & St-Jacques, M. (2022). On modelling of resiliency events using building performance simulation: A multi-objective approach. *Journal of Building Performance Simulation*, *15*(3), 307–322. https://doi.org/10.1080/19401493.2022.2044906

Caieiro Da Costa, V. A., Soares Chvatal, K. M., Melo, A. P., & Souza Fernandes, R. A. (2026). Optimized design solutions for multifamily housing: A multi-objective approach to thermal resilience under heatwave conditions. *Energy and Buildings*, *353*, 116886. https://doi.org/10.1016/j.enbuild.2025.116886

Calvin, K., Dasgupta, D., Krinner, G., Mukherji, A., Thorne, P. W., Trisos, C., Romero, J., Aldunce, P., Barrett, K., Blanco, G., Cheung, W. W. L., Connors, S., Denton, F., Diongue-Niang, A., Dodman, D., Garschagen, M., Geden, O., Hayward, B., Jones, C., … Ha, M. (with Lee, H.). (2023). *IPCC, 2023: Climate Change 2023: Synthesis Report. Contribution of Working Groups I, II and III to the Sixth Assessment Report of the Intergovernmental Panel on Climate Change [Core Writing Team, H. Lee and J. Romero (eds.)]. IPCC, Geneva, Switzerland.* (P. Arias, M. Bustamante, I. Elgizouli, G. Flato, M. Howden, C. Méndez-Vallejo, J. J. Pereira, R. Pichs-Madruga, S. K. Rose, Y. Saheb, R. Sánchez Rodríguez, D. Ürge-Vorsatz, C. Xiao, N. Yassaa, J. Romero, J. Kim, E. F. Haites, Y. Jung, R. Stavins, … C. Péan, Eds.; First). Intergovernmental Panel on Climate Change (IPCC). https://doi.org/10.59327/IPCC/AR6-9789291691647

Dias, J. M. (2025). Enhancing the resilience of urban buildings against extreme wind events: Evaluation, mitigation, and diagnostic approaches. *Sustainable Cities and Society: Advances*, *1*(1), 100008. https://doi.org/10.1016/j.scsadv.2025.100008

Directive (EU) 2024/1275. (2024). *Directive (EU) 2024/1275 of the European Parliament and of the Council of 24 April 2024 on the energy performance of buildings (recast) (Text with EEA relevance)*.

Duan, H., Dong, Y., & Ji, Q. (2026). Multi-objective optimization of windows and PV louvers on the south façade for cold-region office buildings using machine learning and NSGA-II. *Building and Environment*, *288*, 113984. https://doi.org/10.1016/j.buildenv.2025.113984

Eissa, M., Metwally, O., Alawode, K. J., Elawady, A., & Lori, G. (2025). Performance of high-rise building façades under wind loading: A state-of-the-art review. *Journal of Building Engineering*, *113*, 114072. https://doi.org/10.1016/j.jobe.2025.114072

European Comission. (2021). *Forging a climate-resilient Europe—The new EU Strategy on Adaptation to Climate Change*.

European Environment Agency (EEA). (2025, October 14). *Economic losses from weather- and climate-related extremes in Europe*. European Environment Agency (EEA). https://www.eea.europa.eu/en/analysis/indicators/economic-losses-from-climate-related?activeAccordion=ecdb3bcf-bbe9-4978-b5cf-0b136399d9f8

FEMA P-58-1. (2018). *Seismic Performance Assessment of Buildings*. *1*(2nd Edition).

Fonseca Cerda, M. D. S., De Moel, H., Van Ederen, D., Aerts, J. C. J. H., Botzen, W. J. W., & Haer, T. (2025). Empirical evaluation of windstorm losses and meteorological variables over the Netherlands. *Natural Hazards*, *121*(5), 6085–6106. https://doi.org/10.1007/s11069-024-07024-y

Gacu, J., Kantoush, S., Candelario, R., Falculan, J., Moaje, K. V., Famaran, M. J., Nepomuceno, M., Ebon, J. A., Parungao, R., Ignacio, R., Merida, M., Pastrana, P. M., & Quinton, E. (2025). Integrated multi-hazard risk assessment under compound disasters using analytical

hierarchy process (AHP). *Heliyon*, *11*(11), e43173. https://doi.org/10.1016/j.heliyon.2025.e43173

Geurts, C. P. W., van Staalduinen, P. C., & de Wit, M. S. (2004). Towards a reliable design of facade and roof elements against wind loading. *TNO Building and Construction Research*, *49*(2).

Guo, X., Lu, S., Huang, Y., Gu, S., & Guo, Q. (2026). Pedestrian-level wind environment prediction and Human-AI collaborative optimization in football stadium-centered high-density urban blocks. *Building and Environment*, *288*, 113970. https://doi.org/10.1016/j.buildenv.2025.113970

Gupta, H. S., Adluri, T., Sanderson, D., González, A. D., Nicholson, C. D., & Cox, D. (2024). Multi-objective optimization of mitigation strategies for buildings subject to multiple hazards. *International Journal of Disaster Risk Reduction*, *100*, 104125. https://doi.org/10.1016/j.ijdrr.2023.104125

Javanroodi, K., Nik, V. M., & Adl-Zarrabi, B. (2020). A multi-objective optimization framework for designing climate-resilient building forms in urban areas. *IOP Conference Series: Earth and Environmental Science*, *588*(3), 032036. https://doi.org/10.1088/1755-1315/588/3/032036

Kastner, P., & Dogan, T. (2022). Eddy3D: A toolkit for decoupled outdoor thermal comfort simulations in urban areas. *Building and Environment*, *212*, 108639. https://doi.org/10.1016/j.buildenv.2021.108639

Kim, K., D'Amore, S., Luna-Navarro, A., Konstantinou, T., Overend, M., Pampanin, S., & Bianchi, S. (2025). *Integrating Heat and Seismic Risk: A Multi-Objective Decision-Making Approach for Facade Retrofit Design*.

Kim, K., Luna-Navarro, A., Ciurlanti, J., & Bianchi, S. (2024). A multi-criteria decision support framework for designing seismic and thermal resilient facades. *Architecture, Structures and Construction*, *4*(2–4), 195–210. https://doi.org/10.1007/s44150-024-00116-0

Krelling, A. F., Lamberts, R., Malik, J., Zhang, W., Sun, K., & Hong, T. (2024). Defining weather scenarios for simulation-based assessment of thermal resilience of buildings under current

and future climates: A case study in Brazil. *Sustainable Cities and Society*, *107*, 105460. https://doi.org/10.1016/j.scs.2024.105460

Lima-Castillo, I. F., Gómez-Martínez, R., & Pozos-Estrada, A. (2018). Methodology to Develop Fragility Curves of Glass Façades Under Wind-Induced Pressure. *International Journal of Civil Engineering*, *17*, 347–359. https://doi.org/https://doi.org/10.1007/s40999-018-0360-6

Navarro, A. L., Kim, K., & Böke, J. (2024). *D5.1 Multi-Criteria Framework for Resilient Facades and Components*.

NEN-EN 1991-1-4+A1+C2/NB+C2. (1991).

NEN-EN 16612. (2019). *Glass in building—Determination of the lateral load resistance of glass panes by calculation*.

NOAA. (2019). [Dataset]. https://www.ncei.noaa.gov/data/global-hourly/access/2019/06240099999.csv

Omidian, P., & Khaji, N. (2022). A multi-objective optimization framework for seismic resilience enhancement of typical existing RC buildings. *Journal of Building Engineering*, *52*, 104361. https://doi.org/10.1016/j.jobe.2022.104361

Ouyang, Z., & Spence, S. M. J. (2019). A performance-based damage estimation framework for the building envelope of wind-excited engineered structures. *Journal of Wind Engineering and Industrial Aerodynamics*, *186*, 139–154. https://doi.org/10.1016/j.jweia.2019.01.001

Ouyang, Z., & Spence, S. M. J. (2020). A Performance-Based Wind Engineering Framework for Envelope Systems of Engineered Buildings Subject to Directional Wind and Rain Hazards. *Journal of Structural Engineering*, *146*(5), 04020049. https://doi.org/10.1061/(ASCE)ST.1943-541X.0002568

Ouyang, Z., & Spence, S. M. J. (2021). A Performance-Based Wind Engineering Framework for Engineered Building Systems Subject to Hurricanes. *Frontiers in Built Environment*, *7*, 720764. https://doi.org/10.3389/fbuil.2021.720764

Patterson, M. (2022). Resilience by design: Building facades for tomorrow. In *Rethinking Building Skins* (pp. 359–375). Elsevier. https://doi.org/10.1016/B978-0-12-822477-9.00002-4

Pérez-Bella, J. M., Domínguez-Hernández, J., Orna-Carmona, M., López-Julián, P. L., & Ibarz-Montaner, E. (2025). Comprehensive and enhanced characterisation of wind-driven rain exposure on building façades throughout the Netherlands. *Building and Environment*, *271*, 112631. https://doi.org/10.1016/j.buildenv.2025.112631

Perkins, S. E., & Alexander, L. V. (2013). On the Measurement of Heat Waves. *Journal of Climate*, *26*(13), 4500–4517. https://doi.org/10.1175/JCLI-D-12-00383.1

Pyrgou, A., Castaldo, V. L., Pisello, A. L., Cotana, F., & Santamouris, M. (2017). On the effect of summer heatwaves and urban overheating on building thermal-energy performance in central Italy. *Sustainable Cities and Society*, *28*, 187–200. https://doi.org/10.1016/j.scs.2016.09.012

Qin, H., Niu, X., & Zhai, C. (2025). Resilience Assessment for Urban High-rise Buildings Subjected to Typhoon-induced Wind and Rain Hazards. *Journal of Building Engineering*, 114800. https://doi.org/10.1016/j.jobe.2025.114800

Qin, H., Niu, X., & Zhai, C. (2026). Resilience assessment for urban high-rise buildings subjected to typhoon-induced wind and rain hazards. *Journal of Building Engineering*, *118*, 114800. https://doi.org/10.1016/j.jobe.2025.114800

Sadaphal, A. (2024). *A Digital Design Tool for Floods and Heatwaves Resilient Facade System*.

Sayyaadi, H. (2021). Optimization basics. In *Modeling, Assessment, and Optimization of Energy Systems* (pp. 327–430). Elsevier. https://doi.org/10.1016/B978-0-12-816656-7.00006-3

Tokgoz, B. E., & Gheorghe, A. V. (2013). Resilience quantification and its application to a residential building subject to hurricane winds. *International Journal of Disaster Risk Science*, *4*(3), 105–114. https://doi.org/10.1007/s13753-013-0012-z

United Nations Office for Disaster Risk Reduction (UNDRR). (2025). *GLOBAL ASSESSMENT REPORT ON DISASTER RISK REDUCTION 2025: Resilience pays*. UNITED NATIONS.

Yu, Q.-Q., Liu, L.-H., Gu, X.-L., & Zhang, Y.-Y. (2025a). Probabilistic multi-hazard risk assessment of high-rise buildings subjected to concurrent earthquakes and strong winds. *Engineering Structures*, *331*, 119972. https://doi.org/10.1016/j.engstruct.2025.119972

Yu, Q.-Q., Liu, L.-H., Gu, X.-L., & Zhang, Y.-Y. (2025b). Probabilistic multi-hazard risk assessment of high-rise buildings subjected to concurrent earthquakes and strong winds. *Engineering Structures*, *331*, 119972. https://doi.org/10.1016/j.engstruct.2025.119972

Appendix A

Grasshopper Script that are used for the whole framework are presented here

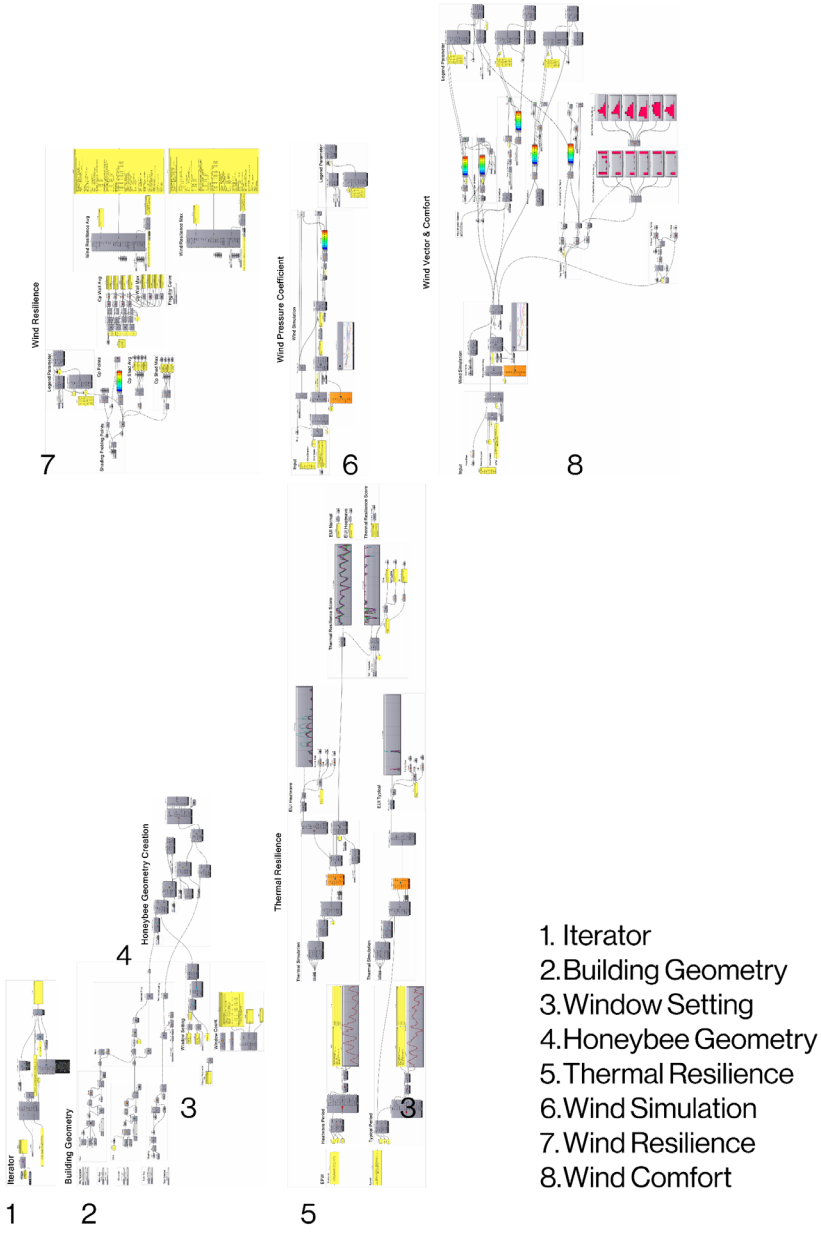

Appendix 1. Grasshopper Script for the framework (Author)

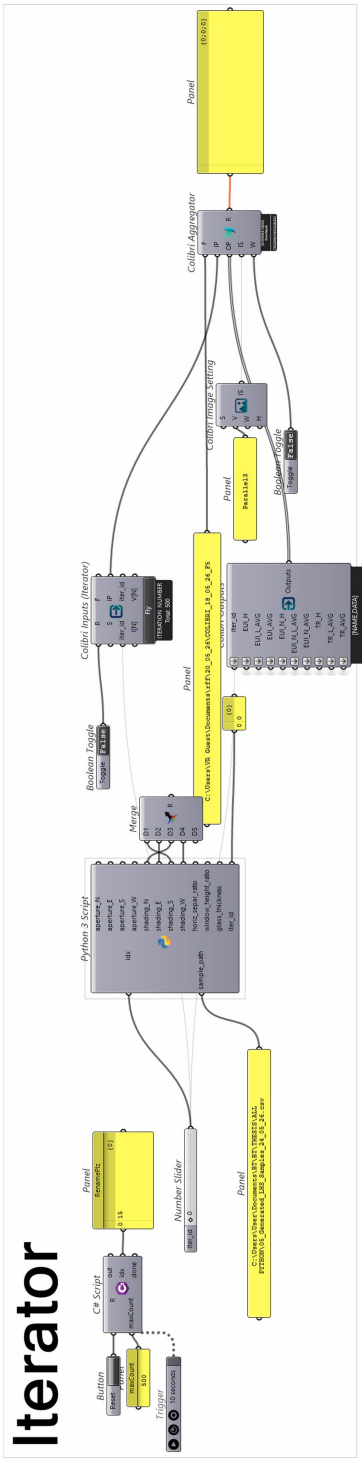

Appendix 2. Grasshopper Script 1: Iterator

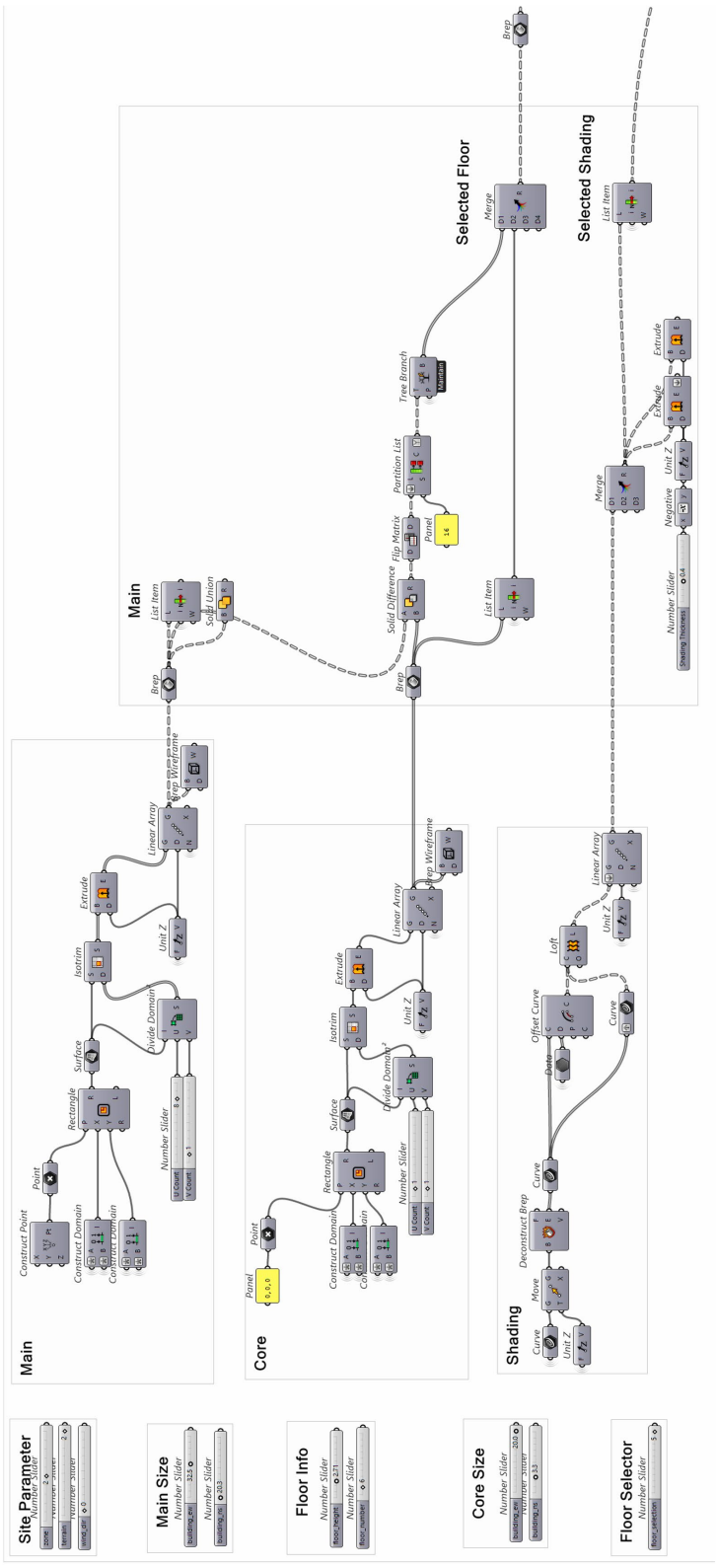

Appendix 3. Grasshopper Script 2: Building Geometry (Author)

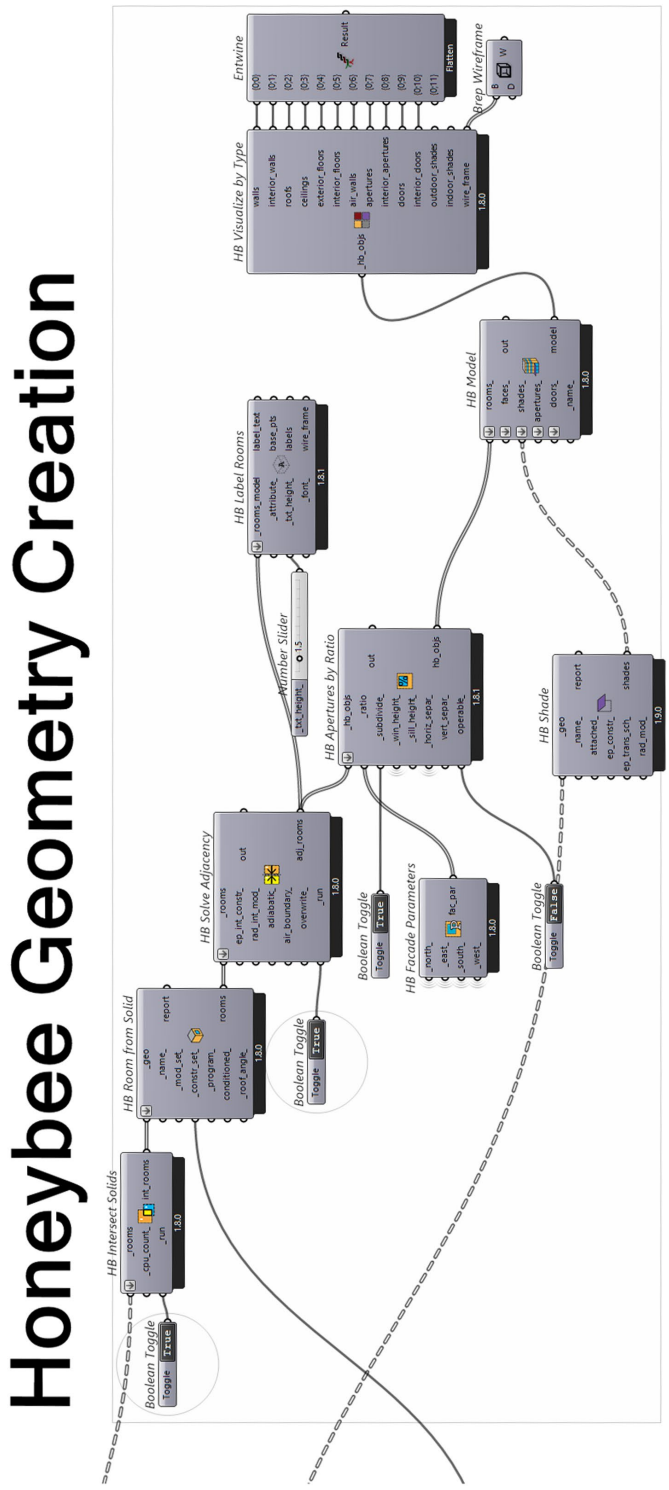

Appendix 4. Grasshopper Script 3: Honeybee Geometry Creation (Author)

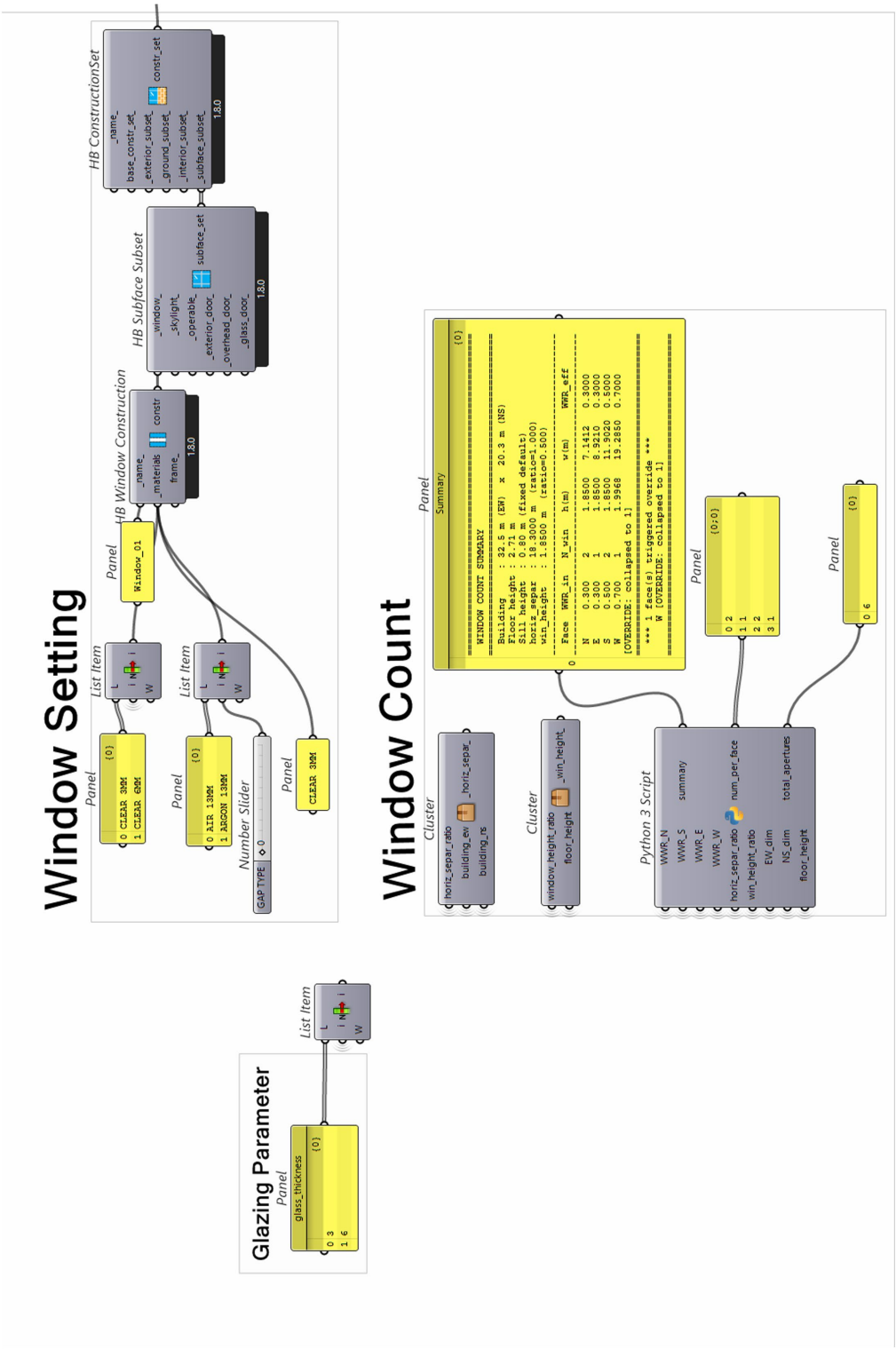

Appendix 5. Grasshopper Script 4: Window Setting

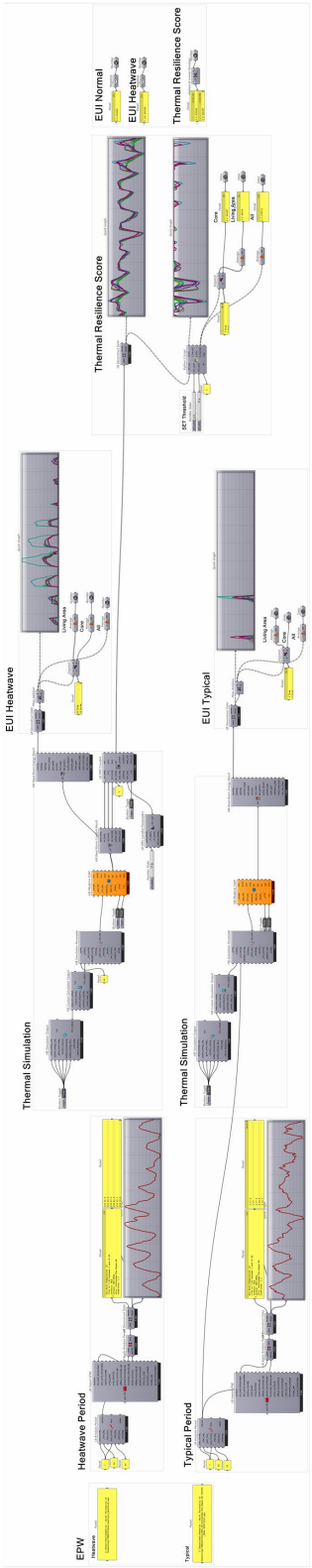

Appendix 6. Grasshopper Script 5: Thermal Resilience (Author)

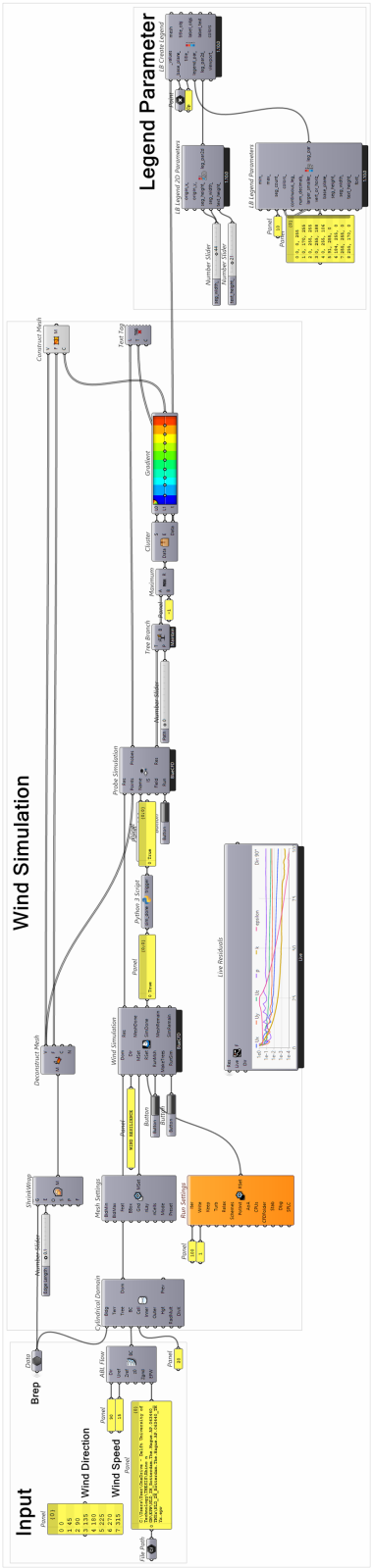

Appendix 7. Grasshopper Script 6: Wind Simulation (Author)

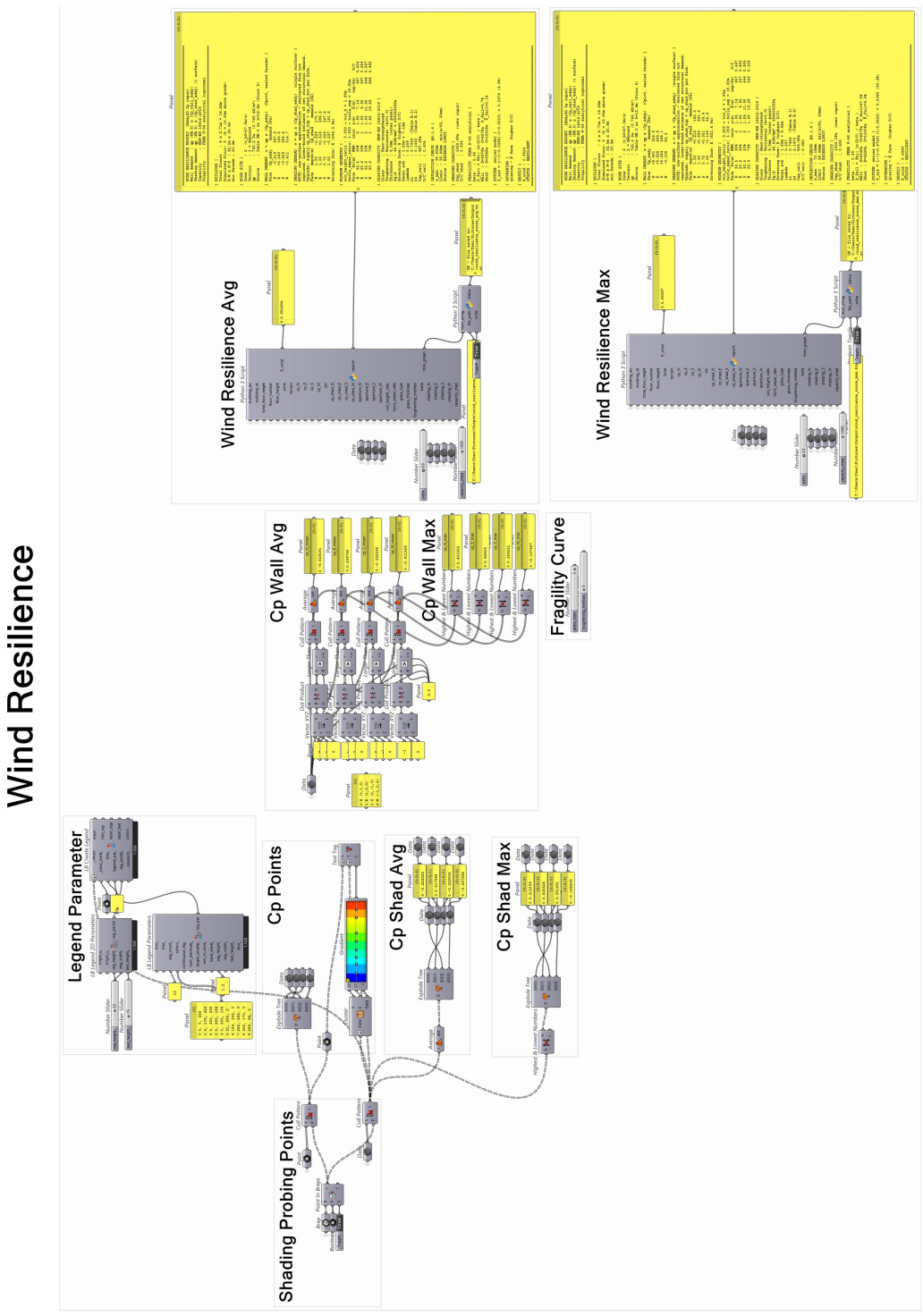

Appendix 8. Grasshopper Script 7: Wind Resilience (Author)

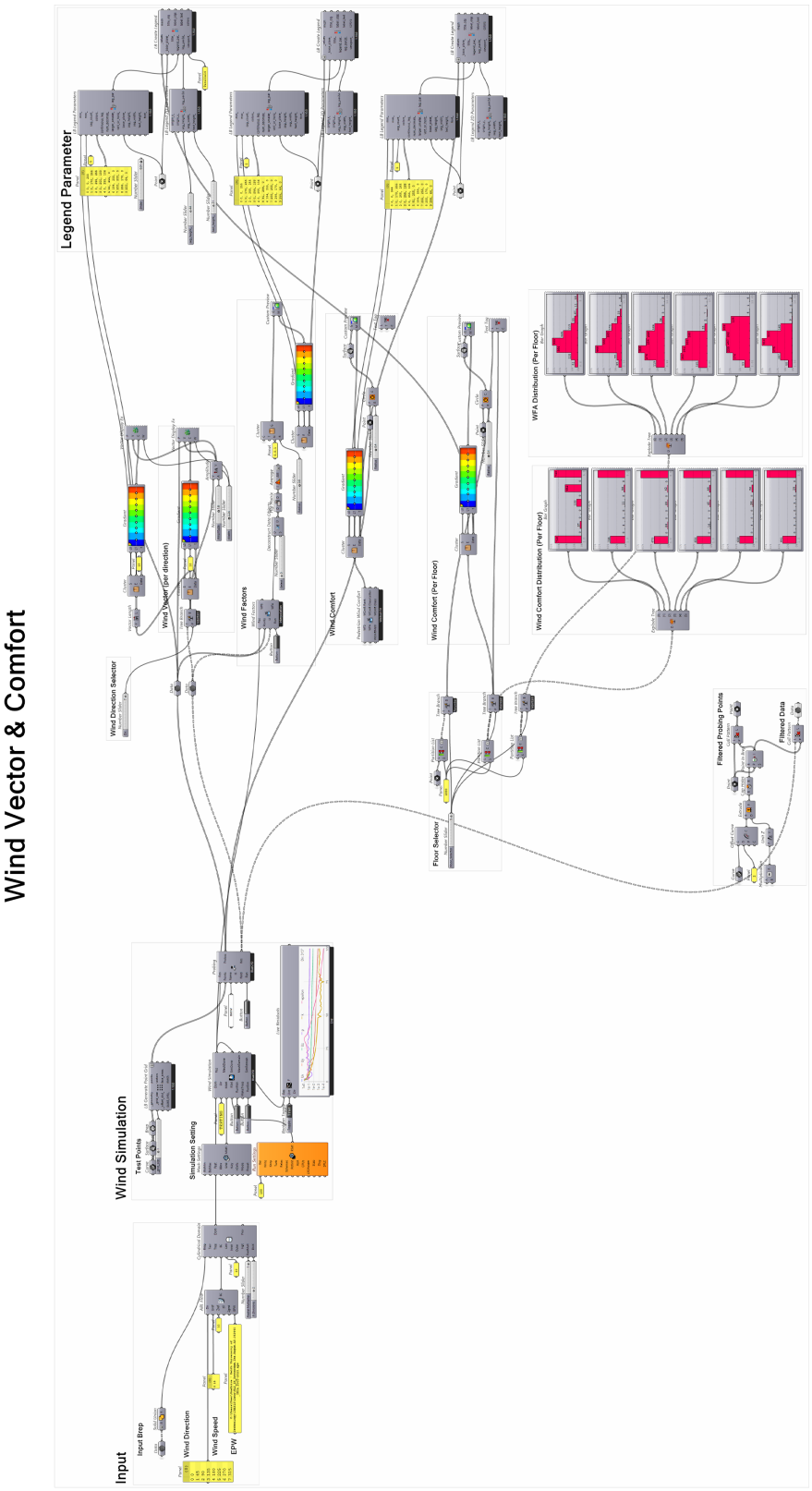

Appendix 9. Grasshopper Script 8: Wind Comfort (Author)

Appendix B

Python script for identifying heatwave events from historical weather data

Python script for thermal resilience calculations

```
"""
Q(t) = 1                    if SET(t) ≤ SET_comf
Q(t) = 0                    if SET(t) ≥ SET_alert
Q(t) = (SET_alert - SET(t))/(SET_alert - SET_comf)  otherwise

L_thermal = ∫[1 - Q(t)] dt
"""

Q_list = []
L_thermal = 0.0
L_max = 0.0
R_thermal = None
msg = ""

if SET_list and len(SET_list) > 0:
    try:
        comf = float(SET_comf)
        alert = float(SET_alert)
        dt_val = float(dt)
    except:
        msg = "Numeric inputs needed"
    else:
        if alert > comf:
            denom = alert - comf

            # COMPUTE Q_k EXACTLY AS YOUR FORMULA
            for S in SET_list:
                s_val = float(S)

                if s_val <= comf:
                    Q = 1.0
                elif s_val >= alert:
                    Q = 0.0
                else:
                    Q = (alert - s_val) / denom  # <- YOUR FORMULA

                Q_list.append(Q)
```

```
            # RESILIENCE LOSS
            loss_per_step = [1.0 - Q for Q in Q_list]
            L_thermal = sum(loss_per_step) * dt_val
            L_max = len(Q_list) * dt_val
            R_thermal = 1.0 - (L_thermal / L_max)
            msg = "OK: R_thermal = " + str(round(R_thermal,3))
        else:
            msg = "alert > comf required"
else:
    msg = "No SET_list"

# outputs are already set
```

Python script for wind resilience score

```
import math
import traceback

# ╔═══════════════════════════════════════════════════════════════════╗
# ║     WIND RESILIENCE COMPONENT — GHPython  (Eddy3D version)        ║
# ║     Demand  : Cp from Eddy3D (mean RANS) × qp from NB.5           ║
# ║     Capacity: NEN-EN 16612:2019 (glazing)                         ║
# ║     Fragility: FEMA P-58 analytical lognormal                     ║
# ╠═══════════════════════════════════════════════════════════════════╣
# ║  NOTE ON WALL Cp                                                  ║
# ║  Eddy3D gives external Cp on the facade (sealed facade,           ║
# ║  Cpi ≈ 0).  Wall demand: w = qp × |Cp_eddy|                       ║
# ╠═══════════════════════════════════════════════════════════════════╣
# ║  NOTE ON SHADING Cp                                               ║
# ║  cp_shad_N/E/S/W = mean Cp on ONE surface of the overhang.        ║
# ║  This is a lower-bound approximation because the sheltered        ║
# ║  underside contribution is not captured.                          ║
# ║                                                                   ║
# ║  UPGRADE PATH (when top+bottom surfaces are available):           ║
# ║  Replace the single-surface block in STEP 4 with:                 ║
# ║    cp_shad_net[f] = cp_shad_top[f] - cp_shad_bot[f]               ║
# ║    w_shad[f]      = qp × |cp_shad_net[f]|                         ║
# ║  Add GH inputs: cp_shad_top_N/E/S/W, cp_shad_bot_N/E/S/W          ║
# ╠═══════════════════════════════════════════════════════════════════╣
# ║  NOTE ON Cp vs qp                                                 ║
# ║  Eddy3D (RANS) outputs MEAN Cp.                                   ║
# ║  qp from NB.5 is the PEAK velocity pressure (gust-based).         ║
# ║  Multiplying mean Cp × peak qp is a conservative estimate.        ║
# ╠═══════════════════════════════════════════════════════════════════╣
# ║  GH INPUTS                                                        ║
# ║  — Building geometry —                                            ║
# ║  building_ew         float  m    E-W dimension                    ║
# ║  building_ns         float  m    N-S dimension                    ║
# ║  total_floor_height  int         total number of floors           ║
# ║  floor_number        int         floor being simulated            ║
```

```
# ╠  floor_height        float  m    floor-to-floor height      ╣
# ╠  — Wind site (for qp from NB.5) —                           ╣
# ╠  zone                int    1/2/3   NL wind zone            ╣
# ╠  terrain             int    0/1/2   exposure category       ╣
# ╠  — Eddy3D Cp — wall (area-weighted mean per facade) —       ╣
# ╠  cp_N                float        mean Cp on North face     ╣
# ╠  cp_E                float        mean Cp on East face      ╣
# ╠  cp_S                float        mean Cp on South face     ╣
# ╠  cp_W                float        mean Cp on West face      ╣
# ╠  — Eddy3D Cp — shading element (mean, single surface) —    ╣
# ╠  cp_shad_N           float        mean Cp on N overhang     ╣
# ╠  cp_shad_E           float        mean Cp on E overhang     ╣
# ╠  cp_shad_S           float        mean Cp on S overhang     ╣
# ╠  cp_shad_W           float        mean Cp on W overhang     ╣
# ╠  shading_N/E/S/W     float  m    overhang depth (ref only) ╣
# ╠  — Glazing —                                               ╣
# ╠  aperture_N/E/S/W    float  0-1   WWR per face             ╣
# ╠  win_height_ratio     float  0-1   → [0.3, 3.4] m          ╣
# ╠  horiz_separ_ratio    float  0-1   → [0.2, min_facade-2] m ╣
# ╠  glass_type           int    0=anneal 1=toughened 2=HS     ╣
# ╠  glass_thickness      float  mm    outer panel only        ╣
# ╠  toughening_method    int    0=horiz(kv=1) 1=vert(kv=0.6)  ╣
# ╠  — Fragility —                                             ╣
# ╠  beta                 float  0-1   dispersion (FEMA P-58)  ╣
# ╠  capacity_shad        float  Pa   rated pressure of shading ╣
# ╠═══════════════════════════════════════════════════════════╣
# ╠  GH OUTPUTS                                                ╣
# ╠  R_wind      float  0-1   wind resilience index            ╣
# ╠  report      str          plain-text report                ╣
# ╠  html_graph  str          interactive HTML dashboard       ╣
# ╚═══════════════════════════════════════════════════════════╝

try:

    # ═══════════════════════════════════════════════════════
    # UTILITY — standard normal CDF (Abramowitz & Stegun)
    # ═══════════════════════════════════════════════════════
    def normCDF(z):
        t    = 1.0 / (1.0 + 0.2316419 * abs(z))
        poly = t * (0.319381530
              + t * (-0.356563782
              + t * ( 1.781477937
              + t * (-1.821255978
              + t *   1.330274429))))
        cdf  = 1.0 - (1.0 / math.sqrt(2.0 * math.pi)) \
                   * math.exp(-0.5 * z * z) * poly
        return cdf if z >= 0.0 else 1.0 - cdf

    # ═══════════════════════════════════════════════════════
    # STEP 0 — BUILDING GEOMETRY
    # total_floor_height : total number of floors (for reference)
    # floor_number       : floor being simulated → sets qp height
    # qp height = floor_number × floor_height
    # ═══════════════════════════════════════════════════════
    nf_total = max(1, int(total_floor_height))   # total floors
```

```
fn  = max(1, int(floor_number))              # simulated floor
fh  = max(0.1, float(floor_height))
bh  = fn * fh                                # height used for qp
bh_total = nf_total * fh                     # total building height
ew  = max(1.0, float(building_ew))
ns  = max(1.0, float(building_ns))
min_facade = min(ew, ns)
facade_w   = {'N': ew, 'E': ns, 'S': ew, 'W': ns}

# ═══════════════════════════════════════════════════════
# STEP 1 — PEAK VELOCITY PRESSURE qp
# Source: Table NB.5, NEN-EN 1991-1-4 NB:2019+C2:2023
# qp scales all Eddy3D Cp values into Pa.
# ═══════════════════════════════════════════════════════
NB5_heights = [
    1,2,3,4,5,6,7,8,9,10,
    15,20,25,30,35,40,45,50,55,60,
    65,70,75,80,85,90,95,100,110,120,
    130,140,150,160,170,180,190,200,225,250,
    275,300
]
NB5 = {
    1: {
        0: [0.93,1.11,1.22,1.30,1.37,1.42,1.47,1.51,1.55,1.58,
            1.71,1.80,1.88,1.94,2.00,2.04,2.09,2.12,2.16,2.19,
            2.22,2.25,2.27,2.30,2.32,2.34,2.36,2.38,2.42,2.45,
            2.48,2.51,2.54,2.56,2.59,2.61,2.63,2.65,2.70,2.74,
            2.78,2.82],
        1: [0.71,0.71,0.71,0.71,0.78,0.84,0.89,0.94,0.98,1.02,
            1.16,1.27,1.36,1.43,1.50,1.55,1.60,1.65,1.69,1.73,
            1.76,1.80,1.83,1.86,1.88,1.91,1.93,1.96,2.00,2.04,
            2.08,2.12,2.15,2.18,2.21,2.24,2.27,2.29,2.35,2.40,
            2.45,2.50],
        2: [0.69,0.69,0.69,0.69,0.69,0.69,0.69,0.73,0.77,0.81,
            0.96,1.07,1.16,1.23,1.30,1.35,1.40,1.45,1.49,1.53,
            1.57,1.60,1.63,1.66,1.69,1.72,1.74,1.77,1.81,1.85,
            1.89,1.93,1.96,2.00,2.03,2.06,2.08,2.11,2.17,2.23,
            2.28,2.32],
    },
    2: {
        0: [0.78,0.93,1.02,1.09,1.14,1.19,1.23,1.26,1.29,1.32,
            1.43,1.51,1.57,1.63,1.67,1.71,1.75,1.78,1.81,1.83,
            1.86,1.88,1.90,1.92,1.94,1.96,1.98,1.99,2.03,2.05,
            2.08,2.10,2.13,2.15,2.17,2.19,2.20,2.22,2.26,2.30,
            2.33,2.36],
        1: [0.60,0.60,0.60,0.60,0.66,0.71,0.75,0.79,0.82,0.85,
            0.98,1.07,1.14,1.20,1.25,1.30,1.34,1.38,1.42,1.45,
            1.48,1.50,1.53,1.55,1.58,1.60,1.62,1.64,1.68,1.71,
            1.74,1.77,1.80,1.83,1.85,1.88,1.90,1.92,1.97,2.01,
            2.05,2.09],
        2: [0.58,0.58,0.58,0.58,0.58,0.58,0.58,0.62,0.65,0.68,
            0.80,0.90,0.97,1.03,1.09,1.13,1.17,1.21,1.25,1.28,
            1.31,1.34,1.37,1.39,1.42,1.44,1.46,1.48,1.52,1.55,
            1.59,1.62,1.65,1.67,1.70,1.72,1.75,1.77,1.82,1.86,
            1.91,1.95],
```

```
    },
    3: {
        0: None,
        1: [0.49,0.49,0.49,0.49,0.54,0.58,0.62,0.65,0.68,0.70,
            0.80,0.88,0.94,0.99,1.03,1.07,1.11,1.14,1.17,1.19,
            1.22,1.24,1.26,1.28,1.30,1.32,1.33,1.35,1.38,1.41,
            1.44,1.46,1.48,1.50,1.52,1.54,1.56,1.58,1.62,1.66,
            1.69,1.72],
        2: [0.48,0.48,0.48,0.48,0.48,0.48,0.48,0.51,0.53,0.56,
            0.66,0.74,0.80,0.85,0.89,0.93,0.97,1.00,1.03,1.05,
            1.08,1.10,1.13,1.15,1.17,1.18,1.20,1.22,1.25,1.28,
            1.31,1.33,1.35,1.38,1.40,1.42,1.44,1.46,1.50,1.54,
            1.57,1.60],
    },
}

def get_qp(zone_, terrain_, h_):
    z = int(zone_);  t = int(terrain_)
    if z == 3 and t == 0:
        t = 1
    col = NB5[z][t]
    if col is None:
        col = NB5[z][1]
    h_ = max(1.0, min(float(h_), 300.0))
    if h_ <= NB5_heights[0]:
        return col[0] * 1000.0
    if h_ >= NB5_heights[-1]:
        return col[-1] * 1000.0
    for i in range(len(NB5_heights) - 1):
        h0, h1_ = NB5_heights[i], NB5_heights[i+1]
        if h0 <= h_ <= h1_:
            f = (h_ - h0) / float(h1_ - h0)
            return (col[i] + f*(col[i+1]-col[i])) * 1000.0
    return col[-1] * 1000.0

qp_Pa   = get_qp(int(zone), int(terrain), bh)
qp_kNm2 = qp_Pa / 1000.0

# ═══════════════════════════════════════════════════════════
# STEP 2 — EDDY3D Cp INPUTS — WALL
# Area-weighted mean Cp per facade from Eddy3D RANS.
# Sign convention: Cp > 0 = pressure, Cp < 0 = suction.
# ═══════════════════════════════════════════════════════════
cp_eddy = {
    'N': float(cp_N),
    'E': float(cp_E),
    'S': float(cp_S),
    'W': float(cp_W),
}

# ═══════════════════════════════════════════════════════════
# STEP 3 — NET WALL PRESSURE DEMAND  w = qp × |Cp|
# Cpi = 0 assumed (sealed curtain-wall facade).
# ═══════════════════════════════════════════════════════════
wall_dem = {}
```

```python
for face in ['N','E','S','W']:
    wall_dem[face] = abs(qp_Pa * cp_eddy[face])

gov_wall_face_dem = max(wall_dem, key=wall_dem.get)

# ═══════════════════════════════════════════════════════════
# STEP 4 — SHADING ELEMENT DEMAND  w = qp × |Cp_shad|
#
# Cp from Eddy3D on the overhang surface (single surface).
# Limitation: only one surface is probed (zero-thickness
# geometry in HB model). The sheltered underside is not
# captured, so this is a lower-bound estimate of the net
# force on the element.
#
# ── UPGRADE PATH ──────────────────────────────────────────
# When top AND bottom surfaces are available, replace the
# single-surface block below with:
#
#   cp_shad_top = {'N': float(cp_shad_top_N), ...}
#   cp_shad_bot = {'N': float(cp_shad_bot_N), ...}
#   for face in ['N','E','S','W']:
#       cp_shad_net[face] = cp_shad_top[face] - cp_shad_bot[face]
#       shad_dem[face]    = abs(qp_Pa * cp_shad_net[face])
#
# Add GH inputs: cp_shad_top_N/E/S/W, cp_shad_bot_N/E/S/W
# ──────────────────────────────────────────────────────────
# safe_cp: returns 0.0 if input is None/empty (face has no
# shading element → zero demand → P_shad = 0 for that face).
def safe_cp(v):
    try:
        return float(v) if v is not None else 0.0
    except (TypeError, ValueError):
        return 0.0

cp_shad = {
    'N': safe_cp(cp_shad_N),
    'E': safe_cp(cp_shad_E),
    'S': safe_cp(cp_shad_S),
    'W': safe_cp(cp_shad_W),
}

# Shading depth kept for reference in report only (not used
# in demand calculation — geometry is in the Eddy3D model).
sh_depth = {
    'N': safe_cp(shading_N),
    'E': safe_cp(shading_E),
    'S': safe_cp(shading_S),
    'W': safe_cp(shading_W),
}

shad_dem = {}
for face in ['N','E','S','W']:
    shad_dem[face] = abs(qp_Pa * cp_shad[face])

w_shad_max    = max(shad_dem.values())
```

```
    gov_shad_face = max(shad_dem, key=shad_dem.get)

    # ═══════════════════════════════════════════════════════
    # STEP 5 — GLAZING CAPACITY  NEN-EN 16612:2019
    # ═══════════════════════════════════════════════════════
    wwr = {
        'N': max(0.0, min(1.0, float(aperture_N))),
        'E': max(0.0, min(1.0, float(aperture_E))),
        'S': max(0.0, min(1.0, float(aperture_S))),
        'W': max(0.0, min(1.0, float(aperture_W))),
    }

    wh_ratio  = max(0.0, min(1.0, float(win_height_ratio)))
    win_h     = max(0.1, min(0.3 + wh_ratio*3.1, fh*0.98))
    hs_ratio  = max(0.0, min(1.0, float(horiz_separ_ratio)))
    horiz_sep = max(0.2, 0.2 + hs_ratio*(min_facade-2.0-0.2))

    def get_panel_ab(wwr_, fw, fh_, wh, hsep):
        if wwr_ <= 0.001:
            return 0.1, 0.1, 0
        if hsep >= fw:
            n_win = 1
        else:
            n_win = max(1, int(round(fw/hsep)))
        A_glaz = wwr_*fw*fh_
        req_w  = A_glaz/(n_win*wh) if (n_win>0 and wh>0) else 0.0
        if req_w > hsep:
            resolved = False
            for test_n in range(n_win-1, 0, -1):
                test_req = A_glaz/(test_n*wh)
                if test_req <= hsep:
                    n_win = test_n;  req_w = test_req
                    resolved = True;  break
            if not resolved:
                n_win = 1
                req_w = min(fw*0.95, A_glaz/wh)
        win_w = max(0.1, min(req_w, fw*0.98))
        a = min(wh, win_w);  b = max(wh, win_w)
        return a, b, n_win

    pd = {}
    for face in ['N','E','S','W']:
        a_, b_, nw_ = get_panel_ab(
            wwr[face], facade_w[face], fh, win_h, horiz_sep)
        pd[face] = {'a': a_, 'b': b_, 'nw': nw_}

    g_type  = int(glass_type)
    g_tough = int(toughening_method)
    h_mm    = max(3.0, float(glass_thickness))
    h_m     = h_mm/1000.0

    fg_k  = 45.0;   gM_A  = 1.8;   gM_v  = 1.2
    E_gls = 70000.0
    fb_k_map = {0: 0.0, 1: 120.0, 2: 70.0}
    fb_k = fb_k_map.get(g_type, 0.0)
```

```
kv   = 1.0 if g_tough==0 else 0.6
kmod = 1.0;  ksp = 1.0;  ke = 1.0

if g_type == 0:
    fg_d = (ke*kmod*ksp*fg_k)/gM_A
else:
    fg_d = ((kmod*ksp*fg_k)/gM_A
          + (kv*(fb_k-fg_k))/gM_v)
fg_d_Pa = fg_d*1.0e6

lam_pts = [0.1,0.2,0.3,0.4,0.5,0.6,0.7,0.8,0.9,1.0]
k1_pts  = [0.750,0.747,0.724,0.671,0.600,
           0.524,0.449,0.380,0.319,0.268]
k4_pts  = [0.1480,0.1474,0.1421,0.1303,0.1148,
           0.0984,0.0826,0.0683,0.0559,0.0461]

def get_k1_k4(a, b):
    lam = max(lam_pts[0], min(a/b, lam_pts[-1]))
    k1_ = k1_pts[-1];  k4_ = k4_pts[-1]
    for i in range(len(lam_pts)-1):
        if lam_pts[i] <= lam <= lam_pts[i+1]:
            f   = (lam-lam_pts[i])/(lam_pts[i+1]-lam_pts[i])
            k1_ = k1_pts[i]+f*(k1_pts[i+1]-k1_pts[i])
            k4_ = k4_pts[i]+f*(k4_pts[i+1]-k4_pts[i])
            break
    return k1_, k4_, lam

E_Pa = E_gls*1.0e6
cap_data = {}
for face in ['N','E','S','W']:
    a  = pd[face]['a'];  b  = pd[face]['b']
    nw = pd[face]['nw']
    if nw==0 or a<=0:
        cap_data[face] = {
            'cap':999999.0,'k1':0.0,'k4':0.0,
            'lam':0.0,'a':a,'b':b,'dc':0.0}
        continue
    k1_, k4_, lam_ = get_k1_k4(a, b)
    cap = max(100.0, fg_d_Pa*(h_m**2)/(k1_*(a**2)))
    dc  = wall_dem[face]/cap if cap>0 else 999.0
    cap_data[face] = {
        'cap':cap,'k1':k1_,'k4':k4_,
        'lam':lam_,'a':a,'b':b,'dc':dc}

gov_wall_face = max(cap_data, key=lambda f: cap_data[f]['dc'])
gf       = cap_data[gov_wall_face]
cap_wall = gf['cap']
dc_wall  = gf['dc']
w_wall_max = wall_dem[gov_wall_face]

# deflection check
w_defl_mm  = (gf['k4']*(gf['a']**4)/(h_m**3)
              *(w_wall_max/E_Pa)*1000.0)
defl_limit = min(gf['a']*1000.0/65.0, 50.0)
defl_ok    = w_defl_mm <= defl_limit
```

```
cap_shad = max(100.0, float(capacity_shad))
dc_shad  = w_shad_max/cap_shad if cap_shad>0 else 999.0

# ═══════════════════════════════════════════════════════
# STEP 6 — FRAGILITY  (FEMA P-58 analytical)
# P_fail = Phi( ln(D/C) / beta )
# System = series: P_sys = 1-(1-P_wall)(1-P_shad)
# R_wind = 1 - P_sys
# ═══════════════════════════════════════════════════════
b = max(0.01, float(beta))

def frag(demand, cap):
    if demand<=0: return 0.0
    if cap<=0:    return 1.0
    return normCDF(math.log(demand/cap)/b)

P_wall = frag(w_wall_max, cap_wall)
P_shad = frag(w_shad_max, cap_shad)
P_sys  = 1.0-(1.0-P_wall)*(1.0-P_shad)
R_wind = max(0.0, min(1.0, 1.0-P_sys))

governing = ("shading — {} face".format(gov_shad_face)
             if dc_shad>=dc_wall else
             "glazing — {} face".format(gov_wall_face))

# ═══════════════════════════════════════════════════════
# STEP 7 — FRAGILITY CURVES for HTML
# ═══════════════════════════════════════════════════════
curve_pts = 120
x_max  = qp_Pa * 3.0
x_dem  = [x_max*i/float(curve_pts) for i in range(curve_pts+1)]

y_wall = [frag(x, cap_wall) for x in x_dem]
y_shad = [frag(x, cap_shad) for x in x_dem]

_hs    = qp_Pa/math.log(50.0)
y_haz  = [round(min(1.0, max(0.0, math.exp(-x/_hs))),6)
          if x>0 else 1.0 for x in x_dem]

y_face = {}
for face in ['N','E','S','W']:
    cap_f = cap_data[face]['cap']
    y_face[face] = [frag(x, cap_f) for x in x_dem]

# ═══════════════════════════════════════════════════════
# STEP 8 — PLAIN-TEXT REPORT
# ═══════════════════════════════════════════════════════
_ter_name  = {0:"Kust",1:"Onbebouwd",2:"Bebouwd"}
_zone_vb   = {1:29.5, 2:27.0, 3:24.5}
_type_name = {0:"Annealed",
              1:"Thermally toughened",
              2:"Heat-strengthened"}
_tough_name= {0:"Horizontal (kv=1.0)",
              1:"Vertical   (kv=0.6)"}
```

```
report_lines = [
    "="*62,
    "  WIND RESILIENCE REPORT  [Eddy3D Cp input]",
    "  Wall demand   : qp (NB.5) x |Cp_wall_eddy|",
    "  Shading demand: qp (NB.5) x |Cp_shad_eddy| (1 surface)",
    "  Capacity      : NEN-EN 16612:2019",
    "  Fragility     : FEMA P-58 analytical lognormal",
    "="*62,
    "",
    "[ BUILDING ]",
    "  Total floors   : {:d} x {:.2f}m = {:.2f}m".format(nf_total,fh,bh_total),
    "  Simulated floor: {:d}  (h = {:.2f}m above grade)".format(fn,bh),
    "  E-W x N-S  : {:.1f}m x {:.1f}m".format(ew,ns),
    "  min facade : {:.1f}m".format(min_facade),
    "",
    "[ WIND SITE ]",
    "  Zone       : {:d}  (v_b0={:.1f}m/s)".format(
        int(zone), _zone_vb.get(int(zone),27.0)),
    "  Terrain    : {:d} = {}".format(
        int(terrain), _ter_name.get(int(terrain),"?")),
    "  qp         : {:.1f} Pa  ({:.3f} kN/m²)".format(
        qp_Pa, qp_kNm2),
    "  Source     : Table NB.5 at h={:.1f}m (floor {:d})".format(bh,fn),
    "",
    "[ WALL DEMAND  w = qp x |Cp_eddy|  (Cpi=0, sealed facade) ]",
    "  Face   Cp_eddy    demand [Pa]",
]
for face in ['N','E','S','W']:
    report_lines.append(
        "   {:s}     {:+.3f}    {:.1f}".format(
            face, cp_eddy[face], wall_dem[face]))

report_lines += [
    "",
    "[ SHADING DEMAND  w = qp x |Cp_shad_eddy|  (single surface) ]",
    "  NOTE: one-surface approximation — sheltered face not",
    "  captured. Lower-bound estimate of net structural demand.",
    "  Upgrade: supply cp_shad_top + cp_shad_bot per face.",
    "  Face   depth(m)  Cp_shad    demand [Pa]",
]
for face in ['N','E','S','W']:
    report_lines.append(
        "   {:s}     {:.2f}     {:+.3f}    {:.1f}".format(
            face, sh_depth[face], cp_shad[face], shad_dem[face]))

report_lines += [
    "  Governing face: {} ({:.1f} Pa)".format(
        gov_shad_face, w_shad_max),
    "",
    "[ WINDOW GEOMETRY ]",
    "  win_height_ratio : {:.3f} → win_h = {:.2f}m".format(
        wh_ratio, win_h),
    "  horiz_separ_ratio: {:.3f} → horiz_sep = {:.2f}m".format(
        hs_ratio, horiz_sep),
```

```
        "  Face  fw(m)  WWR   nwin  a(m)   b(m)   cap(Pa)   D/C",
    ]
    for face in ['N','E','S','W']:
        report_lines.append(
            "   {:s}  {:5.1f}  {:4.0f}%  {:4d}  {:5.2f}  {:5.2f}  {:8.0f}  {:5.3f}".fo
rmat(
                face, facade_w[face], wwr[face]*100,
                pd[face]['nw'],
                cap_data[face]['a'], cap_data[face]['b'],
                cap_data[face]['cap'], cap_data[face]['dc']))

    report_lines += [
        "",
        "[ GLAZING CAPACITY  NEN-EN 16612:2019 ]",
        "  Glass      : {}".format(_type_name.get(g_type,"?")),
        "  Toughening : {}".format(_tough_name.get(g_tough,"?")),
        "  Thickness  : {:.1f}mm  (outer panel)".format(h_mm),
        "  fg;d       : {:.2f}N/mm² = {:.0f}Pa".format(fg_d,fg_d_Pa),
        "  Governing face: {} (highest D/C)".format(gov_wall_face),
        "  Panel a×b  : {:.2f}m × {:.2f}m".format(gf['a'],gf['b']),
        "  lambda     : {:.3f}".format(gf['lam']),
        "  k1         : {:.4f}  (Table B.1)".format(gf['k1']),
        "  k4         : {:.4f}  (Table B.2)".format(gf['k4']),
        "  Cap_wall   : {:.1f}Pa".format(cap_wall),
        "  D/C wall   : {:.3f}".format(dc_wall),
        "",
        "[ DEFLECTION CHECK  §9.1.4 ]",
        "  w_max  : {:.2f}mm".format(w_defl_mm),
        "  Limit  : {:.2f}mm  min(a/65, 50mm)".format(defl_limit),
        "  Status : {}".format("OK" if defl_ok else "EXCEEDS LIMIT"),
        "",
        "[ SHADING CAPACITY ]",
        "  Cap_shad   : {:.1f}Pa  (user input)".format(cap_shad),
        "  D/C shad   : {:.3f}".format(dc_shad),
        "",
        "[ FRAGILITY  FEMA P-58 analytical ]",
        "  beta   : {:.2f}".format(b),
        "  P_fail = Phi( ln(D/C) / beta )",
        "  Wall  : D={:.0f}Pa  C={:.0f}Pa  P_fail={:.1f}%".format(
            w_wall_max, cap_wall, P_wall*100),
        "  Shad  : D={:.0f}Pa  C={:.0f}Pa  P_fail={:.1f}%".format(
            w_shad_max, cap_shad, P_shad*100),
        "",
        "[ SYSTEM  series model ]",
        "  P_sys = 1-(1-{:.4f})(1-{:.4f}) = {:.4f} ({:.1f}%)".format(
            P_wall, P_shad, P_sys, P_sys*100),
        "",
        "[ GOVERNING ]",
        "  {}  (higher D/C)".format(governing),
        "",
        "[ RESULT ]",
        "  R_wind : {:.4f}".format(R_wind),
        "  STATUS : " + (
            "RESILIENT" if dc_wall<=1.0 and dc_shad<=1.0
            else "VULNERABLE"),
```

```
    "="*62,
]

report = "\n".join(report_lines)

# ═══════════════════════════════════════════════════════════
# STEP 9 — HTML DASHBOARD
# ═══════════════════════════════════════════════════════════
def js_arr(lst):
    return "["+",".join("{:.4f}".format(v) for v in lst)+"]"
def js_int(lst):
    return "["+",".join("{:.0f}".format(v) for v in lst)+"]"

bar_labs = ["Wall N","Wall E","Wall S","Wall W",
            "Shad N","Shad E","Shad S","Shad W"]
bar_dems = [wall_dem['N'],wall_dem['E'],
            wall_dem['S'],wall_dem['W'],
            shad_dem['N'],shad_dem['E'],
            shad_dem['S'],shad_dem['W']]
bar_caps = [cap_data['N']['cap'],cap_data['E']['cap'],
            cap_data['S']['cap'],cap_data['W']['cap'],
            cap_shad,cap_shad,cap_shad,cap_shad]
bar_cd   = ["#178CE0"]*4+["#EF9F27"]*4
bar_cc   = ["rgba(23,140,224,0.25)"]*4+\
           ["rgba(239,159,39,0.25)"]*4

sv = {
    'zone' : str(int(zone)),
    'ter'  : _ter_name.get(int(terrain),"?"),
    'bh'   : "{:.1f}".format(bh),
    'nf'   : str(nf_total), 'fn': str(fn), 'fh': "{:.1f}".format(fh),
    'gtype': _type_name.get(g_type,"?"),
    'hmm'  : "{:.0f}".format(h_mm),
    'fgd'  : "{:.1f}".format(fg_d),
    'capw' : "{:.0f}".format(cap_wall),
    'caps' : "{:.0f}".format(cap_shad),
    'rval' : "{:.3f}".format(R_wind),
    'rcl'  : ("good" if R_wind>=0.7 else "warn" if R_wind>=0.4 else "bad"),
    'pval' : "{:.1f}".format(P_sys*100),
    'pcl'  : ("good" if P_sys<=0.3  else "warn" if P_sys<=0.6  else "bad"),
    'pwval': "{:.1f}".format(P_wall*100),
    'pwcl' : ("good" if P_wall<=0.3 else "warn" if P_wall<=0.6 else "bad"),
    'pwdec': "{:.4f}".format(P_wall),
    'psval': "{:.1f}".format(P_shad*100),
    'pscl' : ("good" if P_shad<=0.3 else "warn" if P_shad<=0.6 else "bad"),
    'psdec': "{:.4f}".format(P_shad),
    'pdec' : "{:.4f}".format(P_sys),
    'dcwb' : "b-ok" if dc_wall<=1.0 else "b-bad",
    'dcsb' : "b-ok" if dc_shad<=1.0 else "b-bad",
    'dcw'  : "{:.2f}".format(dc_wall),
    'dcs'  : "{:.2f}".format(dc_shad),
    'gov'  : governing,
    'dwall': "{:.0f}".format(w_wall_max),
    'dshad': "{:.0f}".format(w_shad_max),
    'beta' : "{:.4f}".format(b),
```

```
        'wh'   : "{:.2f}".format(win_h),
        'hs'   : "{:.2f}".format(horiz_sep),
        'qpmax': "{:.0f}".format(x_max),
        'qpdes': str(int(qp_Pa)),
        'xdem' : js_int(x_dem),
        'ywall': js_arr(y_wall),
        'yshad': js_arr(y_shad),
        'yhaz' : js_arr(y_haz),
        'yN'   : js_arr(y_face['N']),
        'yE'   : js_arr(y_face['E']),
        'yS'   : js_arr(y_face['S']),
        'yW'   : js_arr(y_face['W']),
        'blabs': str(bar_labs).replace("'",'"'),
        'bdem' : js_arr(bar_dems),
        'bcap' : js_arr(bar_caps),
        'bcd'  : str(bar_cd).replace("'",'"'),
        'bcc'  : str(bar_cc).replace("'",'"'),
        'cpN'  : "{:+.3f}".format(cp_eddy['N']),
        'cpE'  : "{:+.3f}".format(cp_eddy['E']),
        'cpS'  : "{:+.3f}".format(cp_eddy['S']),
        'cpW'  : "{:+.3f}".format(cp_eddy['W']),
        'csN'  : "{:+.3f}".format(cp_shad['N']),
        'csE'  : "{:+.3f}".format(cp_shad['E']),
        'csS'  : "{:+.3f}".format(cp_shad['S']),
        'csW'  : "{:+.3f}".format(cp_shad['W']),
    }
    for face in ['N','E','S','W']:
        sv['nw'+face]   = str(pd[face]['nw'])
        sv['cap'+face]  = "{:.0f}".format(cap_data[face]['cap'])
        sv['a'+face]    = "{:.2f}".format(pd[face]['a'])
        sv['b'+face]    = "{:.2f}".format(pd[face]['b'])
        sv['wwr'+face]  = "{:.0f}".format(wwr[face]*100)
        sv['dem'+face]  = "{:.0f}".format(wall_dem[face])
        sv['sdem'+face] = "{:.0f}".format(shad_dem[face])

    html_graph = (
"<!DOCTYPE html>\n<html>\n<head>\n<meta charset='utf-8'>\n"
"<title>Wind Resilience — Eddy3D</title>\n"
"<script
src='https://cdnjs.cloudflare.com/ajax/libs/Chart.js/4.4.1/chart.umd.js'></script>\n"
"<style>\n"
"*{box-sizing:border-box;}\n"
"body{font-family:Arial,sans-
serif;background:#f5f5f5;margin:0;padding:20px;color:#333;}\n"
"h2{font-size:14px;font-weight:600;margin:14px 0 3px;color:#222;}\n"
".sub{font-size:11px;color:#777;margin-bottom:10px;}\n"
".card{background:#fff;border-radius:8px;border:1px solid #ddd;"
"padding:16px;margin-bottom:14px;}\n"
".row{display:flex;gap:10px;margin-bottom:14px;flex-wrap:wrap;}\n"
".met{background:#f0f0f0;border-radius:6px;padding:10px 14px;"
"flex:1;min-width:110px;}\n"
".met .lbl{font-size:10px;color:#888;margin-bottom:3px;}\n"
".met .val{font-size:20px;font-weight:700;}\n"
".good{color:#1D9E75;}.warn{color:#EF9F27;}.bad{color:#D85A30;}\n"
".cw2{position:relative;height:260px;}\n"
```

```
".cw3{position:relative;height:280px;}\n"
".badge{display:inline-block;padding:1px 7px;border-radius:4px;"
"font-size:10px;font-weight:600;margin-left:5px;}\n"
".b-ok{background:#d4edda;color:#155724;}\n"
".b-bad{background:#f8d7da;color:#721c24;}\n"
".formula{font-family:monospace;font-size:11px;background:#f8f8f8;"
"padding:10px 14px;border-radius:4px;line-height:2.0;"
"border-left:3px solid #178CE0;color:#333;}\n"
".note{font-size:10px;color:#999;font-style:italic;"
"border-left:3px solid #EF9F27;padding:6px 10px;"
"background:#fffbf5;border-radius:4px;margin-top:6px;}\n"
".sw{background:#f0f0f0;border-radius:8px;padding:16px;"
"margin-bottom:14px;border:1px solid #ddd;}\n"
".sw label{font-size:12px;color:#555;display:block;margin-bottom:8px;}\n"
".sw input[type=range]{width:100%;accent-color:#178CE0;}\n"
".sw-row{display:flex;justify-content:space-between;"
"font-size:11px;color:#888;margin-top:4px;}\n"
".rd{display:flex;gap:12px;margin-top:12px;flex-wrap:wrap;}\n"
".ri{flex:1;min-width:110px;background:#fff;border-radius:6px;"
"padding:8px 12px;text-align:center;border:1px solid #ddd;}\n"
".ri .rl{font-size:10px;color:#888;}\n"
".ri .rv{font-size:17px;font-weight:700;}\n"
".cp-grid{display:grid;grid-template-columns:1fr 1fr 1fr 1fr;"
"gap:8px;margin-top:8px;}\n"
".cp-cell{background:#f8f8f8;border-radius:6px;padding:8px 12px;"
"font-size:11px;border:1px solid #eee;text-align:center;}\n"
".cp-cell .cc-lbl{color:#888;font-size:10px;margin-bottom:3px;}\n"
".cp-cell .cc-val{font-weight:700;font-size:15px;}\n"
".pos{color:#D85A30;}.neg{color:#178CE0;}\n"
".info-grid{display:grid;grid-template-columns:1fr 1fr;"
"gap:10px;margin-top:8px;}\n"
".info-cell{background:#f8f8f8;border-radius:6px;padding:8px 12px;"
"font-size:11px;border:1px solid #eee;}\n"
".info-cell .ic-lbl{color:#888;margin-bottom:3px;}\n"
".info-cell .ic-val{font-weight:600;color:#333;font-size:12px;}\n"
"@media(max-width:600px){"
".cp-grid{grid-template-columns:1fr 1fr;}"
".info-grid{grid-template-columns:1fr;}}\n"
"</style>\n</head>\n<body>\n"
"\n<h2 style='font-size:17px;margin-bottom:3px;'>"
"Wind resilience — Eddy3D demand + EN 16612 capacity</h2>\n"
"<div class='sub'>Wall: qp(NB.5) &times; |Cp_wall|  |  "
"Shading: qp &times; |Cp_shad| (1 surface)  |  "
"Capacity: NEN-EN 16612:2019  |  "
"Fragility: FEMA P-58  |  "
"Zone "+sv['zone']+"  |  "+sv['ter']+"  |  "
"Floor "+sv['fn']+" of "+sv['nf']+"  |  h="+sv['bh']+"m</div>\n"
"\n<div class='row'>\n"
"<div class='met'><div class='lbl'>R_wind</div>"
"<div class='val "+sv['rcl']+"'>"+sv['rval']+"</div></div>\n"
"<div class='met'><div class='lbl'>P_fail system</div>"
"<div class='val "+sv['pcl']+"'>"+sv['pval']+"%</div></div>\n"
"<div class='met'><div class='lbl'>Wall glazing</div>"
"<div class='val "+sv['pwcl']+"'>"+sv['pwval']+"%"
"<span class='badge "+sv['dcwb']+"'>D/C "+sv['dcw']+"</span></div></div>\n"
```

```
"<div class='met'><div class='lbl'>Shading</div>"
"<div class='val "+sv['pscl']+"'>"+sv['psval']+"%"
"<span class='badge "+sv['dcsb']+"'>D/C "+sv['dcs']+"</span></div></div>\n"
"<div class='met'><div class='lbl'>Governing</div>"
"<div class='val' style='font-size:12px;color:#333;'>"+sv['gov']+"</div></div>\n"
"</div>\n"
"\n<div class='card'>\n"
"<h2>Wall Cp — Eddy3D area-weighted mean per face</h2>\n"
"<div class='sub'>Demand = qp &times; |Cp|   (Cpi = 0, sealed facade)
 |  qp = "+sv['qpdes']+" Pa</div>\n"
"<div class='cp-grid'>\n"
"<div class='cp-cell'><div class='cc-lbl'>North</div>"
"<div class='cc-val "+("pos" if cp_eddy["N"]>0 else "neg")+"'>"+sv['cpN']+"</div>"
"<div style='font-size:10px;color:#555;margin-top:4px;'>"+sv['demN']+"
Pa</div></div>\n"
"<div class='cp-cell'><div class='cc-lbl'>East</div>"
"<div class='cc-val "+("pos" if cp_eddy["E"]>0 else "neg")+"'>"+sv['cpE']+"</div>"
"<div style='font-size:10px;color:#555;margin-top:4px;'>"+sv['demE']+"
Pa</div></div>\n"
"<div class='cp-cell'><div class='cc-lbl'>South</div>"
"<div class='cc-val "+("pos" if cp_eddy["S"]>0 else "neg")+"'>"+sv['cpS']+"</div>"
"<div style='font-size:10px;color:#555;margin-top:4px;'>"+sv['demS']+"
Pa</div></div>\n"
"<div class='cp-cell'><div class='cc-lbl'>West</div>"
"<div class='cc-val "+("pos" if cp_eddy["W"]>0 else "neg")+"'>"+sv['cpW']+"</div>"
"<div style='font-size:10px;color:#555;margin-top:4px;'>"+sv['demW']+"
Pa</div></div>\n"
"</div></div>\n"
"\n<div class='card'>\n"
"<h2>Shading Cp — Eddy3D mean per overhang (single surface)</h2>\n"
"<div class='sub'>Demand = qp &times; |Cp_shad|</div>\n"
"<div class='cp-grid'>\n"
"<div class='cp-cell'><div class='cc-lbl'>North</div>"
"<div class='cc-val "+("pos" if cp_shad["N"]>0 else "neg")+"'>"+sv['csN']+"</div>"
"<div style='font-size:10px;color:#555;margin-top:4px;'>"+sv['sdemN']+"
Pa</div></div>\n"
"<div class='cp-cell'><div class='cc-lbl'>East</div>"
"<div class='cc-val "+("pos" if cp_shad["E"]>0 else "neg")+"'>"+sv['csE']+"</div>"
"<div style='font-size:10px;color:#555;margin-top:4px;'>"+sv['sdemE']+"
Pa</div></div>\n"
"<div class='cp-cell'><div class='cc-lbl'>South</div>"
"<div class='cc-val "+("pos" if cp_shad["S"]>0 else "neg")+"'>"+sv['csS']+"</div>"
"<div style='font-size:10px;color:#555;margin-top:4px;'>"+sv['sdemS']+"
Pa</div></div>\n"
"<div class='cp-cell'><div class='cc-lbl'>West</div>"
"<div class='cc-val "+("pos" if cp_shad["W"]>0 else "neg")+"'>"+sv['csW']+"</div>"
"<div style='font-size:10px;color:#555;margin-top:4px;'>"+sv['sdemW']+"
Pa</div></div>\n"
"</div>\n"
"<div class='note'>One-surface approximation — sheltered underside not captured. "
"Lower-bound estimate. Upgrade by supplying Cp_top and Cp_bot separately.</div>\n"
"</div>\n"
"\n<div class='card'>\n"
"<h2>Window geometry — derived from WWR and building size</h2>\n"
"<div class='sub'>Glass: "+sv['gtype']+"  |  "
```

```
"h="+sv['hmm']+"mm (outer panel)  |  "
"fg;d="+sv['fgd']+"N/mm²  |  "
"win_h="+sv['wh']+"m  |  horiz_sep="+sv['hs']+"m</div>\n"
"<div class='info-grid'>\n"
"<div class='info-cell'><div class='ic-lbl'>North   WWR="+sv['wwrN']+"%  
n="+sv['nwN']+" windows</div>"
"<div class='ic-val'>"+sv['aN']+"m &times; "+sv['bN']+"m &rarr; Cap="+sv['capN']+"
Pa</div></div>\n"
"<div class='info-cell'><div class='ic-lbl'>East    WWR="+sv['wwrE']+"%
  n="+sv['nwE']+" windows</div>"
"<div class='ic-val'>"+sv['aE']+"m &times; "+sv['bE']+"m &rarr; Cap="+sv['capE']+"
Pa</div></div>\n"
"<div class='info-cell'><div class='ic-lbl'>South   WWR="+sv['wwrS']+"%  
n="+sv['nwS']+" windows</div>"
"<div class='ic-val'>"+sv['aS']+"m &times; "+sv['bS']+"m &rarr; Cap="+sv['capS']+"
Pa</div></div>\n"
"<div class='info-cell'><div class='ic-lbl'>West    WWR="+sv['wwrW']+"%
  n="+sv['nwW']+" windows</div>"
"<div class='ic-val'>"+sv['aW']+"m &times; "+sv['bW']+"m &rarr; Cap="+sv['capW']+"
Pa</div></div>\n"
"</div></div>\n"
"\n<div class='sw'>\n"
"<label>Hazard intensity slider [Pa]  "
"<strong id='sliderVal' style='color:#178CE0;'>"+sv['dwall']+" Pa</strong></label>\n"
"<input type='range' id='hazSlider' min='0' max='"+sv['qpmax']+"' "
"value='"+sv['dwall']+"' step='10' oninput='onSlider(this.value)'>\n"
"<div class='sw-row'><span>0 Pa</span>"
"<span>"+sv['qpdes']+" Pa (qp)</span>"
"<span>"+sv['qpmax']+" Pa</span></div>\n"
"<div class='rd'>\n"
"<div class='ri'><div class='rl'>P_fail wall</div><div class='rv bad' id='sl_wall'>-
</div></div>\n"
"<div class='ri'><div class='rl'>P_fail shading</div><div class='rv bad'
id='sl_shad'>-</div></div>\n"
"<div class='ri'><div class='rl'>P_fail system</div><div class='rv bad' id='sl_sys'>-
</div></div>\n"
"<div class='ri'><div class='rl'>R_wind</div><div class='rv good' id='sl_r'>-
</div></div>\n"
"</div></div>\n"
"\n<div class='card'>\n"
"<h2>Fragility curves — system + per face</h2>\n"
"<div class='sub'>"
"Solid blue = governing wall face (Cap="+sv['capw']+" Pa)  |  "
"Dashed = other faces  |  "
"Orange = shading (Cap="+sv['caps']+" Pa)  |  "
"Grey dashed = hazard curve</div>\n"
"<div class='cw3'><canvas id='fragChart'></canvas></div></div>\n"
"\n<div class='card'>\n"
"<h2>Demand vs capacity — per orientation</h2>\n"
"<div class='sub'>Blue = wall glazing  |  Orange = shading  | 
Line = capacity</div>\n"
"<div class='cw2'><canvas id='barChart'></canvas></div></div>\n"
"\n<div class='card'>\n"
"<h2>System fragility — series model</h2>\n"
"<div class='formula'>\n"
```

```
"Wall demand  : w = qp &times; |Cp_wall|   (Cpi=0)   [Pa]<br>\n"
"Shading demand: w = qp &times; |Cp_shad|   (1 surface)   [Pa]<br>\n"
"Capacity: C = fg;d &times; h&sup2; / (k1 &times; a&sup2;)   [NEN-EN
16612]<br>\n"
"P_fail = &Phi;( ln(D/C) / &beta; )   &beta;="+sv['beta']+"<br>\n"
"P_fail,wall = "+sv['pwval']+"%<br>\n"
"P_fail,shad = "+sv['psval']+"%<br>\n"
"P_fail,system = 1-(1-"+sv['pwdec']+")(1-"+sv['psdec']+")"
" = <b>"+sv['pval']+"%</b><br>\n"
"R_wind = 1-"+sv['pdec']+" = <b>"+sv['rval']+"</b>\n"
"</div></div>\n"
"\n<script>\n"
"var xD="+sv['xdem']+";\n"
"var yWall="+sv['ywall']+";\n"
"var yShad="+sv['yshad']+";\n"
"var yHaz="+sv['yhaz']+";\n"
"var yN="+sv['yN']+";\n"
"var yE="+sv['yE']+";\n"
"var yS="+sv['yS']+";\n"
"var yW="+sv['yW']+";\n"
"var capWall="+sv['capw']+";\n"
"var capShad="+sv['caps']+";\n"
"var beta="+sv['beta']+";\n"
"var desDem="+sv['dwall']+";\n"
"function normCDF(z){\n"
"  var t=1/(1+0.2316419*Math.abs(z));\n"
"  var p=t*(0.31938153+t*(-0.356563782"
"+t*(1.781477937+t*(-1.821255978+t*1.330274429))));\n"
"  var c=1-(1/Math.sqrt(2*Math.PI))*Math.exp(-0.5*z*z)*p;\n"
"  return z>=0?c:1-c;\n"
"}\n"
"function frag(D,C){if(D<=0)return 0;if(C<=0)return 1;"
"return normCDF(Math.log(D/C)/beta);}\n"
"var govData=xD.map(function(x,i){return{x:x,y:yWall[i]};});\n"
"var shadData=xD.map(function(x,i){return{x:x,y:yShad[i]};});\n"
"var hazData =xD.map(function(x,i){return{x:x,y:yHaz[i]};});\n"
"var nData=xD.map(function(x,i){return{x:x,y:yN[i]};});\n"
"var eData=xD.map(function(x,i){return{x:x,y:yE[i]};});\n"
"var sData=xD.map(function(x,i){return{x:x,y:yS[i]};});\n"
"var wData=xD.map(function(x,i){return{x:x,y:yW[i]};});\n"
"var slPlugin={\n"
"  id:'slPlugin',\n"
"  afterDraw:function(chart){\n"
"    if(chart.canvas.id!=='fragChart')return;\n"
"    var ctx=chart.ctx,xs=chart.scales.x,ys=chart.scales.y;\n"
"    var sv=parseFloat(document.getElementById('hazSlider').value);\n"
"    function vl(xv,col,t1,t2,dy){\n"
"      var px=xs.getPixelForValue(xv);\n"
"      ctx.save();ctx.strokeStyle=col;ctx.lineWidth=1.6;\n"
"      ctx.setLineDash([5,4]);\n"
"      ctx.beginPath();ctx.moveTo(px,ys.top);"
"ctx.lineTo(px,ys.bottom);ctx.stroke();\n"
"      ctx.setLineDash([]);ctx.fillStyle=col;\n"
"      ctx.font='bold 10px Arial';\n"
"      ctx.fillText(t1,px+3,ys.top+12+(dy||0));\n"
```

```
"      ctx.font='10px Arial';\n"
"      ctx.fillText(t2,px+3,ys.top+24+(dy||0));\n"
"      ctx.restore();}\n"
"    vl(sv,'#333','Slider',Math.round(sv)+' Pa',0);\n"
"    vl(desDem,'#D85A30','Design',Math.round(desDem)+' Pa',16);\n"
"    vl(capWall,'#178CE0','Cap wall',Math.round(capWall)+' Pa',32);\n"
"    vl(capShad,'#EF9F27','Cap shad',Math.round(capShad)+' Pa',48);\n"
"  }\n"
"};\n"
"var fragChart=new Chart(document.getElementById('fragChart'),{\n"
"  type:'scatter',\n"
"  data:{datasets:[\n"
"    {label:'Wall govern. face',data:govData,"
"borderColor:'rgb(23,140,224)',backgroundColor:'rgba(23,140,224,0.08)',"
"fill:true,borderWidth:2.5,pointRadius:0,showLine:true,yAxisID:'y'},\n"
"    {label:'Face N',data:nData,borderColor:'rgba(23,140,224,0.35)',"
"borderWidth:1,borderDash:[3,3],pointRadius:0,showLine:true,yAxisID:'y'},\n"
"    {label:'Face E',data:eData,borderColor:'rgba(23,140,224,0.35)',"
"borderWidth:1,borderDash:[6,3],pointRadius:0,showLine:true,yAxisID:'y'},\n"
"    {label:'Face S',data:sData,borderColor:'rgba(23,140,224,0.35)',"
"borderWidth:1,borderDash:[2,4],pointRadius:0,showLine:true,yAxisID:'y'},\n"
"    {label:'Face W',data:wData,borderColor:'rgba(23,140,224,0.35)',"
"borderWidth:1,borderDash:[8,2],pointRadius:0,showLine:true,yAxisID:'y'},\n"
"    {label:'Shading element',data:shadData,"
"borderColor:'rgb(239,159,39)',backgroundColor:'rgba(239,159,39,0.06)',"
"fill:true,borderWidth:2.5,pointRadius:0,showLine:true,yAxisID:'y'},\n"
"    {label:'Annual exceedance',data:hazData,"
"borderColor:'#bbb',borderWidth:1.2,borderDash:[4,3],"
"pointRadius:0,fill:false,showLine:true,yAxisID:'y2'}\n"
"  ]},\n"
"  options:{responsive:true,maintainAspectRatio:false,animation:false,\n"
"    plugins:{legend:{position:'bottom',"
"labels:{boxWidth:12,font:{size:10},color:'#444'}}},\n"
"    scales:{\n"
"      x:{type:'linear',title:{display:true,"
"text:'Wind pressure demand [Pa]',font:{size:10},color:'#666'},\n"
"         ticks:{maxTicksLimit:8,color:'#666',"
"callback:function(v){return Math.round(v)+' Pa';}},\n"
"         grid:{color:'rgba(0,0,0,0.06)'}},\n"
"      y:{min:0,max:1,title:{display:true,"
"text:'Probability of failure',font:{size:10},color:'#666'},\n"
"         ticks:{color:'#666',"
"callback:function(v){return(v*100).toFixed(0)+'%';}},\n"
"         grid:{color:'rgba(0,0,0,0.06)'}},\n"
"      y2:{min:0,max:1,position:'right',\n"
"          title:{display:true,text:'Annual exceedance',"
"font:{size:10},color:'#999'},\n"
"          ticks:{color:'#999',"
"callback:function(v){return(v*100).toFixed(1)+'%';}},\n"
"          grid:{drawOnChartArea:false}}\n"
"    }},plugins:[slPlugin]\n"
"});\n"
"function onSlider(val){\n"
"  var v=parseFloat(val);\n"
"  document.getElementById('sliderVal').textContent=Math.round(v)+' Pa';\n"
```

```
"  var pw=frag(v,capWall),ps=frag(v,capShad);\n"
"  var psys=1-(1-pw)*(1-ps),rw=1-psys;\n"
"  document.getElementById('sl_wall').textContent=(pw*100).toFixed(1)+'%';\n"
"  document.getElementById('sl_shad').textContent=(ps*100).toFixed(1)+'%';\n"
"  document.getElementById('sl_sys').textContent=(psys*100).toFixed(1)+'%';\n"
"  document.getElementById('sl_r').textContent=rw.toFixed(3);\n"
"  document.getElementById('sl_wall').style.color="
"pw>0.5?'#D85A30':pw>0.3?'#EF9F27':'#1D9E75';\n"
"  document.getElementById('sl_shad').style.color="
"ps>0.5?'#D85A30':ps>0.3?'#EF9F27':'#1D9E75';\n"
"  document.getElementById('sl_sys').style.color="
"psys>0.5?'#D85A30':psys>0.3?'#EF9F27':'#1D9E75';\n"
"  document.getElementById('sl_r').style.color="
"rw>=0.7?'#1D9E75':rw>=0.4?'#EF9F27':'#D85A30';\n"
"  fragChart.update('none');\n"
"}\n"
"onSlider(desDem);\n"
"new Chart(document.getElementById('barChart'),{\n"
"  type:'bar',\n"
"  data:{labels:"+sv['blabs']+",datasets:[\n"
"    {label:'Demand [Pa]',data:"+sv['bdem']+","
"backgroundColor:"+sv['bcd']+",borderRadius:4},\n"
"    {label:'Capacity [Pa]',data:"+sv['bcap']+","
"backgroundColor:"+sv['bcc']+","
"borderColor:"+sv['bcd']+",borderWidth:1.5,type:'line',"
"pointRadius:3,tension:0}\n"
"  ]},\n"
"  options:{responsive:true,maintainAspectRatio:false,\n"
"    plugins:{legend:{position:'bottom',"
"labels:{boxWidth:12,font:{size:10},color:'#444'}}},\n"
"    scales:{\n"
"      x:{ticks:{font:{size:10},color:'#666'},"
"grid:{color:'rgba(0,0,0,0.06)'}},\n"
"      y:{title:{display:true,text:'Pressure [Pa]',"
"font:{size:10},color:'#666'},\n"
"         beginAtZero:true,ticks:{color:'#666'},"
"grid:{color:'rgba(0,0,0,0.06)'}}\n"
"    }}\n"
"});\n"
"</script>\n</body>\n</html>\n"
    )

except Exception as e:
    R_wind     = -1.0
    html_graph = ""
    report     = "ERROR:\n" + traceback.format_exc()
```

```
"""
Q(t) = 1                    if SET(t) ≤ SET_comf
Q(t) = 0                    if SET(t) ≥ SET_alert
Q(t) = (SET_alert - SET(t))/(SET_alert - SET_comf)  otherwise

L_thermal = ∫[1 - Q(t)] dt
"""

Q_list = []
L_thermal = 0.0
L_max = 0.0
R_thermal = None
msg = ""

if SET_list and len(SET_list) > 0:
    try:
        comf = float(SET_comf)
        alert = float(SET_alert)
        dt_val = float(dt)
    except:
        msg = "Numeric inputs needed"
    else:
        if alert > comf:
            denom = alert - comf

            # COMPUTE Q_k EXACTLY AS YOUR FORMULA
            for S in SET_list:
                s_val = float(S)

                if s_val <= comf:
                    Q = 1.0
                elif s_val >= alert:
                    Q = 0.0
                else:
                    Q = (alert - s_val) / denom  # <- YOUR FORMULA

                Q_list.append(Q)

            # RESILIENCE LOSS
            loss_per_step = [1.0 - Q for Q in Q_list]
            L_thermal = sum(loss_per_step) * dt_val
            L_max = len(Q_list) * dt_val
            R_thermal = 1.0 - (L_thermal / L_max)
            msg = "OK: R_thermal = " + str(round(R_thermal,3))
        else:
```

Appendix C

Timeline

ACTIVITY	START	DURATION	1	2	3	4	5	6	7	8	A1 9	10	11	12	13	14	15	16	17	A2 18	19	20	21	22	23	24	25	26	A3 27	28	29	30	A4
															16-Feb	23-Feb	2-Mar	9-Mar	16-Mar	23-Mar	30-Mar	6-Apr	13-Apr	20-Apr	27-Apr	4-May	11-May	18-May	26-May	1-Jun	8-Jun	15-Jun	22-Jun
TOPIC SELECTION																																	
Literature Review	1	8																															
Problem Statement	3	6																															
Research Questions	3	6																															
THEORETICAL FRAMEWORK																																	
Define Façade Parameter	8	3																															
Define (Thermal) Hazard Parameter	8	4																															
Define (Wind) Hazard Parameter	8	4																															
Define Resilience Quantificaiton	8	6																															
CASE STUDY																																	
Location Selection	8	3																															
Façade Retrofit Type Selection	8	3																															
DATASET GENERATION																																	
Thermal Dynamic Simulation	13	5																															
Wind Simulation/Structure Simulation	13	5																															
Thermal Resilience Quantification	15	4																															
Wind Resilience Quantification	15	4																															
MULTI OBJECTIVE OPTIMIZATION																																	
Set Resilience Score as Objective	18	2																															
Run Multi-Objective Optimization	20	4																															
CONCLUSION																																	
Analyze Results	22	2																															
Draw Conclusions	25	1																															
Write Thesis Document	1	16																															
Review and Revise	25	2																															
Prepare Presentation	27	3																															